A BEAM STEERING TECHNIQUE USING DIELECTRIC WEDGES

by

MOHAMMAD REZWAN KHAN

A thesis submitted to the University of London for the Degree of Doctor of Philosophy in Electronic and Electrical Engineering.

Department of Electronic and Electrical Engineering
University College London
December 1985

IN THE NAME OF GOD, THE MERCIFUL

AND BENEFICENT

Dedicated to my parents

Abstract

The thesis describes a method of beam steering aimed at producing a useful amount of deflection of an antenna beam from boresight, by a simple and inexpensive method. For large antennas, it is difficult, as well as expensive, to steer the beam by more than a few beamwidths. The method studied was developed with particular reference to the beam steering requirements of Direct Broadcast Satellite flat plate antennas.

The method involves two dielectric wedges, having circular faces, placed in front of the antenna. By adjusting the relative angular position of the wedges, the beam can be steered in any direction, up to a maximum value from the antenna boresight direction. The maximum value of the deflection is determined by the wedge angle and the dielectric constant of the wedge material. This method of beam steering is independent of frequency. Frequency limitations are, however, set by the need for a matching layer on the wedge faces to reduce the loss due to reflection and also due to interference of multiple reflection effects on the radiation pattern.

Extensive investigations are made (both theoretical and experimental) to predict the performance of the wedges as the beam is steered. The effect of reflection is studied

and a new matching technique is devised. Other practical considerations for example, stepping the wedges for weight reduction, the effect of loss in the dielectric material and cross polar performance are also taken into account. Some effort is given to explore the possibility of using metal loaded artificial dielectrics using polyurethane as the base material.

Finally, a number of charts are presented to determine the amount of beam steering for an arbitrary position of the wedges.

ACKNOWLEDGEMENT

The author is indebted to Mr. C.D. McEwen for his supervision and guidance during the course of this project. The author is grateful to Mr. H.D. Griffiths and Dr. A.G. Chapman for their help and useful suggestions on this work and compilation of the thesis.

Sincere thanks are due to Professor D.E.N. Davies and Professor K. Milne for their valuable advice and useful discussions.

The author would like to extend his thanks to the Independent Broadcasting Authority for financing this project. Thanks are due to the Department of Electrical Engineering, Queen Mary College, for their co-operation and providing their laboratory facilities for various experiments.

Finally, the author expresses his gratitude to his wife Shahana Begum for her constant encouragement during this research work.

CONTENTS

LIST OF ILLUSTRATIONS

CHAPTER 1 : Introduction

1.1 The Importance of Beam Steering for Direct Broadcast Satellite Antennas

The World Administrative Radio Conference (WARC) in Geneva in January 1977 reached an agreement regarding television broadcasting from satellites for direct household reception. A plan has been put forward for satellite broadcasting covering most of the world except America. The agreement allocated to every country a number of channels at some defined satellite position. The International Radio Consultative Committee (CCIR) defined a reference pattern for the directivity of the receiving aerials which has been widely accepted. This design was based on a G/T ratio of 6dB/^{o}K at a noise figure of 8dB over a frequency range of 11.7 - 12.5 GHz. The copolar and cross polar specifications are shown in fig(1.1). These specifications correspond to an antenna gain of 38dBi (appendix I). This gain can be achieved by a uniformly illuminated circular aperture of 64cm diameter. If an aperture efficiency of 50% is assumed for a parabolic reflector, a 90 cm dish becomes necessary. Amplifier noise figures of better than 5dB have since become possible, so the diameter of the antenna needed has shrunk to nearly 50cm.

Some form of beam steering facility is of great importance

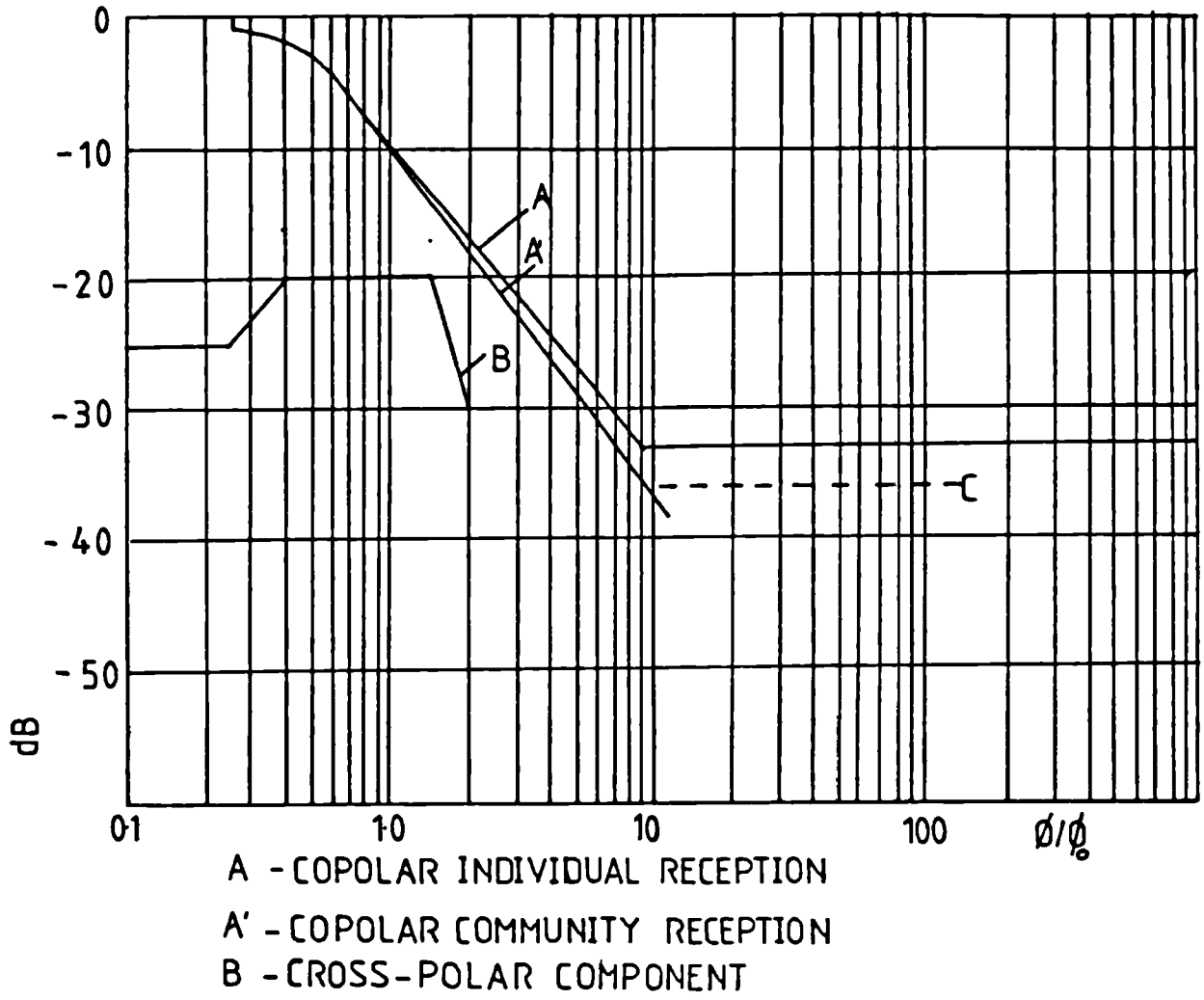

Fig 1.1. Co-polar and cross polar requirements set by CCIR for DBS antennas.

for Direct Broadcast Satellite (DBS) antennas, because the position of the house upon which the antenna is mounted could be such that the satellite is at a large angle from the most convenient roof or side wall. In the worst possible situation this angle can be as high as 54^{o} considering an arbitrary position of the satellite. Mechanical rotation of the antenna for alignment can be quite complicated and it may be necessary for the antenna to project from the side wall or the roof. This may cause excessive stress due to strong wind. Hence, an inexpensive beam steering mechanism can make the problem much simpler and at the same time enable the user to receive signals from several satellites by steering the beam. Even a limited amount of beam steering can make the alignment of the antenna in the right direction much easier.

1.2 Review of Beam Steering Antennas

There are various methods of steering the beam of an antenna without mechanically realigning it. A beam steering antenna requires an arrangement for varying the phase taper on the antenna aperture. The direction of the main beam is normal to the phase front of the antenna hence any change in the tilt of the phase front will change the direction of the main beam.

Beam steering by feed displacement in a parabolic mirror has been studied in optical systems by a number of people [1,2]. Later, it was further developed by Ruze [3] to

apply to parabolic antennas. The technique has limited beam steerability, as the radiation pattern worsens with the steering of the main beam off boresight. Hence the maximum achievable beam steering using this technique is limited to 3-4 beamwidths.

Antenna arrays seem to be the most attractive type of antenna for beam steering purposes. In an array, the individual elements can be fed via phase shifters, each controlled electronically [4]. Hence the beam can be steered by a large amount without degrading the radiation pattern appreciably. Moreover, very fast scanning of the beam is possible as no mechanical movement is involved. It has the disadvantage of high cost of the phase shifters, which make the method extremely expensive for large arrays. However, it is possible to achieve a limited amount of beam steering by dividing the whole array into a number of subarrays and feeding each of the subarrays via a single phase shifter. The number of phase shifters is thus considerably reduced, but a penalty is paid in the grating lobes that come up as the beam is steered.

Another way of obtaining the phase shift for the array elements is the multiple beam forming lens. Rotman and Turner [5] designed a lens to be used at microwave frequencies. Lens design has been improved considerably since then, and Fong and Smith [6] have built a lens in microstrip to feed a 16-element linear array. Instead of

feeding all the ports at the same time, exciting one port at a time will produce only one beam along a certain direction. Changing the feed port mechanically or electronically will produce a new beam in a different direction. This has the disadvantage of producing the beams in fixed positions rather than as a continuum. It can be overcome by designing the angular separation of the beams to be less than the beam width of an individual beam. The lens described in [6] is capable of feeding a linear array only. Research is going on to make a three dimensional version of the lens [7] to feed a planar or conformal array which will enable the beams to be directed in 3-dimensional space.

1.3. The Scheme of Dielectric Wedges

This scheme has been developed to produce a useful amount of beam steering in an inexpensive way. This technique uses a pair of identical dielectric wedges having circular faces. A schematic diagram of a wedge is shown in fig(1.2). The wedges are placed one in front of the other and the whole combination is placed in front of an antenna. Fig(1.3a) and (1.3b) show the two possible orientations of the wedges along with the antenna whose beam is to be steered. The wedges are placed such that they can be rotated individually about their axis. Fig(1.4b) shows the position of the wedges for maximum

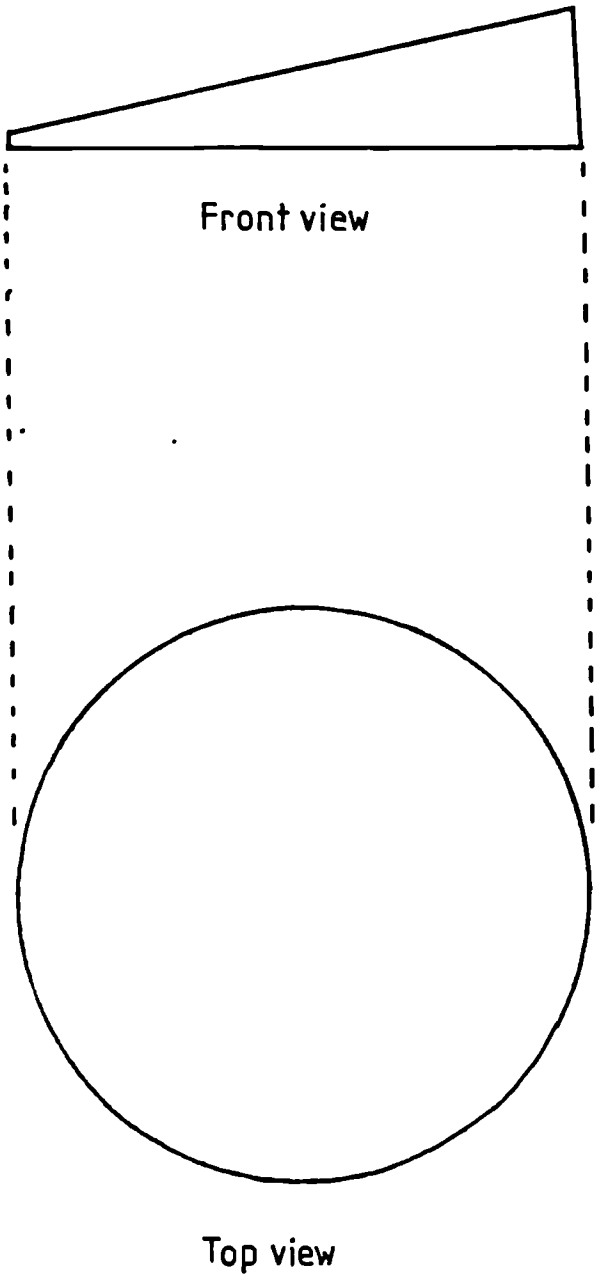

Fig 1.2. A schematic diagram of a wedge.

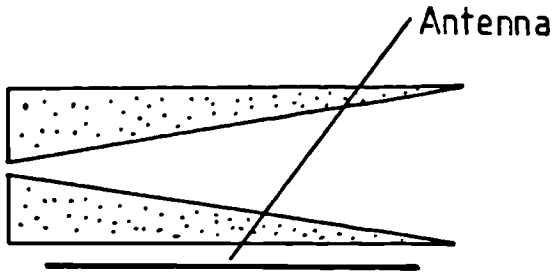

(a)

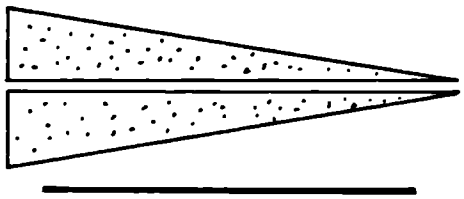

(b)

Fig 1.3. Two possible configurations for the wedges.

steering of the beam. Keeping the relative position of the wedges unchanged, both the wedges can be rotated at the same time to give a conical coverage of the main beam. By changing the relative position of the wedges, the main beam can be positioned in any direction within this cone. Fig(1.4a) shows the relative position of the pair of wedges to give no beam deflection at all. The maximum achievable beam deflection for a pair of wedges depends on the dielectric constant of the material and the

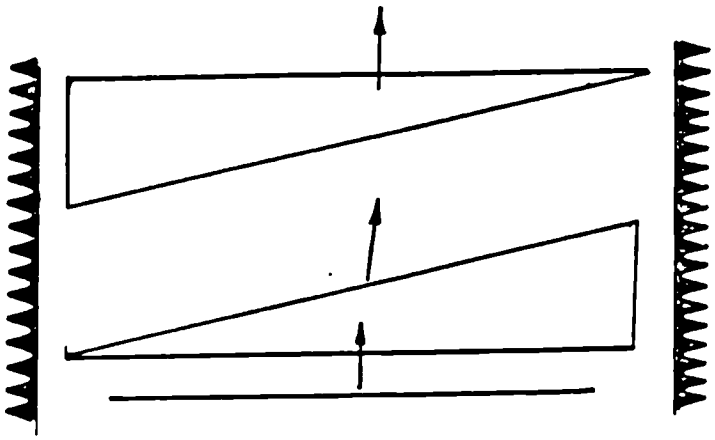

Fig 1.4a. Wedges oriented for zero beam deflection.

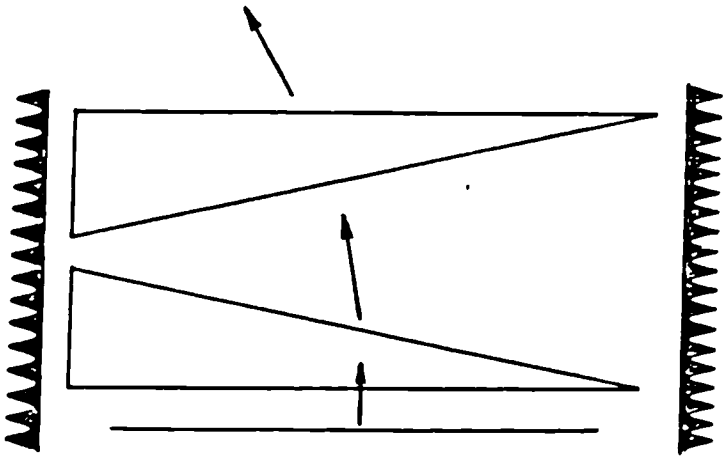

Fig 1.4b. Wedges oriented for maximum beam deflection.

wedge angle. Wedges made of high dielectric constant material can steer the beam by a larger amount for the same wedge angle.

1.4. Outline of the Thesis

An understanding of antenna fundamentals is very important for this project. The performance of the wedges is related to the radiating properties of the antenna used with them. Diffraction theory, which predicts the far field pattern from the aperture distribution is the most important relation used to develop the mathematical model for the overall performance of the system. Chapter 2 discusses all the basic parameters of an antenna and provides a useful discussion on diffraction theory and the concept of the angular spectrum.

Chapter 3 contains a theoretical study of the propagation of electromagnetic waves in a dielectric medium. Detailed discussions are presented on reflection at a dielectric interface, the matching, technique and the change in amplitude of the EM wave due to its transmission from one medium to another. Attenuation in a lossy medium is also included in this discussion.

Chapter 4 presents a detailed analysis of the dielectric wedges. The concept of the angular spectrum is used to develop the mathematical relation for the overall radiation pattern. Experimental measurements show the

importance of matching layers in improving the radiation pattern of the system. Both the computed and the measured results show that there is no significant change in sidelobe levels as the beam is steered. A comparison between the theory and the experiment is presented to justify the mathematical model developed.

A brief discussion is presented in chapter 5 regarding different kinds of dielectric materials including artificial dielectric materials. A wedge was made from artificial dielectric material and its performance investigated experimentally.

Certain quite important aspects of this beam steering technique are discussed in chapter 6. Some analysis is presented on a weight reduction scheme by stepping the wedges which reduces the weight sufficiently to make the wedges a realistic commercial proposition. Stepping of the wedges has the disadvantage of degrading the pattern and reducing the bandwidth. It is shown that the cross polar performance is well within acceptable limits even at large angles of beam steering ($\sim 30^{o}$). In addition, modification of the amplitude distribution due to a lossy wedge and the reduction in gain due to beam steering are also discussed in detail.

Chapter 7 presents some charts to enable the user to point the beam in the right direction, and the analysis behind their developments. Charts are presented to evaluate

maximum deflection of the beam and to determine the azimuth and elevation in relation to the wedge positions.

Some measured results are presented in chapter 8 for circular wedges, using a parabolic dish as the antenna. Comparison between theory and experiment is also presented.

CHAPTER 2: Antenna Fundamentals

2.1 Introduction

The performance of an antenna is expressed in terms of a number of its properties such as gain, sidelobe level, cross polar performance etc. This chapter deals with the definitions of the parameters and their influence on the antenna performance. The radiation pattern of an antenna can be determined from the knowledge of the complex amplitude distribution on the antenna aperture. Our scheme of beam steering places the dielectric wedges in the near field of the antenna. The computation of the steered radiation pattern requires the accurate determination of the radiation pattern from the amplitude distribution. The concepts and relations presented in this chapter are extensively used to develop the mathematical relations to predict the overall performance of the scheme.

2.2 Antenna Parameters

a) Gain and Effective area -

Gain is the measure of the ability of an antenna to transmit or receive power in a particular direction. Gain $G(\theta,\phi)$ of an antenna in a particular direction (θ,ϕ) is

expressed as -

$$G(\theta,\phi) = \frac{\text{Power radiated in any direction/solid angle}}{\text{Power radiated by a lossless isotropic antenna / solid angle}}$$

The gain of an antenna usually refers to the direction of maximum gain. An isotropic or omni-directional antenna is defined as an antenna which radiates equally in all directions; hence has a gain of unity. So, the gain of an antenna can also be defined as the ratio of the intensity of radiation in a given direction to the intensity of radiation of an isotropic antenna fed by the same amount of power. The terms 'directivity' or 'directive gain' refer to the antenna gain considering the antenna to be loss free. The effective area of an antenna is related to its gain by the relation -

$$G = 4\pi A_e/\lambda^2$$

where λ = wavelength

A_e = effective area

If 'A' is the geometric area of an antenna, then the ratio of 'A_e' to 'A' is called the aperture efficiency.

b) Beamwidth -

Beamwidth is most frequently defined as the angle between the half power (-3dB) points of the main beam. Sometimes the angle between the one tenth (-10dB) power points is

also used. Beamwidth in a given plane is closely related to the dimension of the aperture in that plane and also to the nature of the of the aperture excitation. The beamwidth of an antenna gives us a good idea of its directivity. The higher the gain, the smaller should be the beamwidth . This fact establishes the inverse relation between the size of the antenna and the beamwidth.

c) Sidelobes -

The radiation pattern of an antenna usually contains a number of lobes. The lobe in the direction of maximum radiation is called the main beam and the rest are called sidelobes. In the case of a transmitting antenna, power in the sidelobes is wasted as far as the main beam is concerned. On reception sidelobes pick up signals from unwanted directions resulting in an increase in the noise level. Sidelobe levels are not dependent on the size of the antenna, but on the nature of the antenna aperture excitation.

d) Polarization -

Polarization of an antenna refers to the orientation of the radiated electric field. In the case of an antenna, where the direction of the electric field does not change with time, the polarization is said to be linear. On the other hand, a rotating electric field vector with constant

amplitude is called circular polarization. A circular polarization can be resolved into two linear polarizations of equal amplitude, separated both in space and phase by 90 degrees. When the constituent linearly polarized waves are not equal in amplitude, the rotating electric field vector changes amplitude as it rotates. This is known as elliptical polarization.

In the case of a linearly polarized receiving antenna, we must align the antenna so that the polarization of the incident signal coincides with the polarization of the antenna. This is a necessary condition for maximum reception of the incident signal. For circularly polarized signals, the antenna must have the same direction of rotation of the electric field to receive the incident signal.

All practical antennas radiate some energy orthogonal to the expected polarization. These are called cross-polar radiations. In the case of linear polarization the cross polar components have electric fields normal to the expected direction of polarization. For circular polarized antennas, cross polar components are effectively the rotation of the electric field vector in the opposite direction, making the overall polarization elliptic.

2.3 Aperture Excitation and Radiation pattern

The radiation pattern of an aperture antenna can be calculated from the knowledge of its aperture amplitude distribution. In electromagnetism, field distribution refers to both the electric and magnetic fields. In simple structures, knowledge of one of the fields enables us to calculate the other. Hence, the computation of the radiation pattern usually involves the tangential component of the electric field on the radiating aperture.

Two different mathematical relations, although they are very nearly the same, are widely used for the computation of the radiation pattern. Let us consider a radiating aperture, as shown in fig(2.1), whose aperture

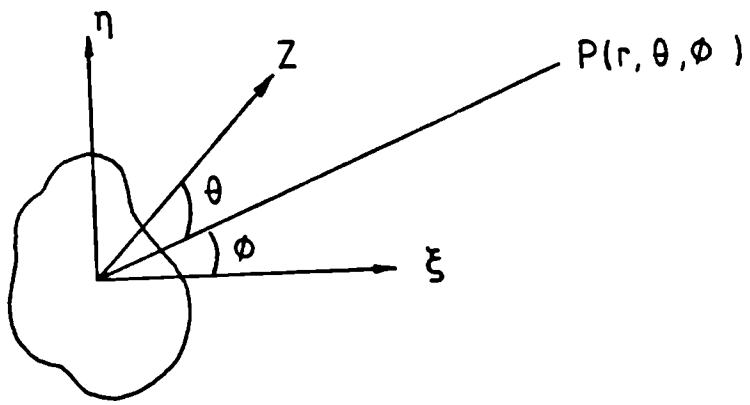

Fig 2.1. A radiating aperture and its co-ordinate system.

illumination is known. Let E_{ax} be the tangential electric field on the aperture. The Fresnel-Kirchoff relation [8] gives the far field pattern -

$$E(\theta,\phi) = -j/(2\lambda r) \iint E_{ax}(1+\cos\theta) \cdot \exp(-jKr)\, d\xi\, d\eta \quad \ldots.(2.1)$$

where K = propagation constant = $2\pi/\lambda$

r = distance from the aperture

θ,ϕ = parameters of spherical co-ordinate system

The above relation use spherical waves, which is evident from the exp(-jKr) term. Although spherical waves are nearer to physical reality, they are difficult to handle mathematically. Booker and Clemmow [9] have developed the concept of the angular spectrum, where they have used the superposition of an infinite number of plane waves approaching from different directions to simulate the aperture distribution on the aperture plane. As the angular spectra represent plane waves, they are simple to handle mathematically.

In fig(2.2) $\bar{u}$ corresponds to the direction of an elemental plane wave component.

$$\bar{u} = \bar{u}_x\alpha + \bar{u}_y\beta + \bar{u}_z\gamma$$

Where $\alpha = \sin\theta\cos\phi$

$\beta = \sin\theta\sin\phi$

$\gamma = \cos\theta$

and $\alpha^2 + \beta^2 + \gamma^2 = 1$

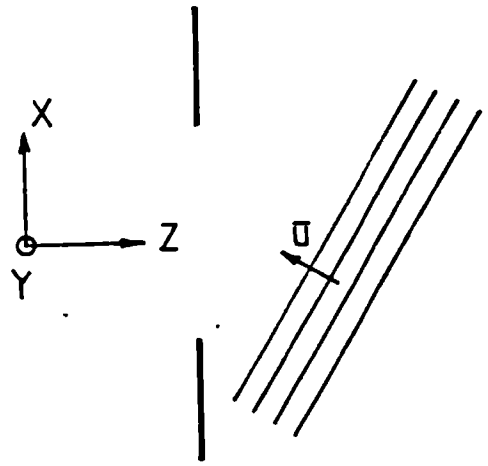

Fig 2.2. An elemental plane wave approaching a radiating aperture.

Using angular spectra we can write down the expressions for the electric field [10], assuming x-polarization -

$$E_{ax}(x,y) = \iint F_x(\alpha,\beta)\exp(-jK(\alpha x+\beta y))\,d\alpha\,d\beta \quad ..(2.2)$$

which is a two dimensional Fourier transformation of the angular spectrum $F_x(\alpha,\beta)$. Using the inverse Fourier transform relation we can find out the angular spectrum when the aperture distribution $E_{ax}(x,y)$ is known.-

$$F_x(\alpha,\beta) = \frac{1}{\lambda^2}\iint E_{ax}(x,y)\exp(jK(\alpha x+\beta y))\,dx\,dy \quad ...(2.3)$$

Considering an arbitrary polarization of the aperture, the far field is given by [11] -

$$\bar{E}(x,y,z) = j\frac{2\pi}{Kr}\exp(-jKr)\,[(\bar{u}_x\gamma - \bar{u}_z\alpha)\,F_x(\alpha,\beta) + (\bar{u}_y\gamma - \bar{u}_z\beta)\,F_y(\alpha,\beta)] \quad ..(2.4)$$

Where $r^2 = x^2+y^2+z^2$ and F_x and F_y are the angular spectra corresponding to the x and y components of the tangential fields of the aperture respectively. From these given relations we can find out the magnetic fields using Maxwell's equations.

When eqn(2.4) is reduced for a two dimensional radiation pattern, assuming x-polarization only, then

$$\bar{E}(x,y,z) = 2\pi/(Kr)\; e^{-jKr}\,(\bar{u}_x\gamma - \bar{u}_z\alpha)\,F_x(\alpha,\beta)$$

If we consider the radiation pattern in the TE (Transverse Electric) plane i.e. in the y-plane , then $\phi = 90^\circ$ and

$$\bar{E}(x,y,z) = 2\pi/(Kr)\; e^{-jKr}\,\bar{u}_x\gamma\,F_x(\alpha,\beta) \quad ....(2.5)$$

where $\gamma = \cos\theta$

Here the far field pattern is the angular spectrum multiplied by a $\cos\theta$ factor, where θ is the angle from boresight.

For the TM case, $\phi=0$ and

$$E(x,y,z) = 2\pi/(Kr)\; e^{-jKr}\,|(\bar{u}_x\gamma - \bar{u}_z\alpha)|\,F_x(\alpha,\beta)$$

$$= 2\pi/(Kr)\; e^{-jKr}\,F_x(\alpha,\beta) \quad ....(2.6)$$

as $\alpha^2 + \gamma^2 = 1$

Here the radiation pattern is the same as the angular spectrum of the aperture.

To look at some other important aspects of the angular spectra, let us consider a one dimensional radiation pattern for a uniformly illuminated aperture having an electric field of E_o. Using eqn(2.3) -

$$F_x(s) = 1/\lambda \int_{-a/2}^{a/2} E_o \, e^{jKsx} \, dx$$

$$= 1/\lambda \; a/2 \; E_o \; (\sin Ks\,a/2)/(Ks\,a/2)$$

$$= \sin(\mu a/2)/(\mu a/2) \; .E_o \; a/2 \; 1/\lambda$$

where $s = \sin\theta$ and $\mu = K \sin\theta$

Fig(2.3) shows the sinc function $\sin(\mu a/2)/(\mu a/2)$, the angular spectrum pattern of the aperture. This function extends from $\mu = -\infty$ to $\mu = \infty$. But actual radiation only occurs for $|s| < 1$, which corresponds to θ from -90^o to $+90^o$. The spectrum for $|s| > 1$ corresponds to the reactive field of the aperture [12]. It is evident from the figure that the radiation pattern is more directive for large values of a, as the value of μ corresponding to $|s| < 1$ is also large. As the value of a decreases, the radiation pattern becomes more broad and for $a < \lambda$ there is no sidelobe. When $a << \lambda$, the radiation pattern becomes almost uniform for all the angles and effectively behaves like an omnidirectional antenna.

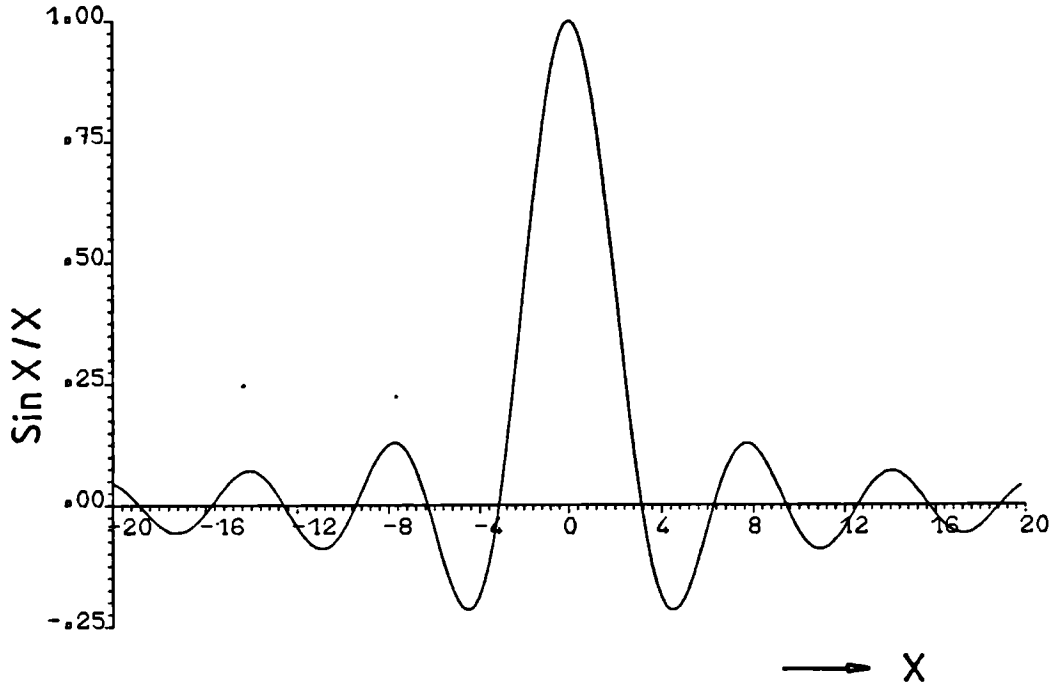

Fig 2.3. Plot of the angular spectrum for a uniformly illuminated aperture.

If we consider different planes at different distances Z from the aperture, the aperture distribution tends to spread out with increasing Z. At Rayleigh's distance ($Z = 2\,a^2/\lambda$) the field distribution is very nearly the angular spectrum pattern. So, the far field distance for an antenna is defined as a distance $Z > 2\,a^2/\lambda$. For large antennas, this distance can be quite large; for an antenna of 1m in diameter and operating at 12GHz, the far field distance is about 80m.

CHAPTER 3: Propagation of Electromagnetic Waves in Dielectric Media

3.1 Introduction

In this chapter we shall be dealing with the effect of propagation of electromagnetic plane waves in dielectric materials and at their interfaces. Reflection from a dielectric interface depends on the dielectric constants of the materials and the polarization of the incident waves. Both the polarization and the incidence angle will vary in our scheme of beam steering as the dielectric wedges are rotated relative to each other. Moreover, a cross polar component will be generated at the air-wedge interface and any loss in the wedge material will modify the amplitude distribution on the wedge faces. So, the propagation characteristics of the electromagnetic waves are vitally important for our analysis of the beam steering technique and understanding its limitations.

3.2 Wave Impedance and Basic Relations

The principal effect of an incident plane wave at the dielectric interface is reflection, which is dependent on the dielectric constant of the materials. The wave impedance and the propagation constant of a dielectric material are given by

$$\eta = \sqrt{\mu/\varepsilon} = \sqrt{\mu_o/\varepsilon_o} \cdot \sqrt{1/\varepsilon_r} \qquad \text{.....(3.1a)}$$

$$K = 2\pi/\lambda = 2\pi/\lambda_o \sqrt{1/\varepsilon_r} \qquad \text{.....(3..1b)}$$

where ε_o= permittivity of free space

μ_o= permeability of free space

ε_r = Relative permittivity or dielectric constant

λ_o, λ = Wavelengths in free space and inside the dielectric respectively.

In the above relation we have assumed that the permeability of the dielectric material is the same as that of free space and that the material is isotropic and loss free.

At normal incidence of a plane wave from one medium to another, having characteristic impedances η_1 and η_2 respectively, the reflection co-efficient is given by

$$\rho = \frac{\eta_2 - \eta_1}{\eta_2 + \eta_1} \qquad \text{.....(3.2)}$$

Hence the transmission co-efficient is

$$\tau = 1 + \rho = \frac{2\eta_2}{\eta_2 + \eta_1} \qquad \text{.....} \quad (3.3)$$

The transmission co-efficient is defined as the ratio of the - transmitted to the incident electric field. So, the total transmitted field, if there is any normal component to the surface, will be greater and can be calculated using Maxwell's equations.

From equation(3.2), it can be easily understood that ρ

can be either positive or negative depending on the values of η_1 and η_2. If we assume that $\eta_1 > \eta_2$ then ρ is negative. But for the same pair of dielectric materials, when the wave is incident from the η_2 side, ρ is positive. Although the sign of ρ changes, the magnitude remains the same. Accordingly, the transmission coefficient is different for these two situations, as $\tau > 1$ for $\rho > 0$ and $\tau < 1$ for $\rho < 0$.

For an arbitrary angle of incidence of plane waves on a dielectric interface, there can be two distinctly different polarizations [13].

Case I - Polarization in the plane of incidence

The situation is shown in fig(3.1). This type of wave is termed a TM (Transverse Magnetic) wave as the magnetic field is normal to the plane of incidence. In this situation, the wave impedance

$$Z_z = E_{x+} / H_{y+} = \eta \cos\theta \qquad ....(3.4)$$

and the propagation constants in the Z and X directions are -

$$K_z = K \cos\theta \quad \text{and} \quad K_x = K \sin\theta \qquad ...(3.5)$$

The total field in medium 1 is the sum of the incident and the reflected fields.

$$E_x = \eta H_+ \cos\theta \, e^{-jK_x x} [e^{-jK_z z} + \rho e^{jK_z z}] \qquad ..(3.6a)$$

$$H_y = H_+ e^{-jK_x x} [e^{-jK_z z} - \rho e^{jK_z z}] \qquad .....(3.6b)$$

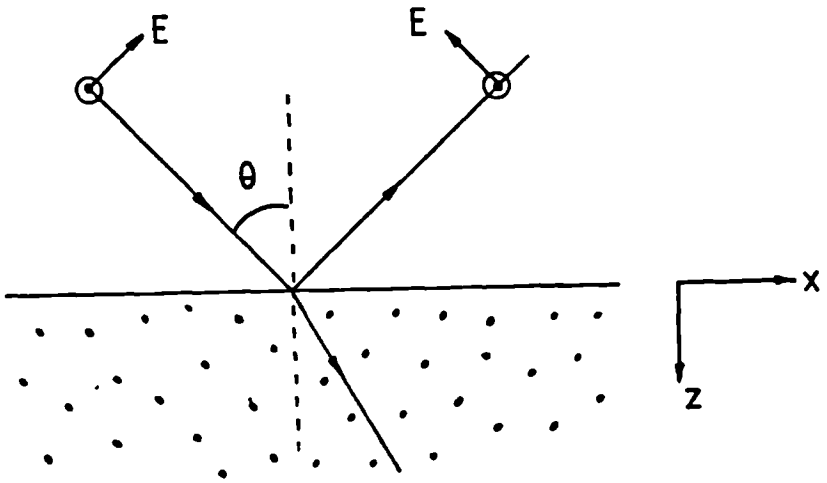

Fig 3.1. Incidence of electrmagnetic waves with the electric field in the plane of incidence.

$$E_z = \eta H_+ \sin\theta\ e^{-jK_x x}[\ e^{-jK_z z} + \rho e^{jK_z z}\ ] \quad ....(3.6c)$$

where ρ is the reflection co-efficient.

Case II - Polarization normal to the plane of incidence

Figure(3.2) illustrates the situation. This type of wave is termed a TE (Transverse Electric) wave as the electric field is normal to the plane of incidence. The wave impedance in the z- direction is

$$Z_z = E_{x+} / H_{y+} = \eta \sec\theta \quad .....(3.7)$$

and the propagation constants :

$$K_z = K\cos\theta \quad \text{and} \quad K_x = K\sin\theta \qquad ...(3.8)$$

The total fields in medium 1 are -

$$E_y = E_+ e^{-jK_x x}\left[e^{-jK_z z} + \rho e^{jK_z z}\right] \qquad ....(3.9a)$$

$$H_x = E_+/\eta \cos\theta\, e^{-jK_x x}\left[e^{-jK_z z} - \rho e^{jK_z z} \right] \qquad ..(3.9b)$$

$$H_z = E_+/\eta \sin\theta\, e^{-jK_x x}\left[e^{-jK_z z} + \rho e^{jK_z z} \right] \qquad ...(3.9c)$$

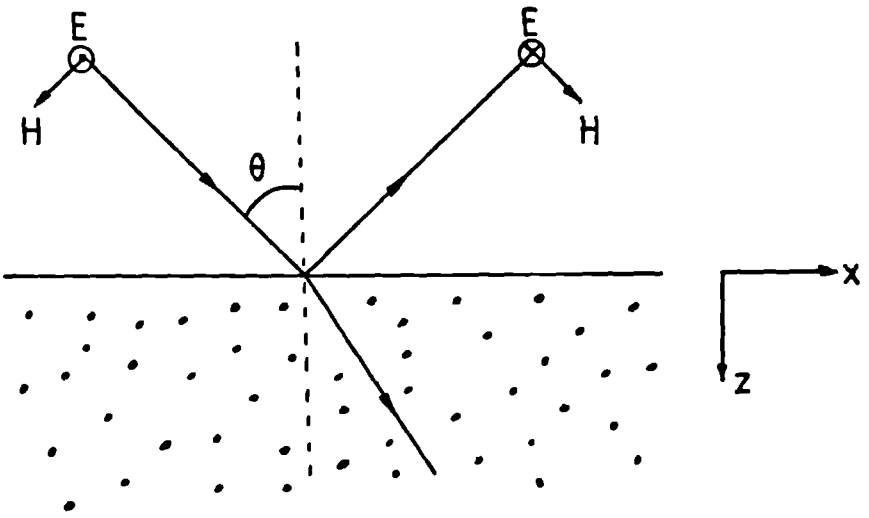

Fig 3.2. Incidence of the electromagnetic waves with the electric field normal to the plane of incidence.

In both situations we can find the propagating field in medium 2 by putting z=0 in all the equations. They then correspond to the amplitude of the waves which propagate within the medium with the new propagation constants.

3.3 Snell's law of refraction

When a plane wave is incident from a dielectric material of dielectric constant ε_1 on a dielectric interface at an angle of i, it is transmitted to the second medium having a dielectric constant of ε_2 ,at an angle of r where

$$\sin(i)/\sin(r) = \sqrt{\varepsilon_2 / \varepsilon_1}$$

This relation is well known in optics as Snell's law. This law holds good at microwave frequencies when we are dealing with a section of plane wave much larger than a wavelength. When the section of the plane wave is small compared to the a wave length, the propagation inside the dielectric can no more be assumed to be a plane wave , as the radiation pattern from a small aperture is quite broad (section 2.3). The transmitted wave is diffracted by the finite aperture producing a scattered pattern of the wave.

Snell's law gives a quick insight to the propagation constant of the waves in a particular direction after they are refracted to the second medium.

3.4 Impedance Matching

The reflection co-efficient can be quite high at a dielectric interface, depending on the angle of incidence and the difference in relative permittivity (dielectric constant) of the materials. To reduce the reflection, one or more intermediate layers of different materials of

definite thickness are introduced in between the materials concerned. This layer or layers of materials act as a matching section and can reduce the reflection considerably.

3.4.1 Quarter wave matching section

The quarter wave matching technique is widely used in microwave transmission line applications and optics. Let us assume that EM wave is incident from a medium of dielectric constant ε_1 to a second medium of dielectric constant ε_2 .The matching layer to be introduced should have a dielectric constant of ε_m, where

$$\varepsilon_m = \sqrt{\varepsilon_1 \cdot \varepsilon_2} \qquad \text{..... (3.10)}$$

The thickness of the layer should be a quarter of a wave length inside the medium.

When we have to deal with oblique incidence, we can still use the relation in eqn(3.10) replacing η by Z (eqn (3.4),(3.7)). Instead of using one layer, a number of layers of matching sections, each of quarter wave thickness, can be used for matching the impedance in a number of steps. Multiple layers are useful when the matching is needed between a very high and very low impedance material. They are also used to provide different types of frequency response. Binomial transformers and Chebyshev transformers [14] use multiple

layers for broadening the bandwidth.

Generally speaking, the bandwidth of a quarter wave matching layer is quite broad, and is given by the relation [15] -

$$\frac{\Delta f}{f_o} = 2 - \frac{4}{\pi} \cos^{-1}\left| \frac{2\rho_m \sqrt{Z_1 Z_2}}{(Z_2 - Z_1)\sqrt{1-\rho_m}} \right| \quad ..(3.11)$$

where Z_1 and Z_2 are the wave impedences for medium 1 and 2 respectively and ρ_m is the maximum tolerable reflection.

Within a given bandwidth, the reflection co-efficient will vary with changes in incidence angle. Fig(3.3) shows the reflection co-efficient for two different dielectrics $\varepsilon_r = 2$ and $\varepsilon_r = 100$ for TE and TM waves without a matching layer. These two values of dielectrics were chosen intentionally to compare the performance of two widely different dielectric material, one on the lower and the other on the higher side. The behaviour of any other dielectric materials can be visualised by comparing the performance of these examples. We can see the strange behaviour of the reflection co-efficients for TM waves which go down to zero and then increase rapidly with increasing incidence angle. This is caused by the total transmission at the Brewster angle [16]. Fig(3.4) shows the reflection co-efficients for the same materials for the TE and TM waves, when a quarter wave matching layer is used to match the normal incidence of the waves. Fig(3.5)

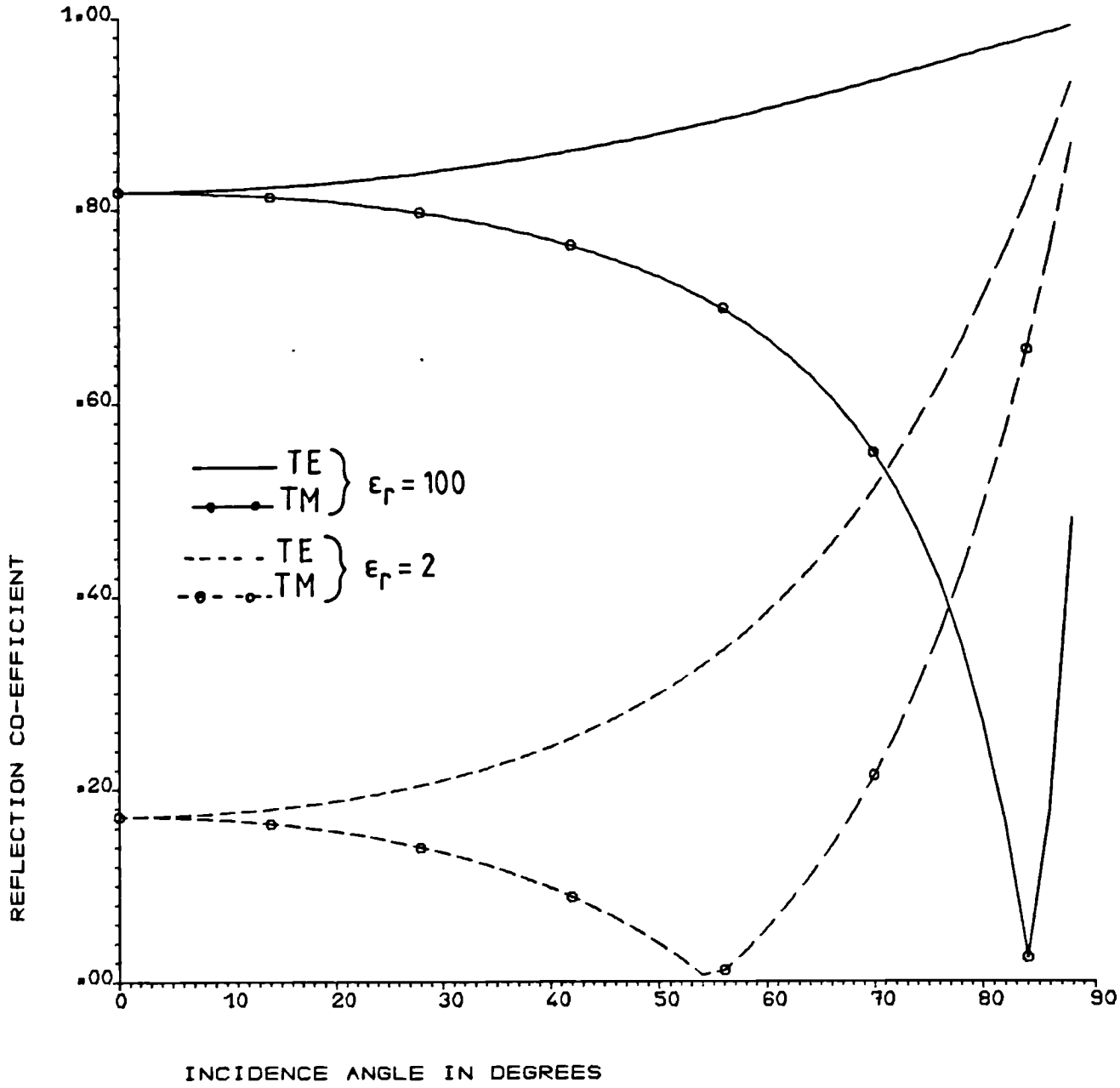

Fig 3.3. Reflection coefficients for two different dielectric materials for TE and TM polarizations for different angles of incidence.

and fig(3.6) show the performance of two different matching layers designed to match for abnormal incidence for TE and TM waves respectively. The incidence angle is chosen to be 30^{o} assuming it to be a reasonably high value for the beam steering angle. In fig(3.5) the reflection coefficient for TE waves goes down to zero at 30^{o} but for the TM waves it increases monotonically. The reverse situation occurs in fig(3.6), as the matching layer is designed for TM waves. However, considering both figures, the difference between the curves for the TE and TM waves are smaller in fig(3.5) which is matched for TE waves.

3.5 Transmission of Electromagnetic Waves

The transmission co-efficient is defined as the ratio of the electric fields of the transmitted wave to the incident wave as described in section(3.2). The effect of the matching layer upon the transmission coefficient must be considered. Using the transmission co-efficient to represent the transmitted field is sometimes misleading as the tangential field may not be the only electric field present. So, the total transmitted field will be considered instead of the transmission coefficient. When the polarization of the electric field is parallel to the plane of incidence, there are two components of the electric field parallel and normal to the surface. So, the resultant field is the sum of these

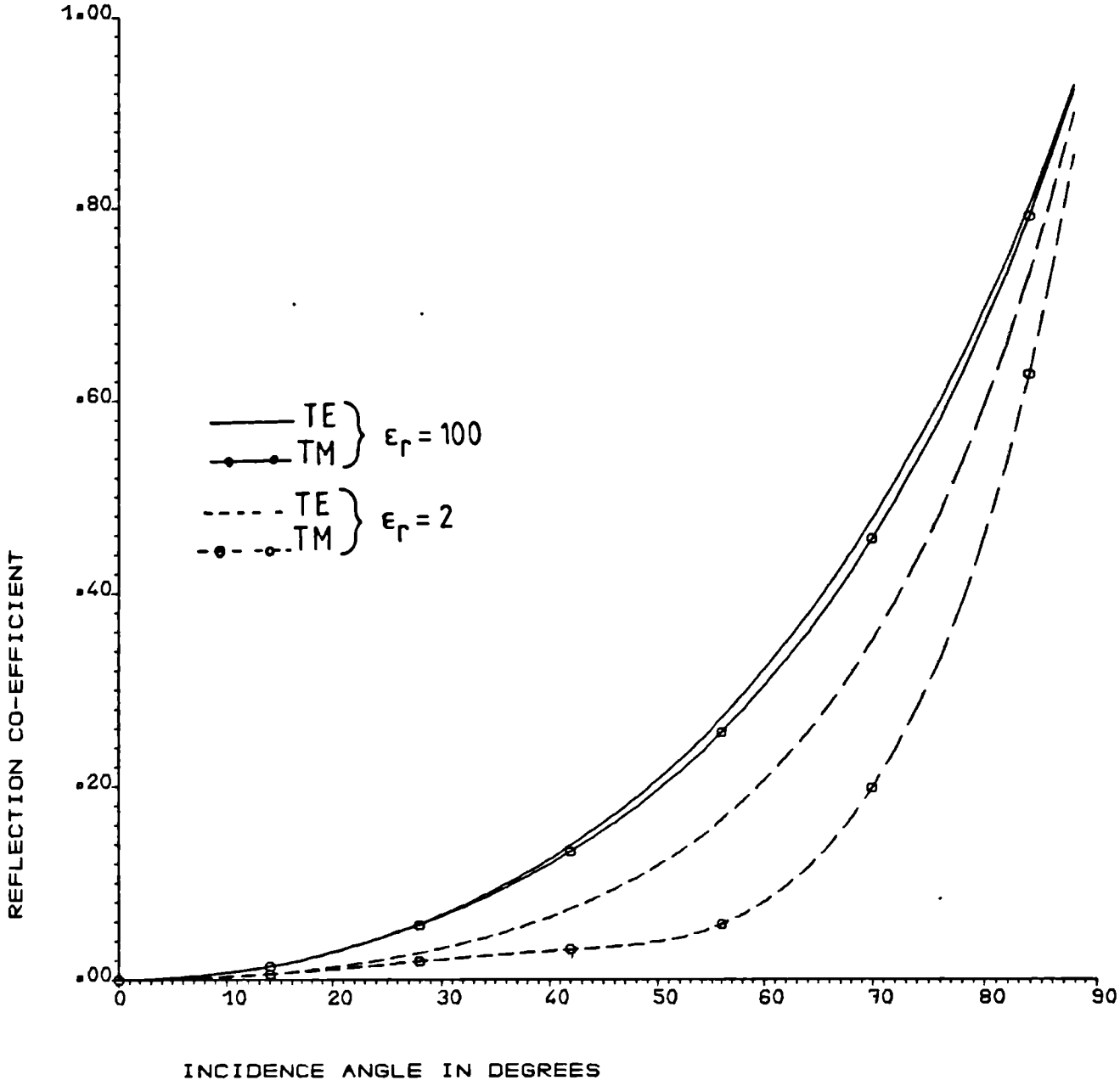

Fig 3.4. Reflection coefficients for two different dielectric materials matched for normal incidence.

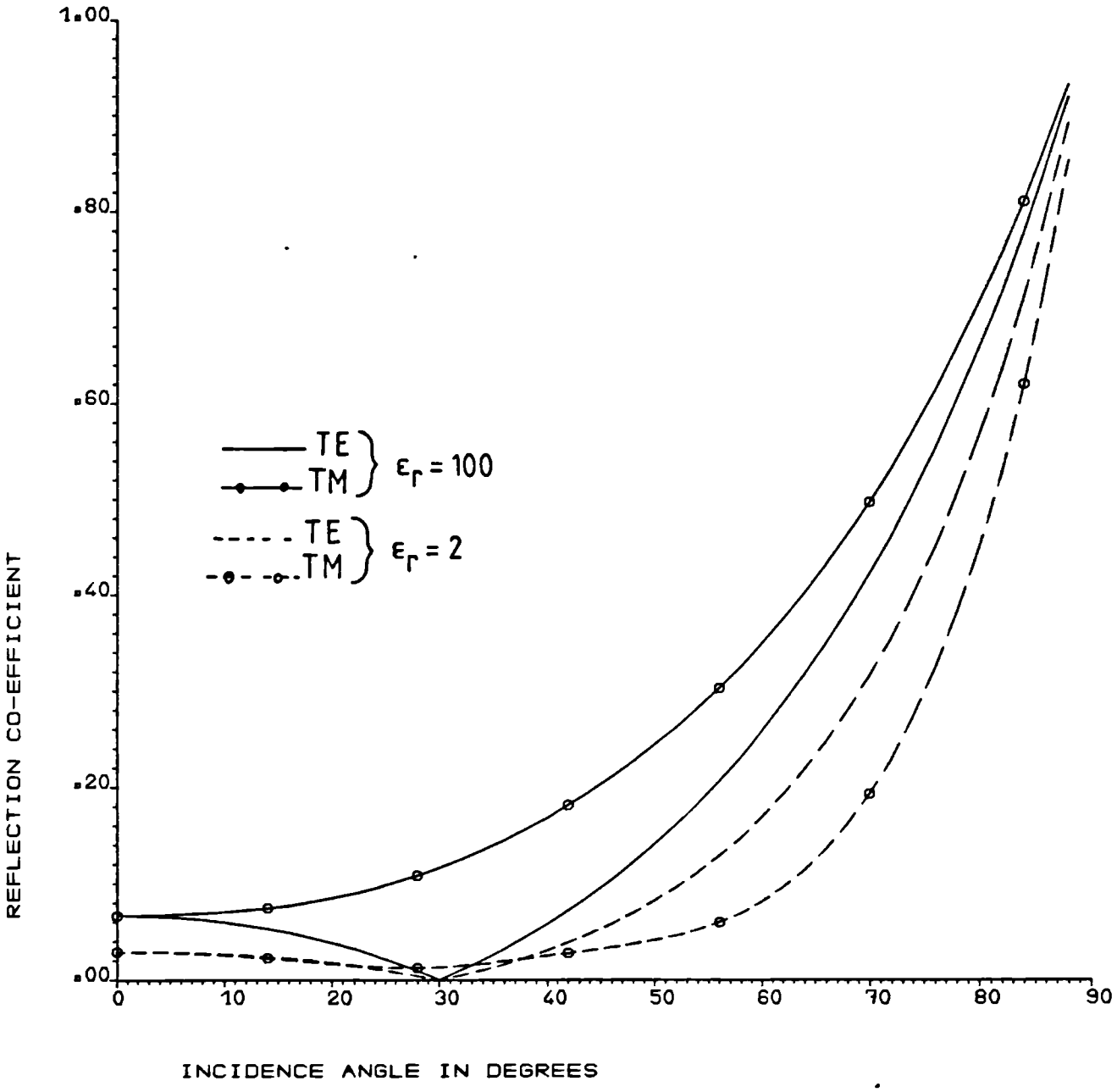

Fig 3.5. Reflection coefficients for two different dielectric materials matched for TE polarization and an incidence angle of 30^{o}.

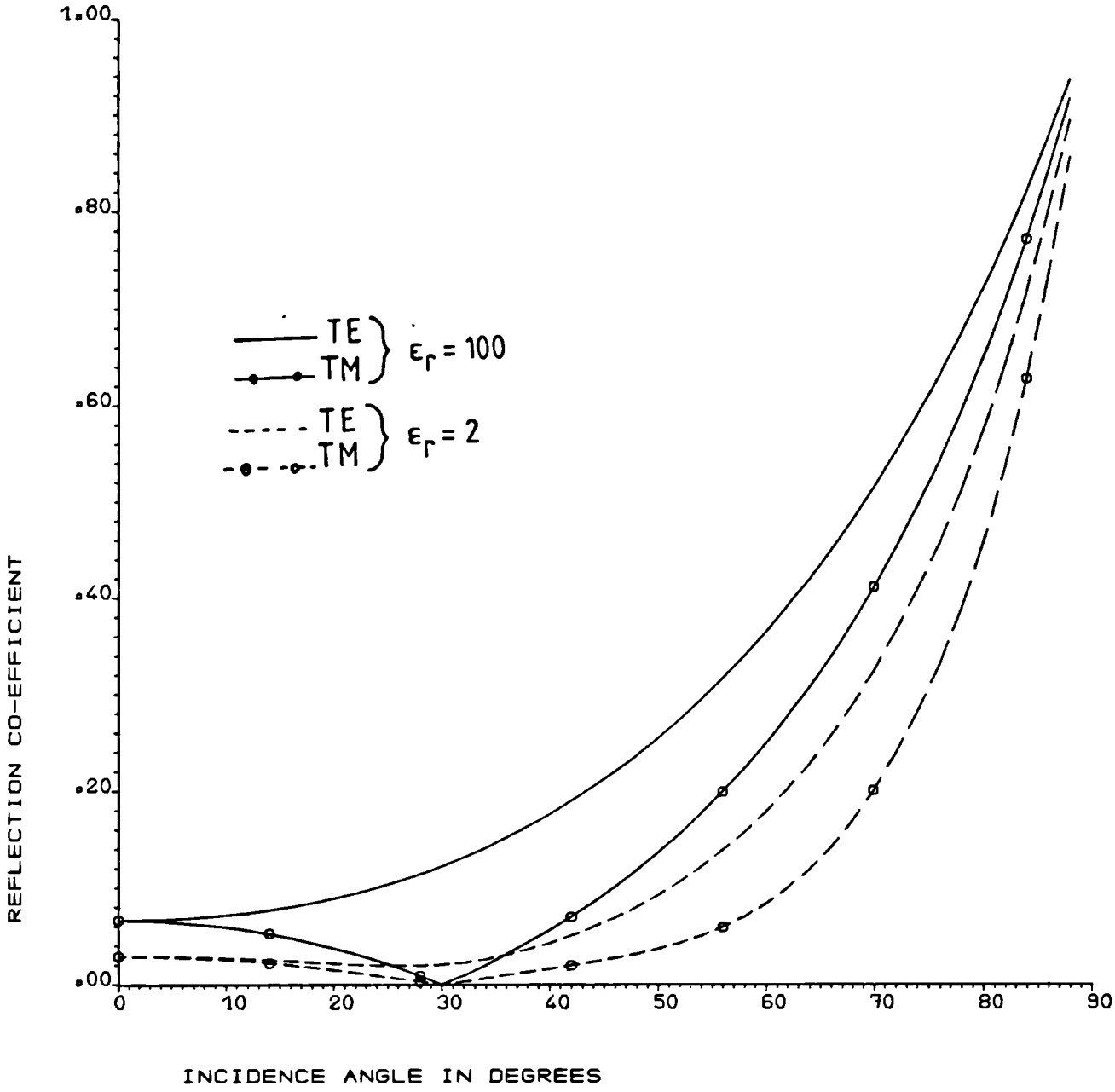

Fig 3.6.Reflection coefficients for two different dielectric materials matched for TM polarization and an incidence angle of 30^{o}.

two fields after the wave is refracted. It is simpler in this situation to evaluate the magnetic field which is parallel to the surface, and find out the total electric field by dividing the magnetic field by the characteristic impedance. When the waves are incident from air to a denser medium, even with the assumption that there is no reflection due to a matching layer, the transmitted field is less than unity. The situation can be explained using conservation of energy.

Let P_o be the incident power from air,

$$P_o = |\bar{E}_o x\ \bar{H}_o|$$
$$= E_o^2/\eta_o$$

When all the power is transmitted in the dielectric , the transmitted power is,

$$P_t = E_t^2/\eta_t = E_t^2\sqrt{\varepsilon_r}/\eta_o = E_o^2/\eta_o$$
$$E_t = E_o\ (\varepsilon_r)^{-1/4}$$

Fig(3.7) shows the transmitted field for TE and TM waves entering a medium from air when perfectly matched for normal incidence.

The reverse situation occurs on emergence from the dielectric to air and the transmitted field is greater than unity. With a change in incidence angle, the reflection increases, but the transmitted field still

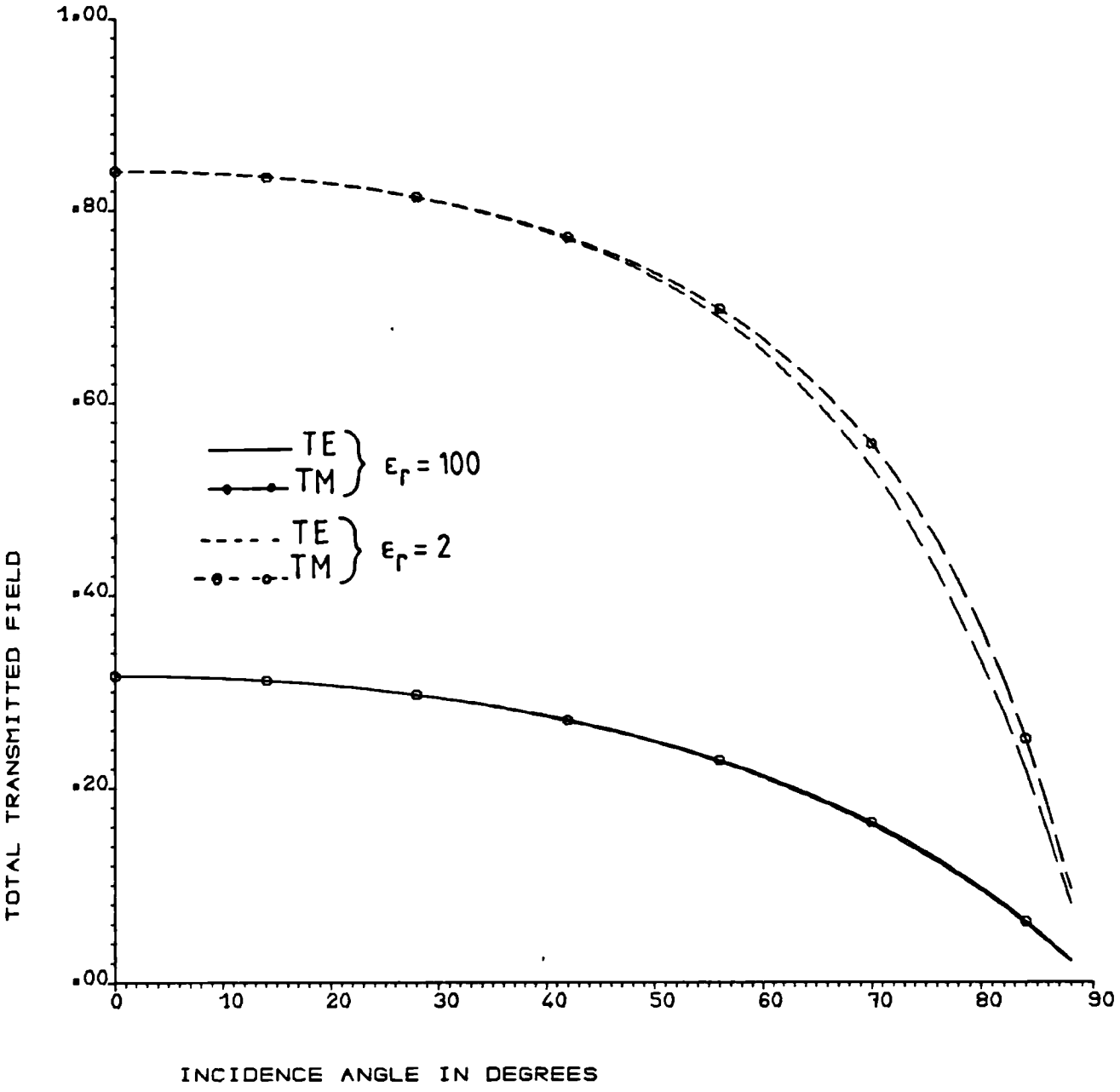

Fig 3.7. Normalised transmitted fields from air to two different dielectrics, matched for normal normal incidence.

increases. This is evident in fig(3.8). This is due to the reduction in projected area of the emergence wave due to inclination to the surface. So, the amplitude goes up considerably to transmit the right amount of power. Even at grazing angles close to 90^{o}, the transmitted field is quite high, but the actual power transmitted is very small due to the internal reflection.

Fig(3.4), (3.5) and (3.6) show that the effect of the Brewster angle is absent when there is a matching layer present. This is due to the change in the incidence angle as the wave enters the matching layer, although the Brewster angle is the same for both materials.

3.6. Loss in dielectric medium

Loss inside a dielectric material can occur due to two reasons -

i) finite conductivity of the material

ii) complex permittivity

For a good dielectric material the conductivity is very small and can be neglected. The loss due to the complex permittivity occurs due to the time varying nature of the electromagnetic field, which induces the electrons and ions inside the material to oscillate and lose some of their energy in the process [17]. Ideally, the permittivity of a material is a real quantity.

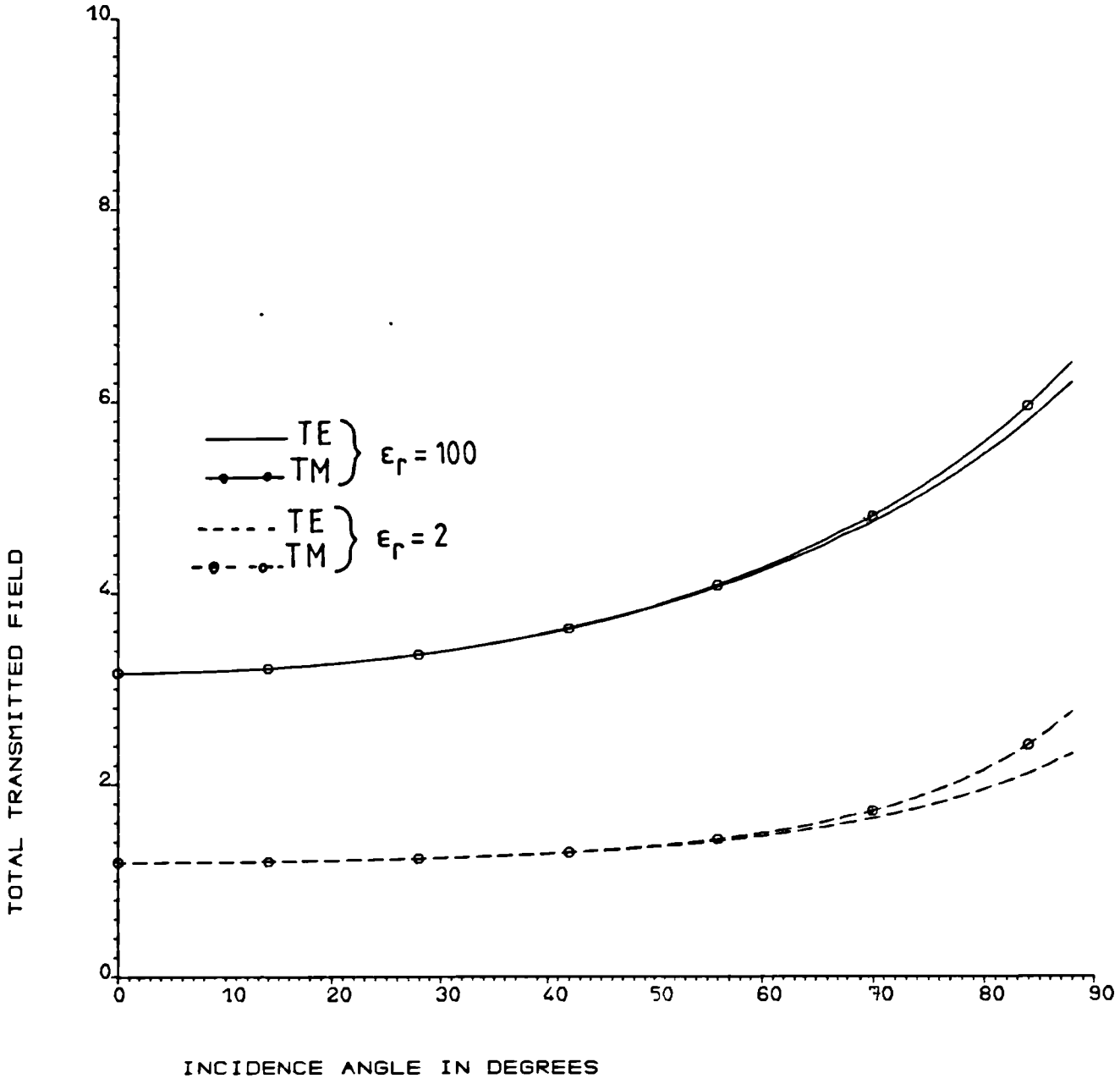

Fig 3.8. Transmitted field from the dielectrics to air normalised to the incident field, matched for normal incidence.

When loss is involved, it is expressed as a complex quantity, with the imaginary part responsible for the loss. If the complex permittivity is expressed as $\varepsilon = \varepsilon' - j\varepsilon''$, then a quantity called loss tangent is expressed as $\tan\delta = \varepsilon''/\varepsilon'$. For an infinite plane wave the propagation constant is given by $K = (\omega^2 \mu \varepsilon)^{1/2}$ for any lossless medium. For a lossy medium K is complex and can be expressed as

$$\begin{aligned} jK &= \alpha_d + j\beta_d \\ &= j\omega\sqrt{\mu\varepsilon'} \cdot [\, 1 - j\varepsilon''/\varepsilon' \,]^{1/2} \\ &= j\omega\sqrt{\mu\varepsilon'} \,(\, 1 - j/2 \;\varepsilon''/\varepsilon' \,) = j\omega\sqrt{\mu\varepsilon'}\,(\, 1 - 1/2 \; j \tan\delta \,) \end{aligned}$$

assuming $\varepsilon'' << \varepsilon'$. We can get a solution for the attenuation

$$\begin{aligned} \alpha_d &= \omega\sqrt{\mu\varepsilon'} \quad .1/2 \tan\delta \\ &= \pi/\lambda \;.\; \tan\delta \end{aligned}$$

This attenuation factor , when expressed in dB is given by the following -

$$\begin{aligned} \text{attenuation in dB} &= 8.686\, \alpha_d \\ &= 8.686\, \pi \sqrt{\varepsilon'} \quad \tan\delta \,/\lambda_o \qquad ...(4.12) \end{aligned}$$

where λ_o = free space wavelength.

CHAPTER 4 : Detailed Analysis of Dielectric Wedges

4.1 Introduction

Snell's law can be used very easily to find out the angle of beam steering by a dielectric wedge. But it does not give any indication of the overall radiation pattern when placed in front of an antenna. We can find out the positions of the sidelobes approximately using Snell's law, but not their power level because the amplitude changes as the electromagnetic waves propagate from one medium to another. A rigorous mathematical analysis has been carried out in this chapter to predict the overall effect of a single wedge upon the radiation pattern. Once we know the performance of a single wedge, we can apply the same formulation for the second wedge to compute the radiation pattern.

The wedges are placed in the near field of the antenna. This ensures that the field incident upon the wedges is almost undistorted, and that there is only negligible spillover loss due to the finite size of the wedges.

The wedges can be configured in two ways (fig 4.1a and 4.1b) for approximately the same steering angle. In fig(4.1a) the parallel face of the first wedge faces the antenna aperture. Hence the reflection from the first surface is incident normal to the antenna aperture and is

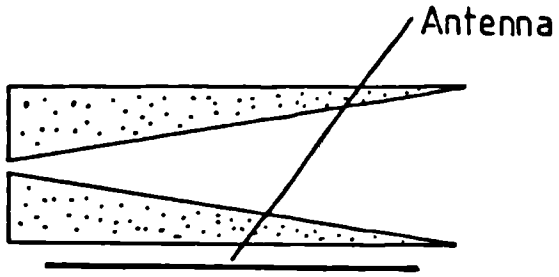

(a)

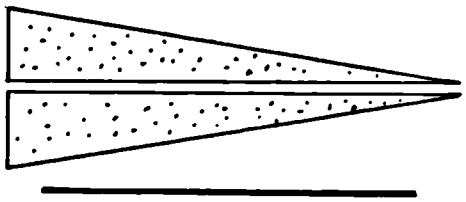

(b)

Fig 4.1. Diagrams showing two different configuarations of the wedges for beam steering.

mainly absorbed in the system. In fig(4.1b), the slanting face of the wedge causes reflections to be incident on the antenna aperture at an abnormal angle and most of the reflected power is scattered rather than being absorbed in the system. So, we have always assumed that the wedge is placed as in fig(4.1a), to reduce the effect of the

reflected waves. A paper [18] has been published on the result of this chapter describing this novel scheme of beam steering with some theoretical and practical results.

4.2 Theoretical Model for the Radiation Pattern

Development of the theoretical model for the radiation pattern uses the concept of angular spectra, as discussed in section(2.3). The effects of the individual angular spectra are considered separately and then summed to obtain the final result. The following assumptions are made for the derivation -

i) The wedge material is isotropic;
ii) Snell's law holds for the dielectric interface;
iii) Dielectric loss is neglected;
iv) The effect of the diffraction at the edges is neglected;
v) Reflected waves are not considered.

Snell's law can be effectively applied when the incident surface is large enough compared to a wavelength, as discussed in section (3.3). Loss in the dielectric material will modify the amplitude pattern over the face of the wedge, and is considered separately in section (6.3). Diffraction from the edges is not important in considering the far field; for the finite size of the

aperture this effect is quite insignificant. The reflection is neglected during the development of the mathematical relations for simplicity. Once the formula is developed, we can easily superimpose the effect of reflection on the overall radiation pattern. The effect of reflection is discussed in section(4.3.3).

A schematic diagram of the wedge and the antenna is shown in fig(4.2).

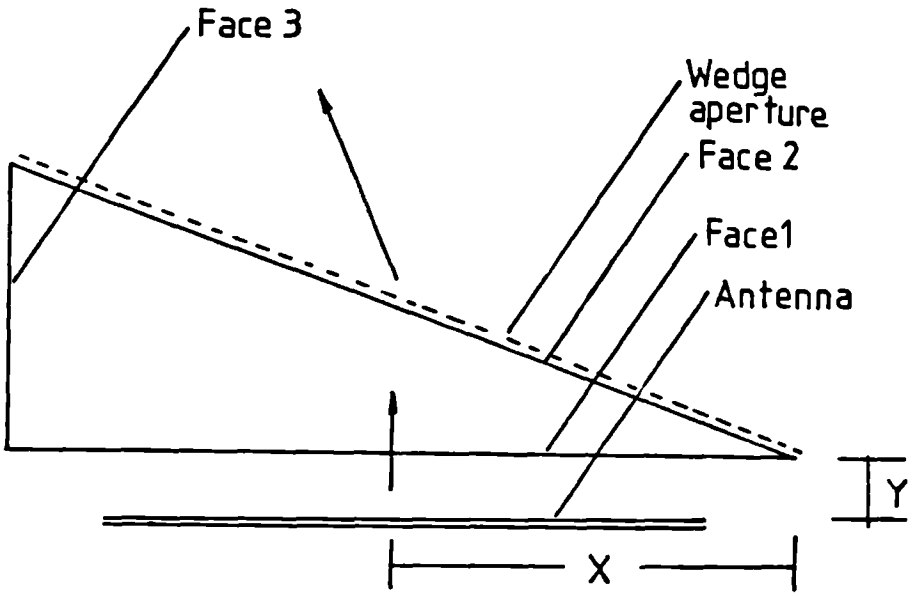

Fig 4.2. Schematic diagram of a wedge placed in front of an antenna.

Let us express the angular spectrum from the wedge aperture by $F_w(\alpha,\beta)$, when the aperture is illuminated by a plane wave of unit amplitude, where

$$\alpha = \sin\theta \cdot \cos\phi \quad \text{and} \quad \beta = \sin\theta \cdot \sin\phi$$

θ and ϕ are measured with respect to the aperture under consideration.

We consider a plane wave incident from the antenna at an arbitrary direction of (θ', Φ'), having an amplitude of $F_a(\alpha', \beta')$. It passes through the wedge and experiences changes both in amplitude and phase. Let the plane wave $F_a(\alpha', \beta')$ suffer phase tilts of e^{-jgx} and e^{-jhy} in the x and y directions respectively and experience an overall change in amplitude by a factor of τ . This plane wave is then radiated from the face of the wedge i.e. the wedge aperture. Hence the angular spectrum for this plane wave $F_a(\alpha', \beta')$ is

$$F(\alpha, \beta) = \frac{\tau}{\lambda^2} \iint_s F_a(\alpha', \beta') \exp(jk \sin\theta(x(\cos\phi - g/k\sin\theta) + y(\sin\phi - h/k\sin\theta)) \, dx \, dy$$

$$= \frac{\tau}{\lambda^2} F_a(\alpha', \beta') \iint_s \exp(jk \sin\theta(x(\cos\phi - g/k\sin\theta) + y(\sin\phi - h/k\sin\theta)) \, dx \, dy \quad \ldots(4.1)$$

Let $\cos\phi - g/k\sin\theta = p \cos\phi''$

$\sin\phi - h/k\sin\theta = p \sin\phi''$

$p \sin\theta = \sin\theta''$

and S = surface defined by the aperture

Substituting these expressions in equation (4.1) -

$$F(\alpha, \beta) = \frac{\tau}{\lambda^2} F_a(\alpha', \beta') \iint_s \exp(jk \cdot p \cdot \sin\theta(x\cos\phi'' + y\sin\phi'')) dx \, dy$$

$$= \frac{\tau}{\lambda^2} F_a(\alpha',\beta') \iint_S \exp(jk\sin\theta''(x\cos\phi'' + y\sin\phi'')) \, dx \, dy$$
$$= \tau/\lambda^2 F_a(\alpha',\beta') \cdot F_w(\alpha'',\beta'') \qquad \ldots\ldots\ldots(4.2)$$

where $\alpha'' = \sin\theta''\cos\phi''$ and $\beta'' = \sin\theta''\cos\phi''$

Equation(4.2) represents the contribution of a plane wave $F_a(\alpha',\beta')$ from the antenna to the overall radiation pattern. Now, if we consider all the plane waves from the antenna, the overall angular spectrum will be -

$$F(\alpha,\beta) = \frac{1}{\lambda^2} \int_{-1}^{+1}\int \tau F_a(\alpha',\beta') F_w(\alpha'',\beta'') \, d\alpha' \, d\beta' \qquad \ldots.(4.3)$$

In equation(4.3) $F_w(\alpha'',\beta'')$ corresponds to the steered pattern of the wedge aperture illuminated by a plane wave. In evaluating $F(\alpha,\beta)$ numerically, we must evaluate F_w over a very wide range of α and β, even in the reactive range of the spectrum as they come out in real angles when the beam is steered.

To make the numerical evaluation of the pattern simpler, the angular spectrum from the antenna F_a can be summed up at the wedge aperture to compute the amplitude distribution. So, the aperture distribution at the emergence face of the wedge is -

$$A_w(x,y) = \int_{-1}^{+1}\int \tau F_a(\alpha',\beta') \exp(jk(\alpha''x + \beta''y) \, d\alpha' \, d\beta' \ldots(4.4a)$$

The Fourier transformation of A_w gives the overall angular

spectrum $F(\alpha, \beta)$ -

$$F(\alpha, \beta) = \frac{1}{\lambda^2} \iint_S A_w(x,y) \exp(jk(\alpha x + \beta y))\, dx\, dy \quad ..(4.4b)$$

Computing the angular spectrum in two steps needs much less computer memory space than using eqn(4.3) directly. When computing the response of a pair of wedges, $F(\alpha, \beta)$ is taken as the incident spectrum for the second wedge in place of F_a in equation(4.3) and the overall pattern can be found out in the similar way as described.

4.3 Experimental Investigation

4.3.1 A Pair of Perspex Wedges

Perspex is a very common plastic-like material. It is inexpensive and can be machined very easily to any particular shape. Measurements on the dielectric constants and loss factor show that it is quite suitable for making wedges for small deflections. The dielectric constant of perspex was measured to be 2.59 and the loss tangent $\tan\delta = 0.0061$ (section 5.3.1). A block of perspex was machined to make a pair of wedges. A single wedge, shown in fig(4.3) is designed to steer the beam by 7.5° from the broadside position. The dimensions make a wedge angle of 11.76°.

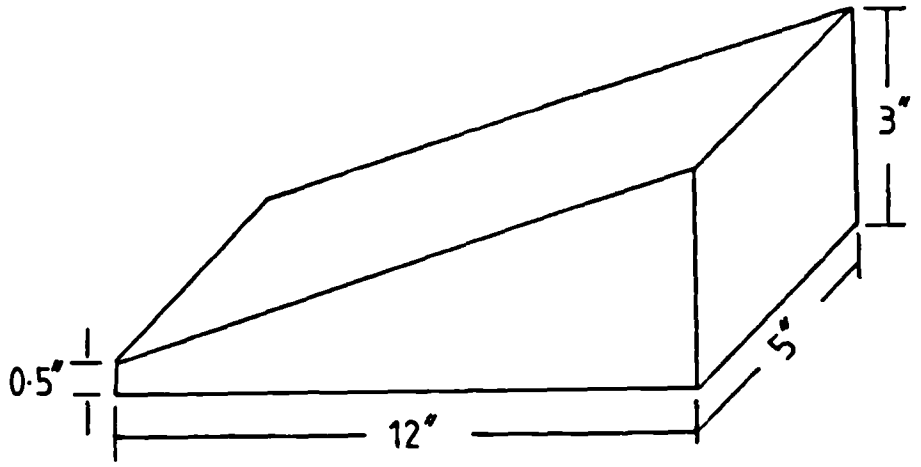

Fig 4.3. Diagram of a rectangular perspex wedge.

4.3.2 An 8-element Array of Printed Antennas

An 8-element printed antenna array was made on RT/DUROID 5880 [19], which has a substrate dielectric constant of 2.2 and a thickness of 0.031 inch. Fig(4.4) shows the array. The elements are fed by a corporate feed network, to provide uniform excitation of the elements. The elements are designed for a centre frequency of 12.0GHz. Design procedures are very well described by James and Hall [20]. The element radiation pattern in the H-plane is shown in fig(4.5). The overall radiation pattern of the array in the H-plane is shown in fig(4.6). Fig(4.7) shows the return loss of the array as a function of frequency. We can see that the antenna is not well matched and has a minimum return loss of -12.0dB.

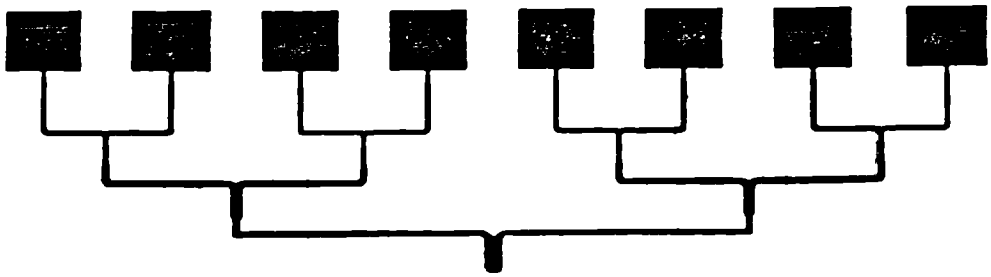

Fig 4.4. An 8-element printed antenna array.

The characteristic impedance of the transmission line on the microstrip is very sensitive to its thickness. So, any small error during fabrication or design can cause mismatch in the system. The impedance of the radiating patches are also sensitive to their dimensions.

4.3.3. Measured Pattern: Effect of Reflection

The radiation pattern of the array was measured in an anechoic chamber by placing a horn in the far field. The length of the 8-element array was 12.8cm which corresponds to a far field distance of 1.3m. The experimental setup for the pattern measurements is shown in fig(4.8). The array was placed on a wooden frame placed on a turntable. One of the perspex wedges was placed in front of the antenna and the radiation pattern was measured. It was found that the radiation pattern changed with the change in position of the wedge. The position co-ordinates x and

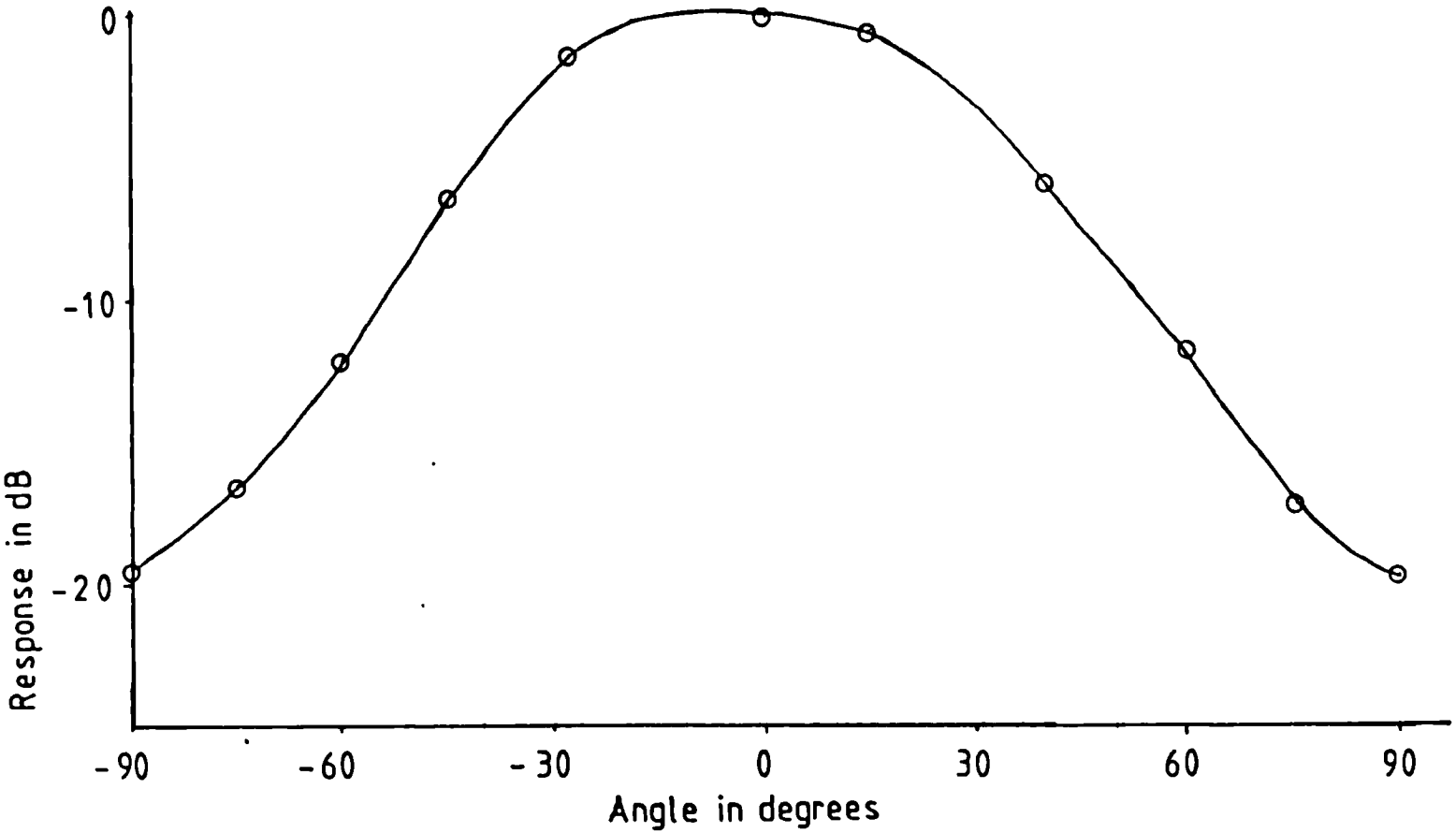

Fig 4.5. Element pattern of the printed antenna.

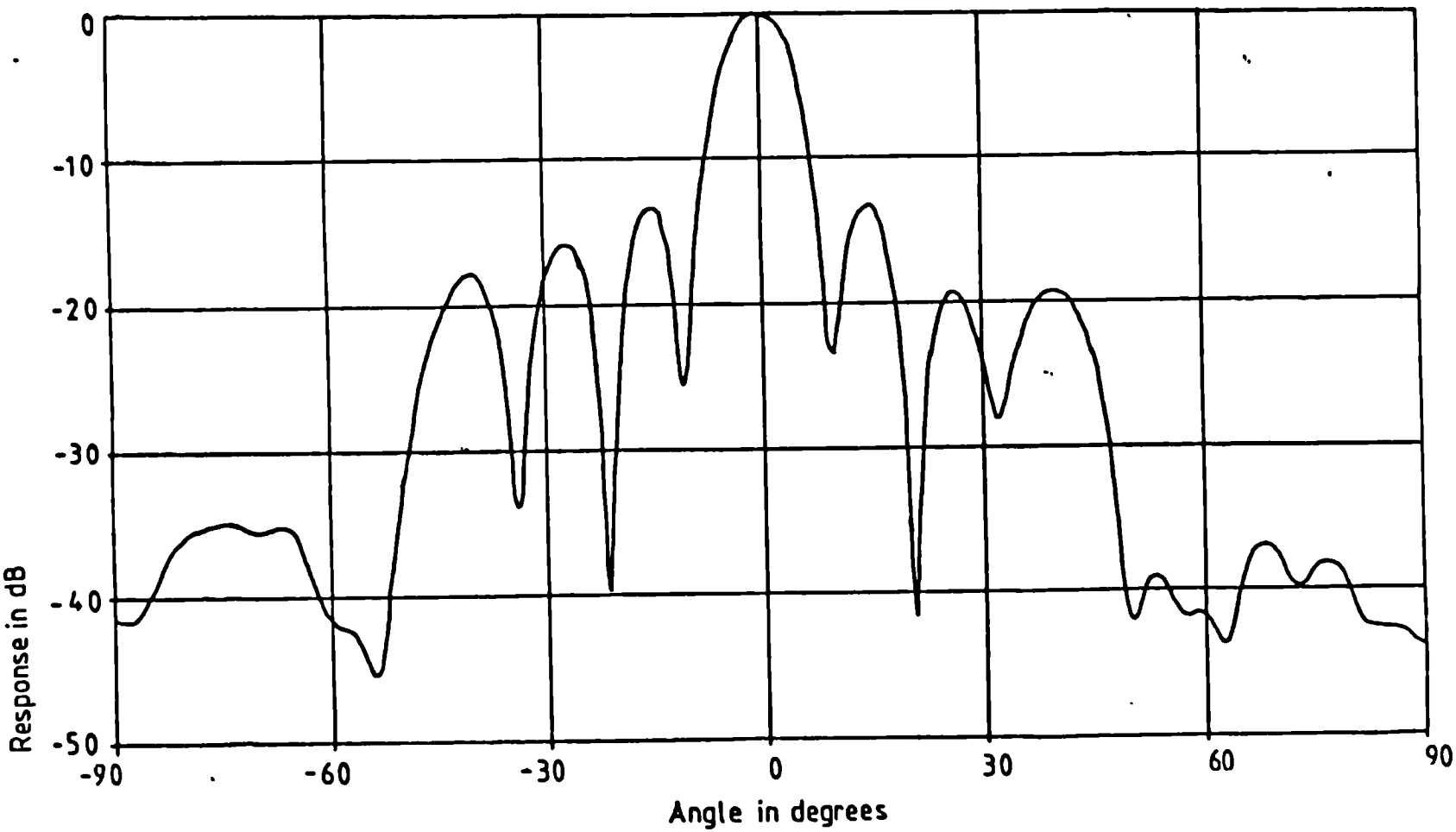

Fig 4.6. Radiation pattern of the 8-element array.

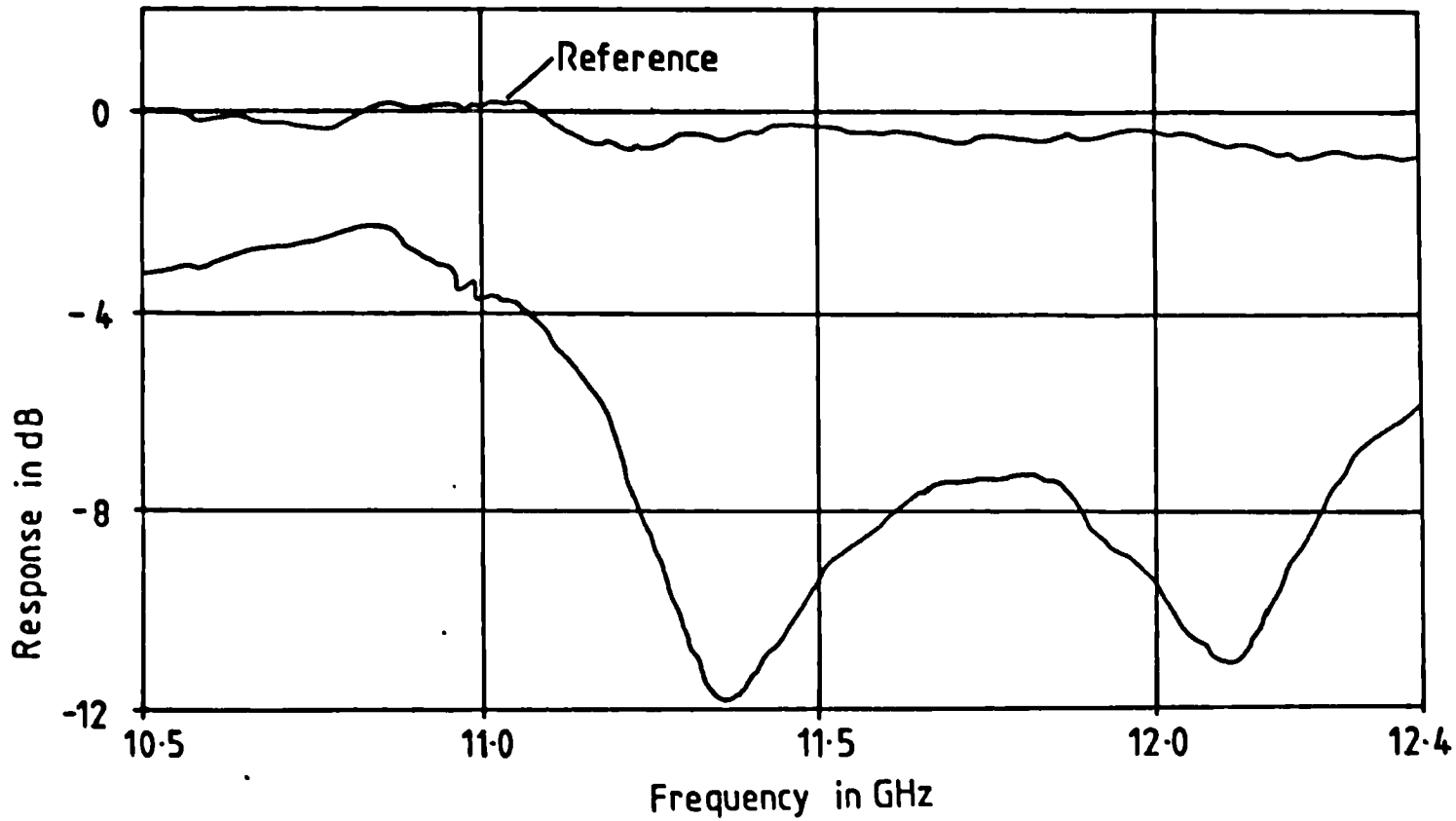

Fig 4.7. Frequency response of the 8-element array.

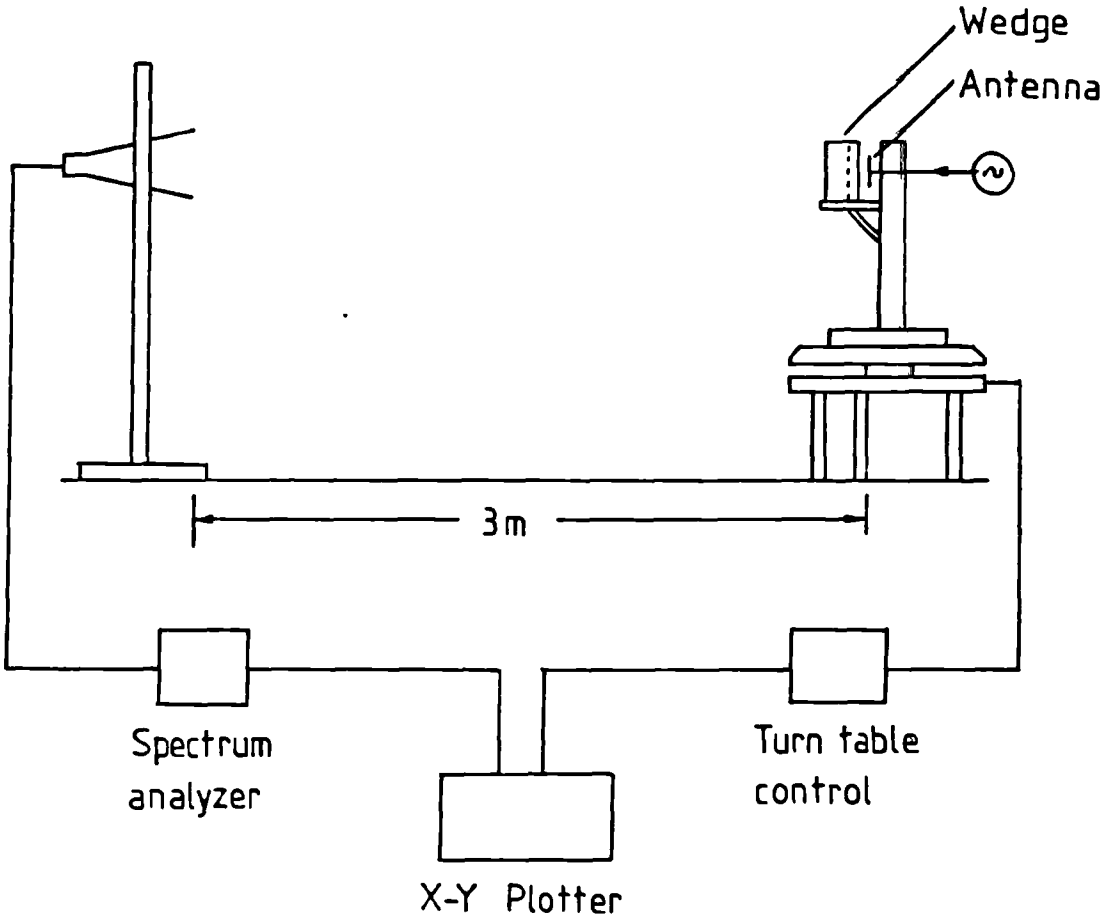

Fig 4.8. Setup for the radiation pattern measurement.

y of the wedge with respect to the antenna are defined in fig(4.2). The variation of the radiation pattern with the variation of x and y is shown in the fig(4.9) and fig(4.10). The first sidelobes change by about 4dB between the highest and the lowest values. As mentioned in section 4.3.1, the dielectric constant of perspex is 2.59,

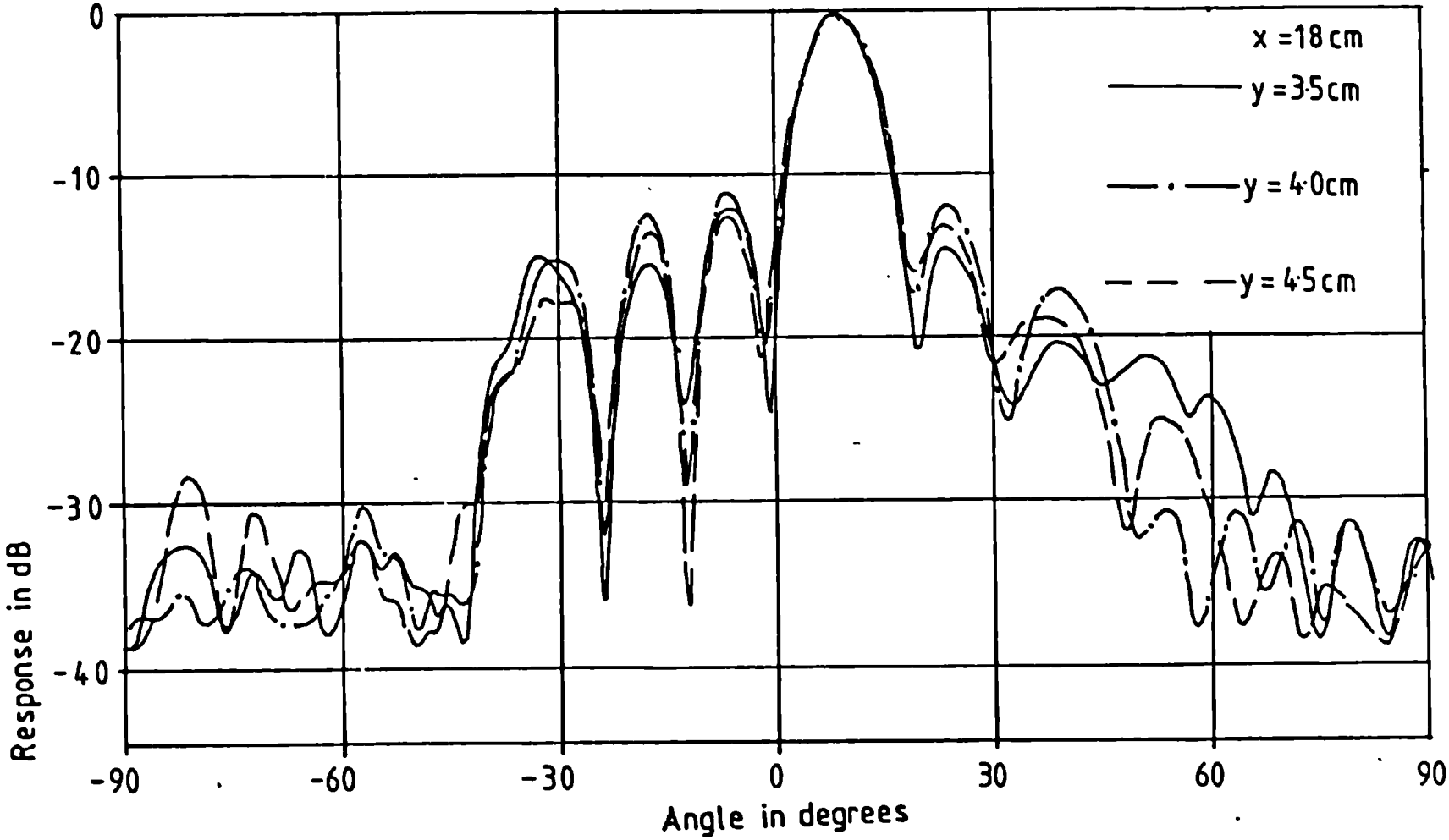

Fig 4.9. Variation of the radiation pattern due to change in position x,y of the wedge.

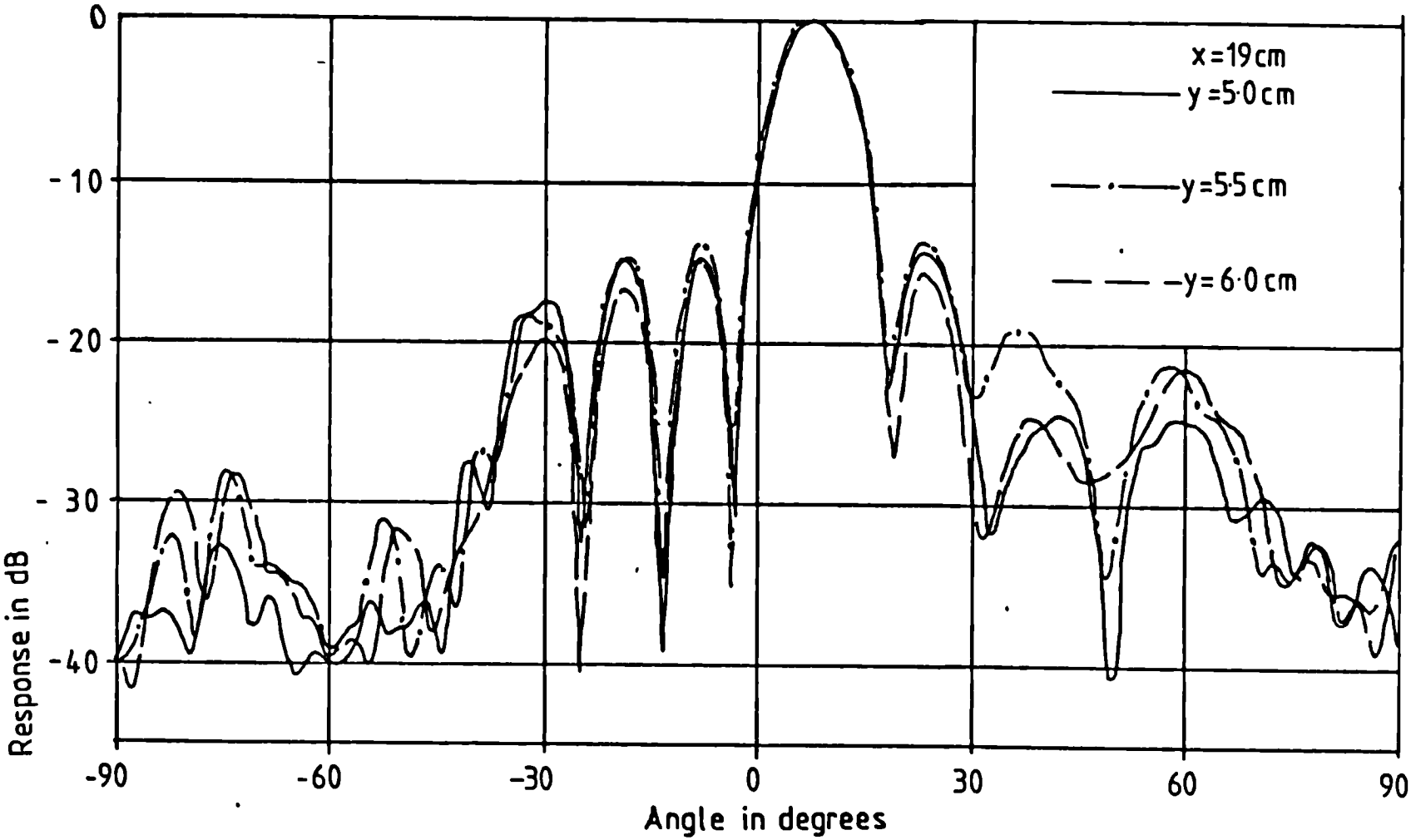

Fig 4.10. Variation of the radiation pattern due to change in position x,y of the wedge.

which implies a reflection coefficient of -12.6 dB for normal incidence of the waves. When the dielectric constant of the wedge is very high, the high value of reflection coefficient will result in considerable loss of power. Although a small reflection co-efficient like -12.6dB does not change the transmitted power by an appreciable amount, the reflected power is scattered and reradiated by the antenna and interferes with the original radiation pattern. A wedge has two reflecting surfaces. So, any change in either x or y will change the overall phase of the reflected waves and hence their resultant interference pattern. The effects are clearly shown in fig(4.9) and fig(4.10).

Fig(4.11) shows a diagram of rays incident on the wedge at various angles (at intervals of 20^{o}). The rays show the incidence and the emergence angles. But the rays suffering total internal reflection do not result in any emergence rays. Some of the rays are reflected from the face 3 and contribute to the overall radiation pattern at large angles. Others are reflected from the face 1 and 2 and are incident on the array at different angles. In the case of the 8-element array and the perspex wedge, the main beam is reflected from the face 1 and is incident normally to the array. But the reflection from the second face is incident at an angle of 39^{o}, most of which is scattered. Multiple reflections can be neglected, as two successive

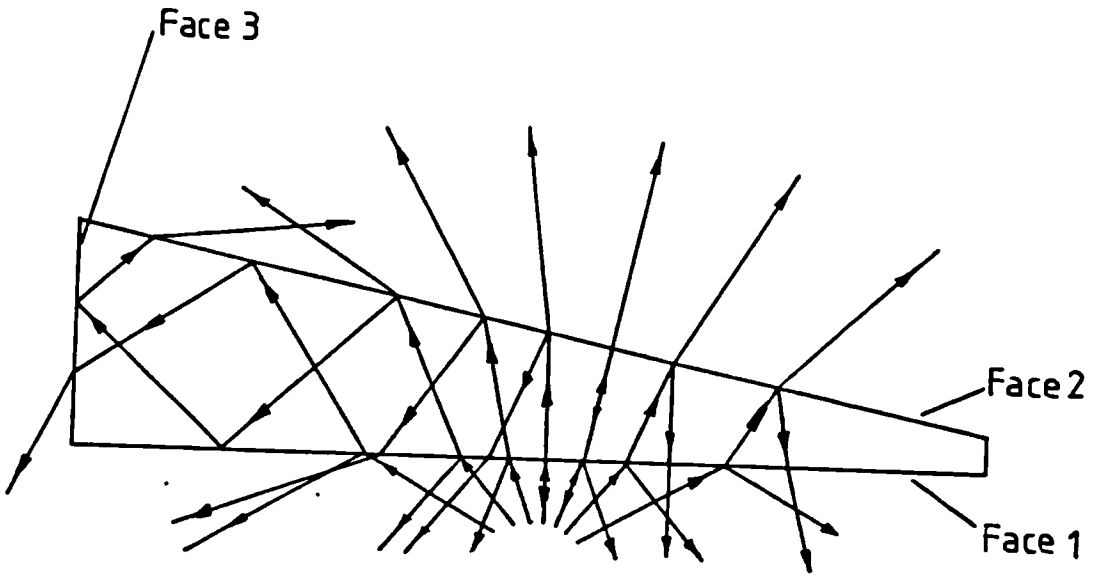

Fig 4.11. A ray diagram showing the reflections from different faces.

reflections reduce the amplitude of the reflected wave by -25dB.

4.3.4 Scattering of The Reflected Waves by The Array

Interference of the reflected waves scattered by the array is seen in fig(4.9) and fig(4.10). It can be seen from the ray diagram in the fig(4.11) that the energy reflected back towards the antenna may not be in the direction of the main beam. As a result, not all the power will appear at the antenna terminal as reflected power; some power will be reradiated from the antenna and hence will affect the overall pattern.

If a plane wave is incident on an array at whatever angle corresponds to the main beam, then all of the antenna elements will be excited with the same amplitude and the correct phase so that the maximum power appears at the antenna terminal. If the antenna is designed for the main beam to appear at the broadside position and there is no amplitude taper, then this will correspond to co-phasal excitation with equal amplitude for all the elements. If we now consider an incident plane wave arriving at an angle other than the direction of the main beam, then the power coupled to the output must be less than that corresponding to the main beam, and hence the remaining power must be reflected. The reflected power coming out of other elements suffers phase changes depending on the length of different sections of the transmission line. In fact there will be a definite set of values for the element excitations under these conditions and we can compute the corresponding radiation pattern for any particular angle of incidence. Details of the analysis are given in appendix II. Figure(4.12) shows the results computed for the 8-element array for radiation incident at 5^{o} to the normal, and figures (4.13) and (4.14) give the results for 40^{o} and 45^{o} respectively. The incident angle of 40^{o} correspond to reflection of the main beam from the second face of the wedge.

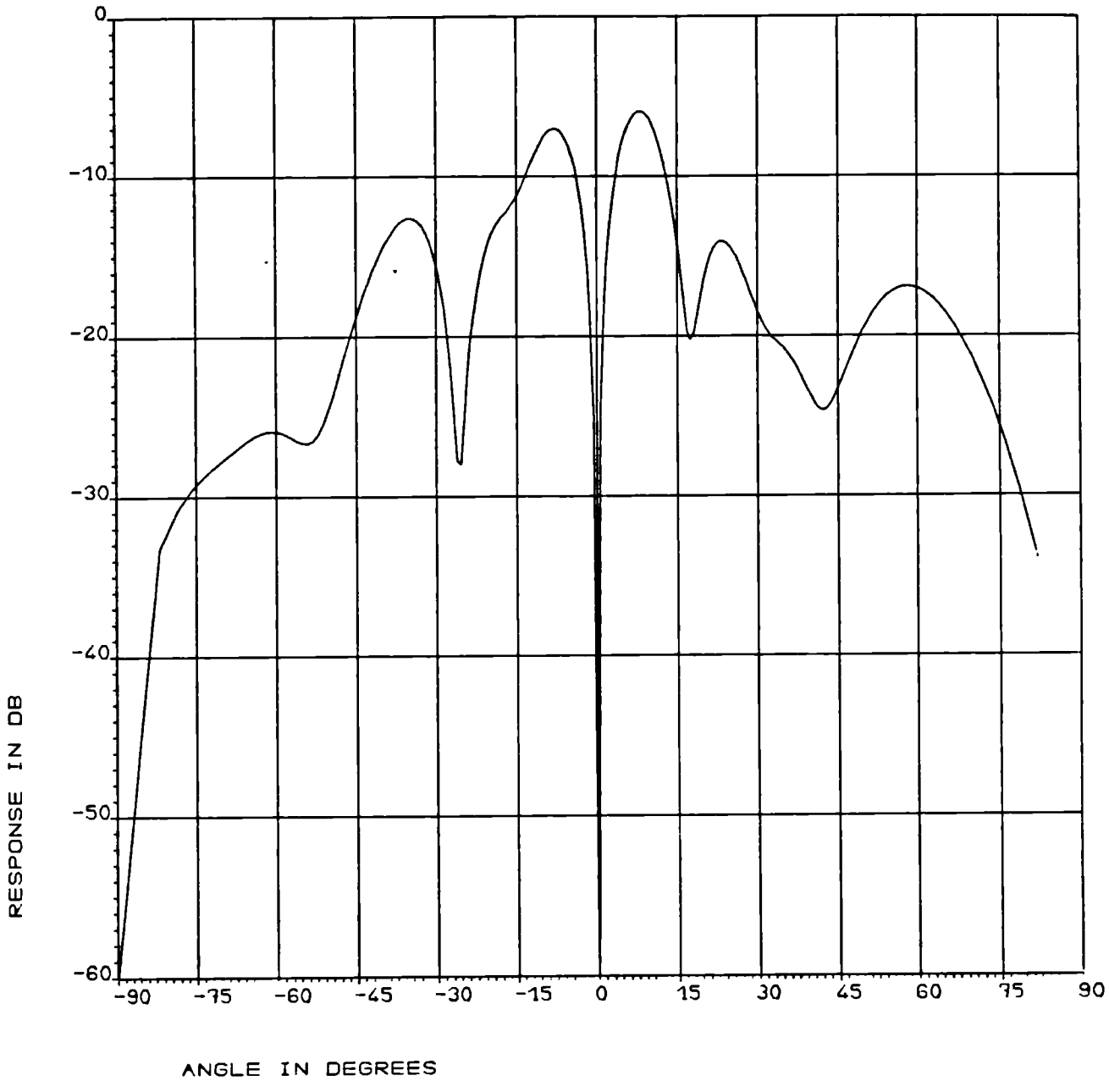

Fig 4.12. Scattered pattern for the 8-element array for a plane wave incident at an angle of 5^{o}.

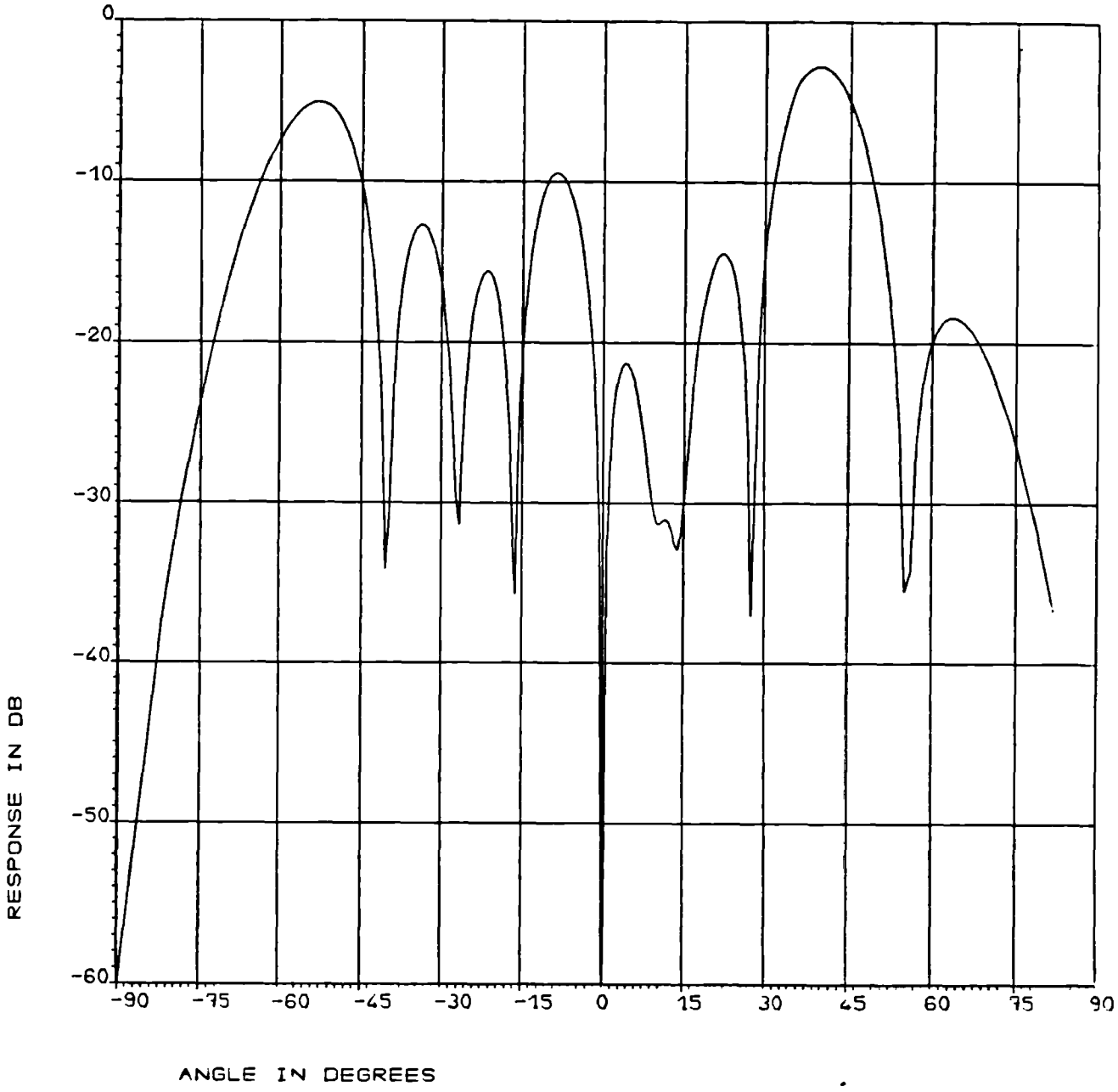

Fig 4.13. Scattered pattern for the 8-element array for a plane wave incident at an angle of 40^{o}.

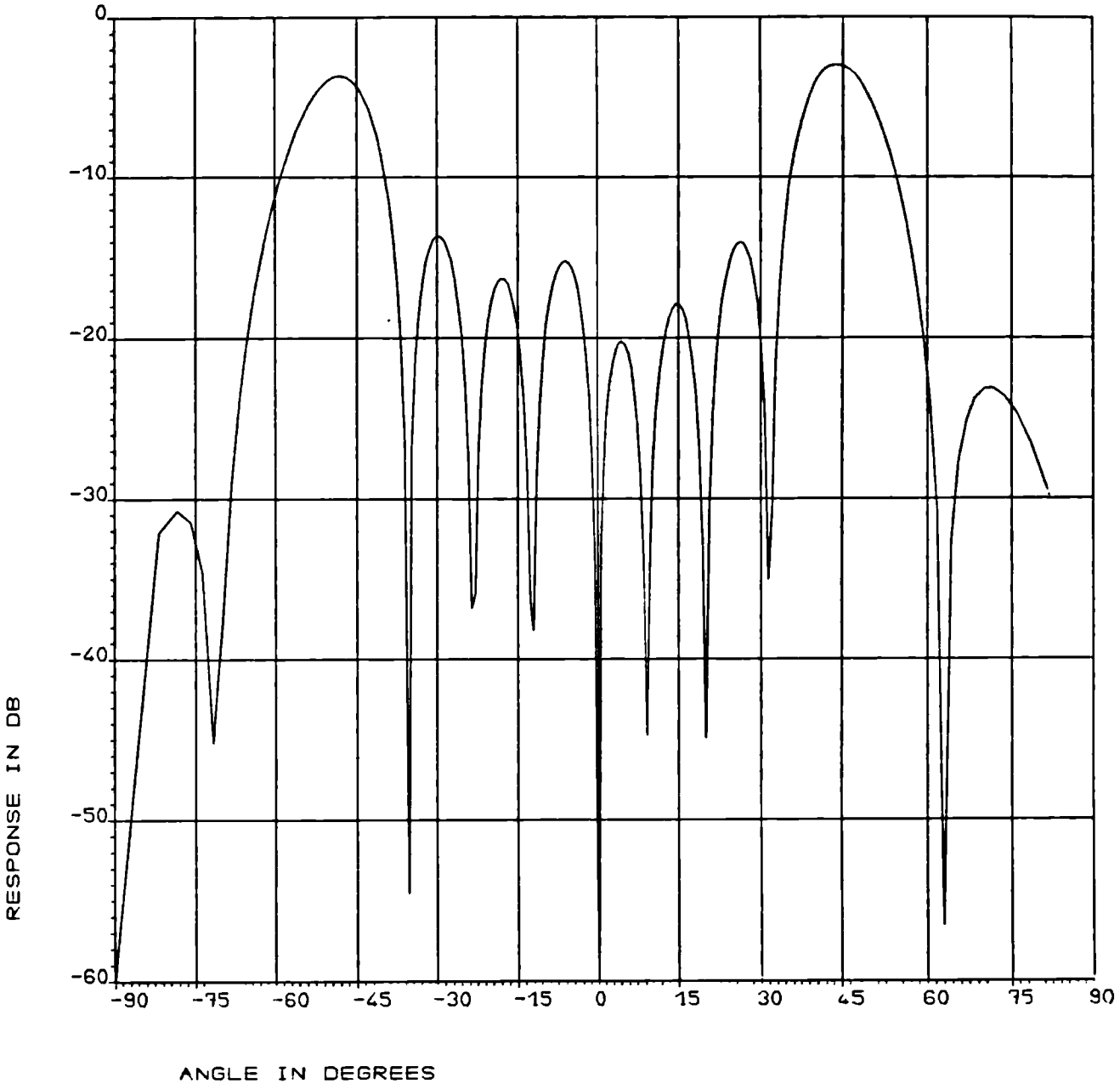

Fig 4.14. Scattered pattern of the 8-element array for a plne wave incident at an angle of 45^{o}.

4.3.5 An Array of a Pair of Horns

As discussed in section 4.3.4, reflected waves from the wedge faces are absorbed by the individual elements of the 8-element array and then they reradiate through the other elements i.e. the power received by one of the elements is transmitted to the other elements as well. To reduce the power coupling between the elements, an array of a pair of horns was fed by a power divider with matched termination. The mode of connection of the power divider to the horns is shown in fig(4.15). The horn dimensions

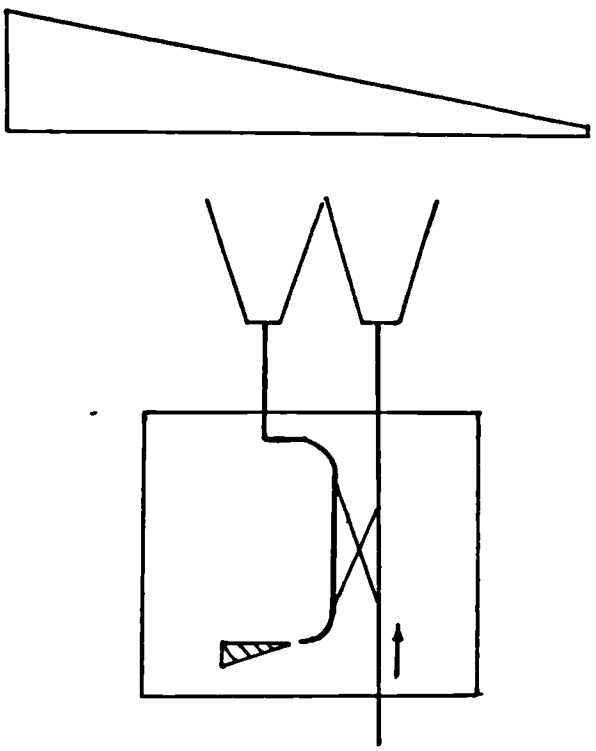

Fig 4.15. Diagram of the power divider connected at the back of the array of horns.

are 7.5cmx4.0cm having flare lengths of 20cm and 22cm in H and E planes respectively. The radiation pattern of a single horn is quite broad as shown in fig(4.16). So, the portion of the power received by individual horns, which do not have correct phase to reach the feed port, is absorbed in the matched load of the power divider. So, the power for reradiation will be considerably reduced. The frequency response of the array with the power divider connected to it is shown in fig(4.17). Fig(4.18) and fig(4.19) shows the computed and the measured radiation patterns of the array respectively at 12.4GHz. There is slight discrepancy in the sidelobes between the computed and the measured pattern. The amplitude distribution is taken to be sinusoidal in the H-plane and uniform in the E-plane. Quadratic phase taper due to the flares are taken into account [21]. But the amplitude distribution may change due to the flares [22] which is not considered during computation. Fig(4.20) and (4.21) shows the measured steered pattern by a single wedge. We can still see the change in sidelobes by a considerable amount (~4dB).

4.3.6 Airgap Matching Layer

It is clear from the discussions in section 4.3.4 and section 4.3.5 that some kind of matching is necessary to improve the performance of the wedges. Matching is possible in a dielectric slab having parallel faces by

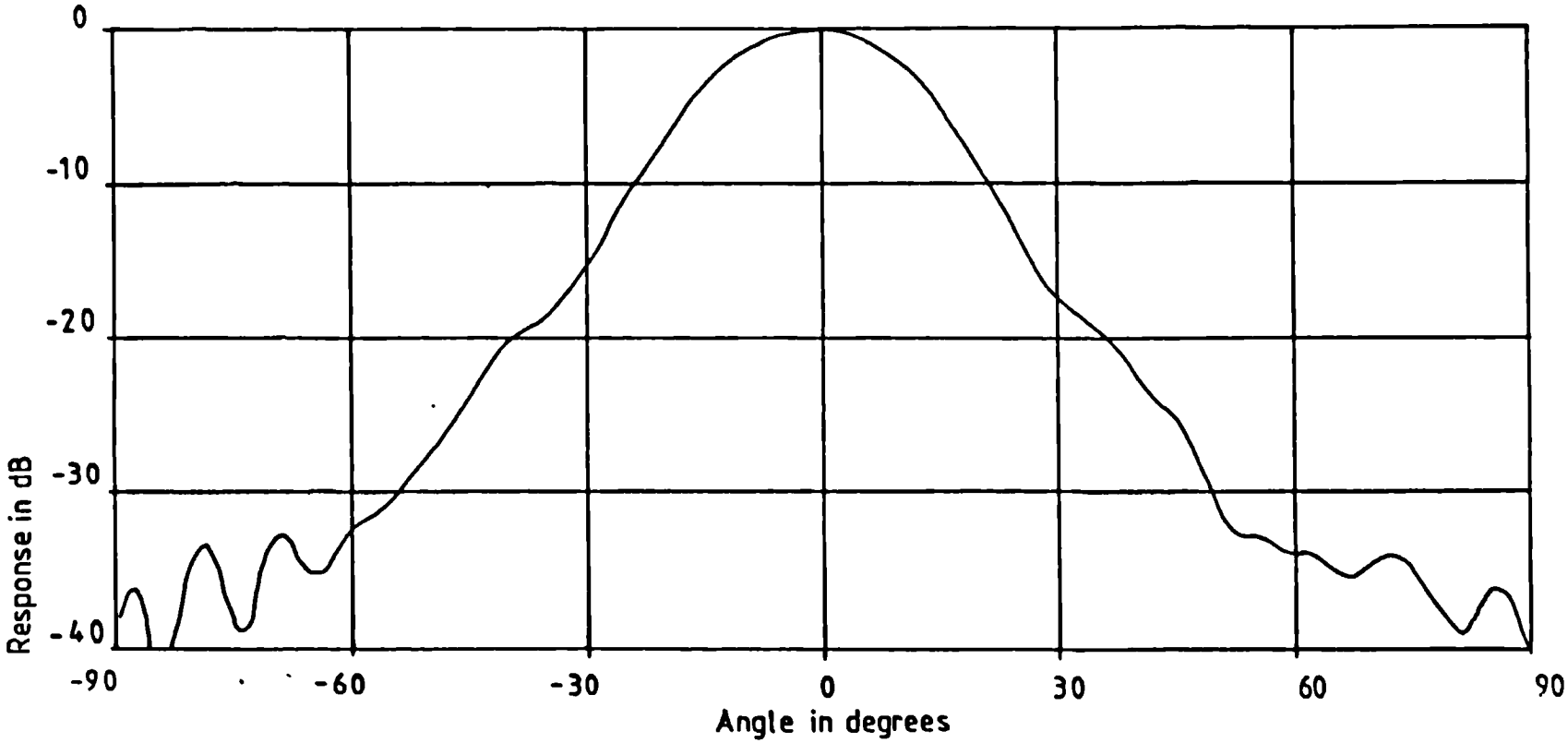

Fig 4.16. Radiation pattern of a single horn. (H-plane)

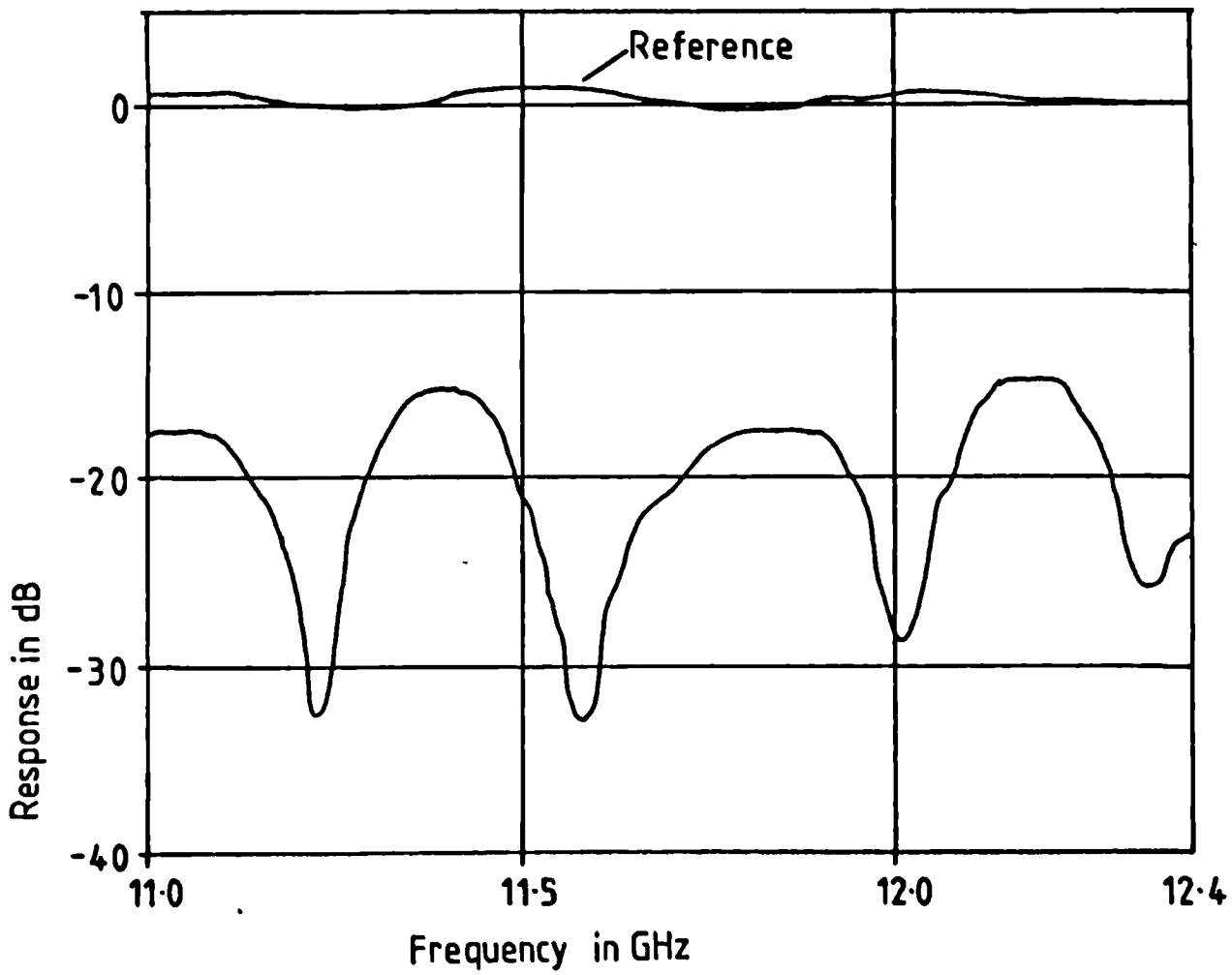

Fig 4.17. Frequency response of the array of horns with power divider.

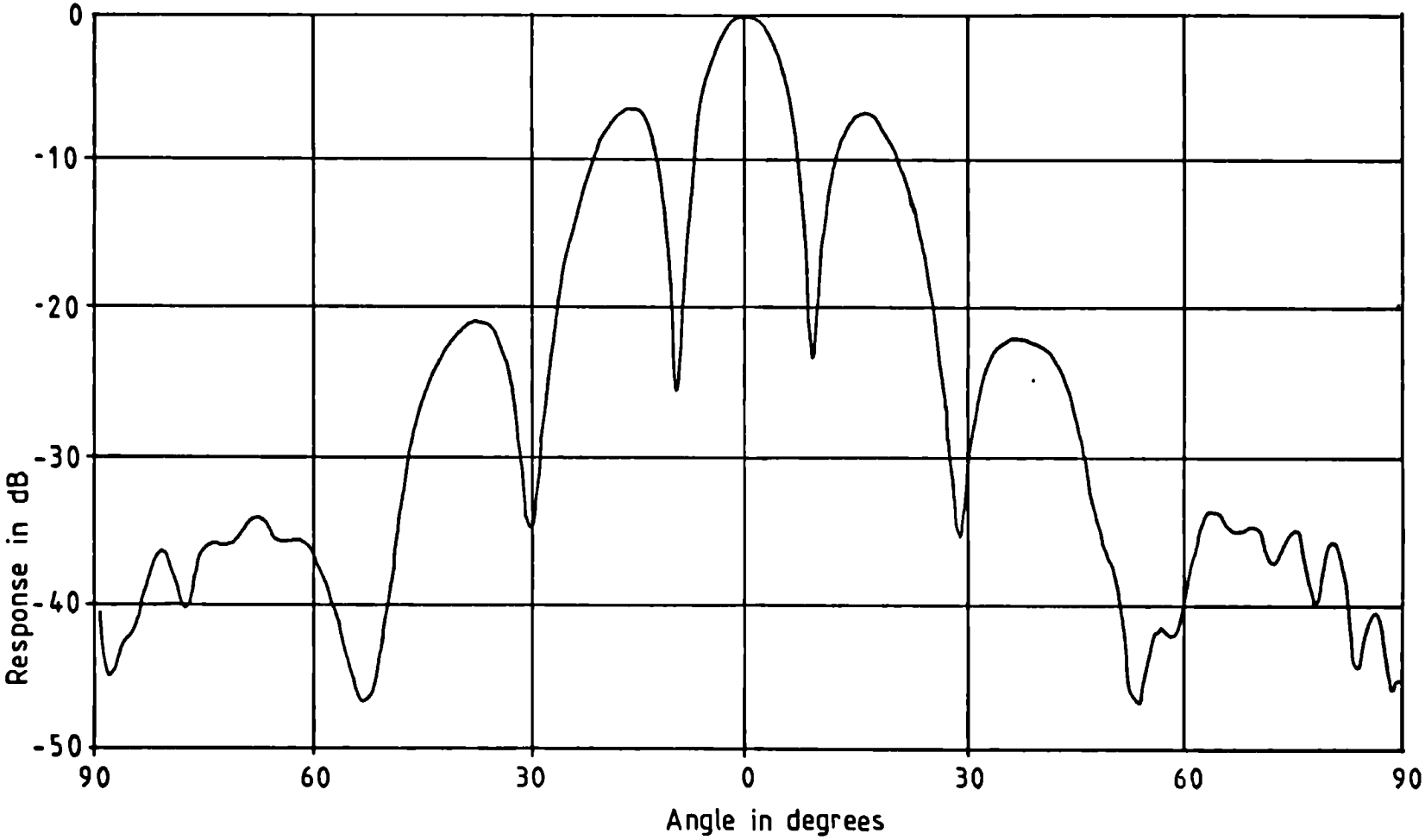

Fig 4.18. Radiation pattern of the array of horns.

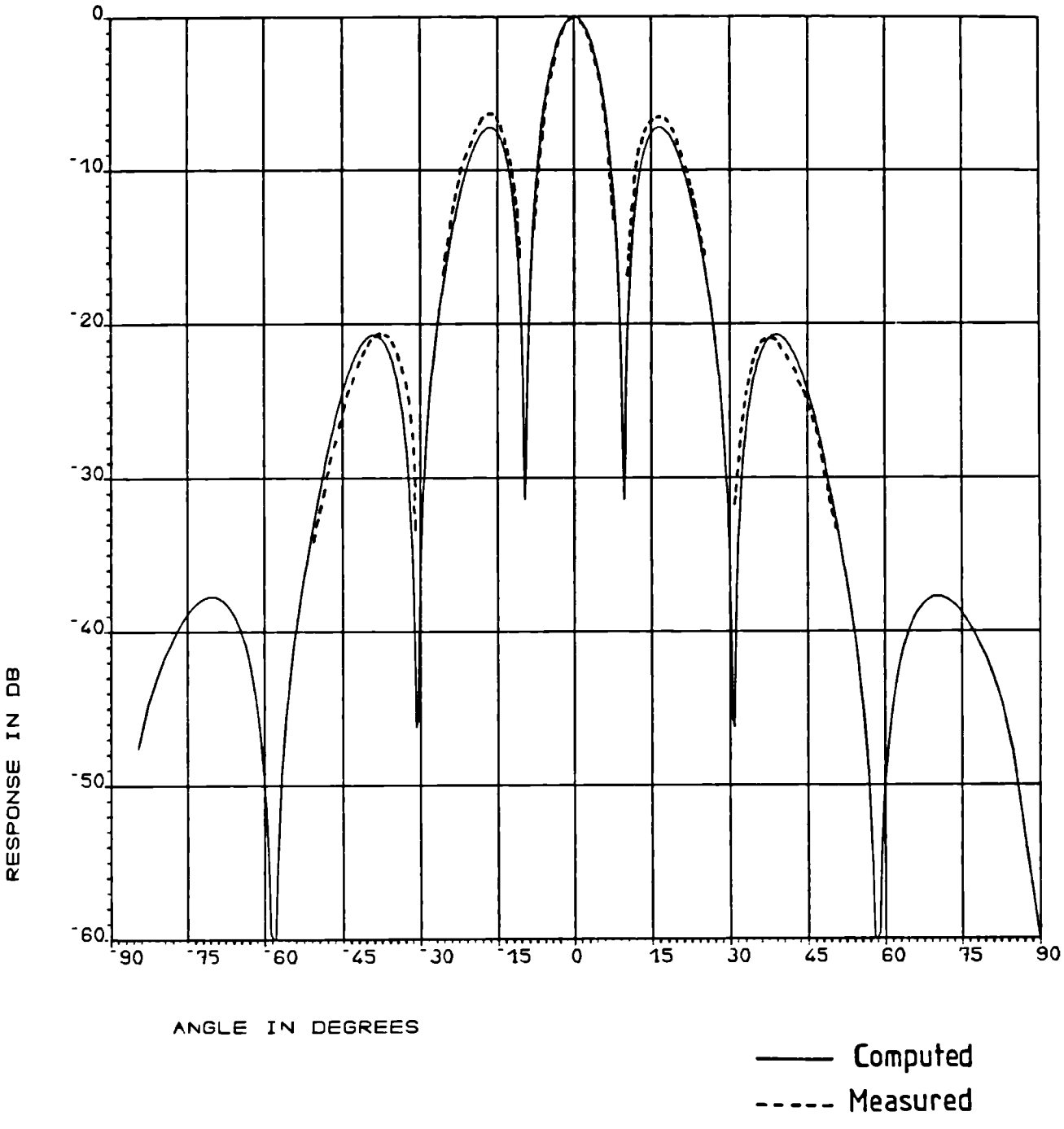

Fig 4.19. Computed pattern for the array of horns.

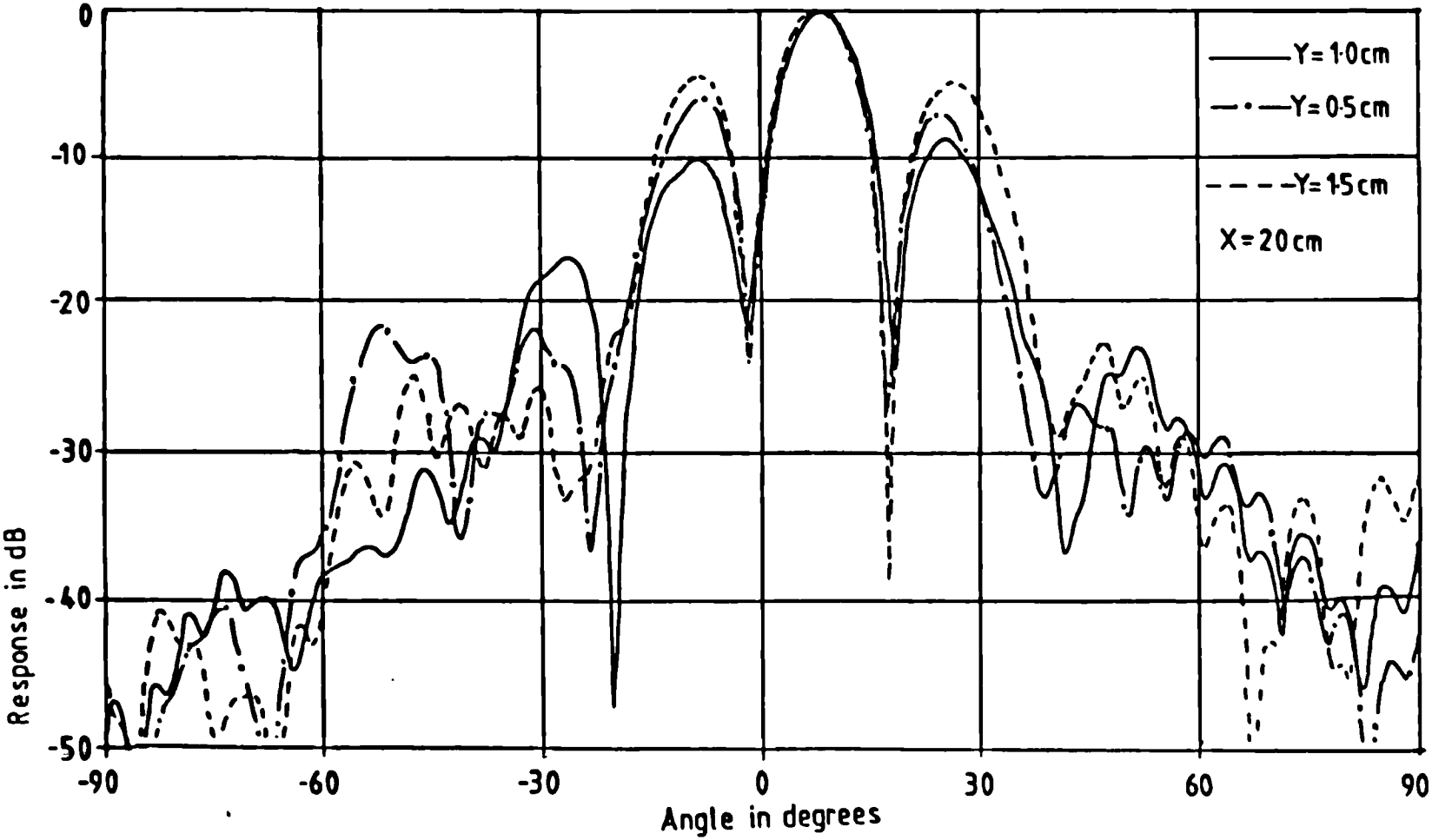

Fig 4.20. Radiation pattern of the array of horns steered by a single wedge for different x and y.

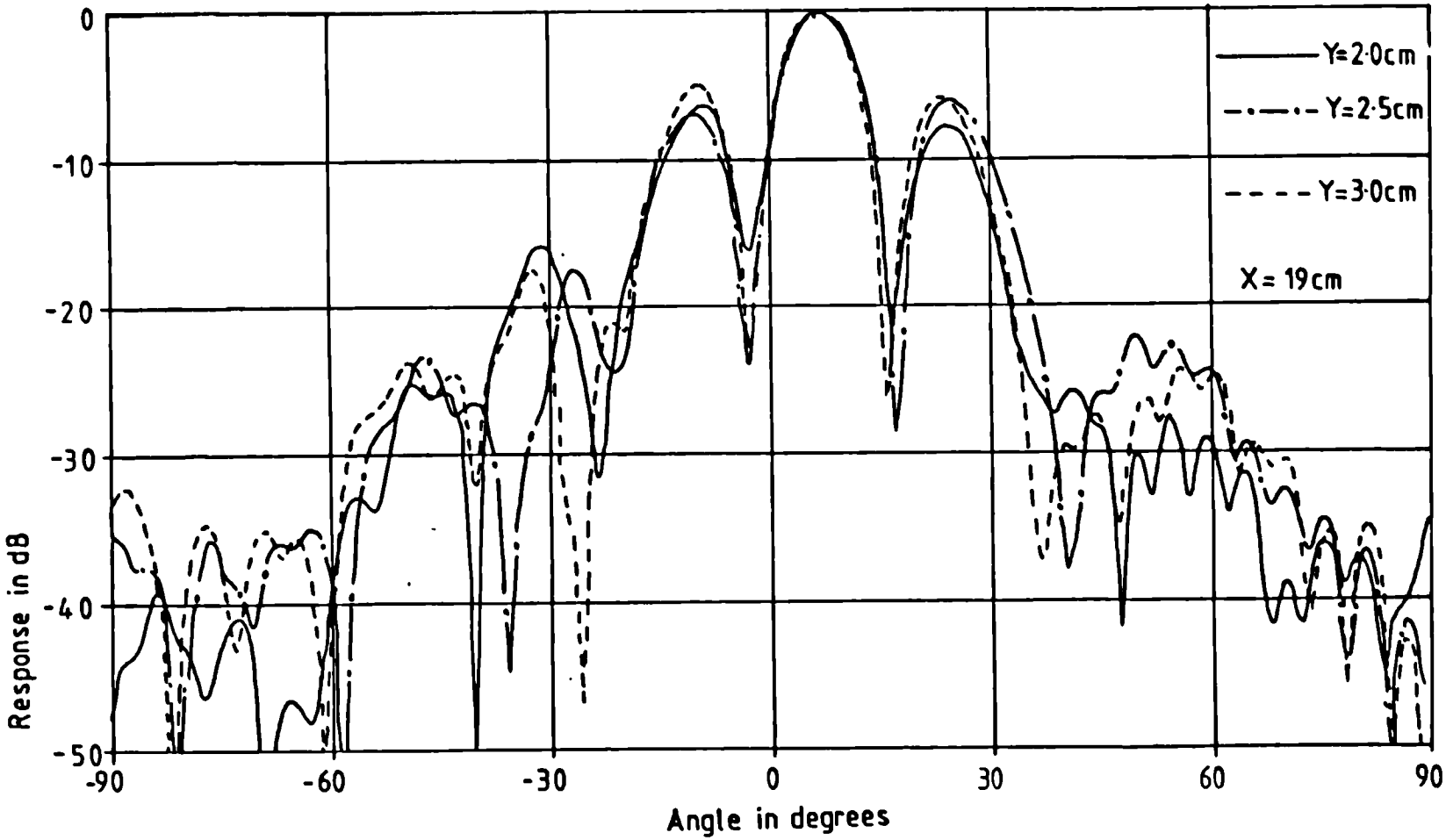

Fig 4.21. Radiation pattern of the array of horns steered by a single wedge for different x and y.

choosing the right thickness of the material. But for a wedge, having faces at an angle to each other, it is not possible. So, some kind of matching layer needs to be introduced on each of the refracting faces of the wedge. The dielectric constant of perspex is 2.59 and a quarter wave matching layer would need a material of dielectric constant $\varepsilon_r = \sqrt{2.59} = 1.61$, which is quite low and not easily available. However, it is possible to match without using a quarter wave matching layer. Different types of matching techniques has been described by Matthaei and others [23]. Hamid and Yunik [24] and Arnold [25] used a single transmission line section to match a complex load. French and Fooks [26] and Day [27] used double section matching instead of a single transmission line segment. However, the technique of Bramham [28] seems to be the most attractive, and can be easily adopted in this case of matching a pair of dielectric materials. Fig(4.22) shows a diagram of the matching sections and its equivalent transmission line analogy. The characteristic impedance of a dielectric medium is proportional to the inverse of the square root of the dielectric constant. Hence we shall take impedance Z of any medium as $\sqrt{1/\varepsilon_r}$.

Let us define the reference plane, as shown in the fig(4.22b), and assume that the impedances looking towards the thin dielectric layer and the air gap are Z_1 and Z_2 repectively. Let the characteristic impedance of air and perspex be Z_o and Z_p and their propagation constants be β_1

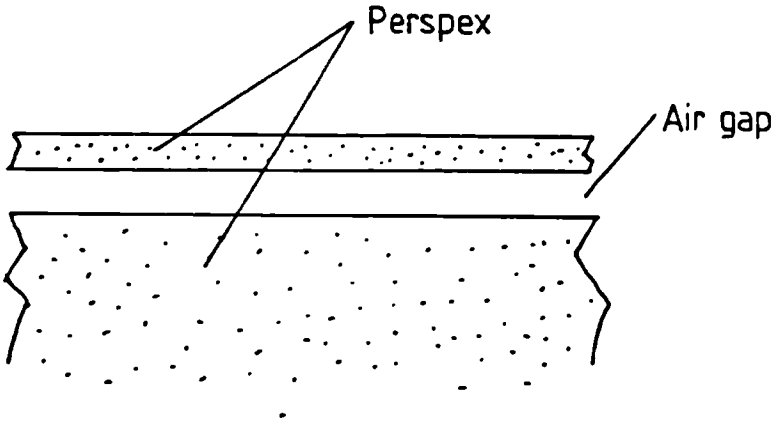

Fig 4.22a. Diagram of the air gap matching layer.

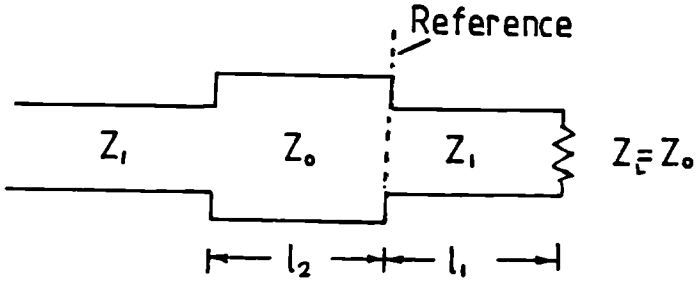

Fig 4.22b. Transmission line analogy of the air gap matching layer.

and β_2 respectively. Using transmission line relations -

$$Z_1 = Z_p \frac{Z_o \cos\beta_2 l_2 + jZ_p \sin\beta_2 l_2}{Z_p \cos\beta_2 l_2 + jZ_o \sin\beta_2 l_2} = Z_p \frac{\cos\theta_2 + jx \sin\theta_2}{x\cos\theta_2 + j \sin\theta_2}$$

$$Z_2 = Z_o \frac{Z_p \cos\beta_1 l_1 + jZ_o \sin\beta_1 l_1}{Z_o \cos\beta_1 l_1 + jZ_p \sin\beta_1 l_1} = Z_o \frac{x\cos\theta_1 + j \sin\theta_1}{\cos\theta_1 + jx \sin\theta_1}$$

where $\theta_1 = \beta_1 l_1$

$$\theta_2 = \beta_2 l_2 \qquad \text{and} \qquad x = Z_p/Z_o$$

For complete matching, the condition required is $Z_1 = Z_2^*$.

$$Z_p \frac{\cos\theta_2 + jx\sin\theta_2}{x\cos\theta_2 + j\sin\theta_2} = Z_o \frac{x\cos\theta_1 - j\sin\theta_1}{\cos\theta_1 - jx\sin\theta_1}$$

After simplifying and equating the imginary parts on both the sides of the equation we get

$$\sin\theta_1 \cos\theta_2 = \cos\theta_1 \sin\theta_2$$

$$\tan\theta_1 = \tan\theta_2 \quad \text{i.e.,} \quad \theta_1 = \theta_2 \qquad \ldots\ldots\ (4.5)$$

Now if we equate the real parts,

$$\tan\theta_1 \tan\theta_2 = x/(1 + x + x^2)$$

Using the relation in equation (4.5)

$$\tan^2\theta_1 = \tan^2\theta_2 = x/(1 + x + x^2)$$

$$\tan\theta_1 = \tan\theta_2 = \sqrt{x/(1 + x + x^2)} \qquad \ldots\ldots\ (4.6)$$

Equations (4.5) and (4.6) are valid for both normal and abnormal incidence angles provided we use the correct values of the impedances and the propagation constants. For a material of very high dielectric constant, dimensions l_1 and l_2 become very small and require greater precision in making the matching layer. The performance of the air gap matching layer is presented in

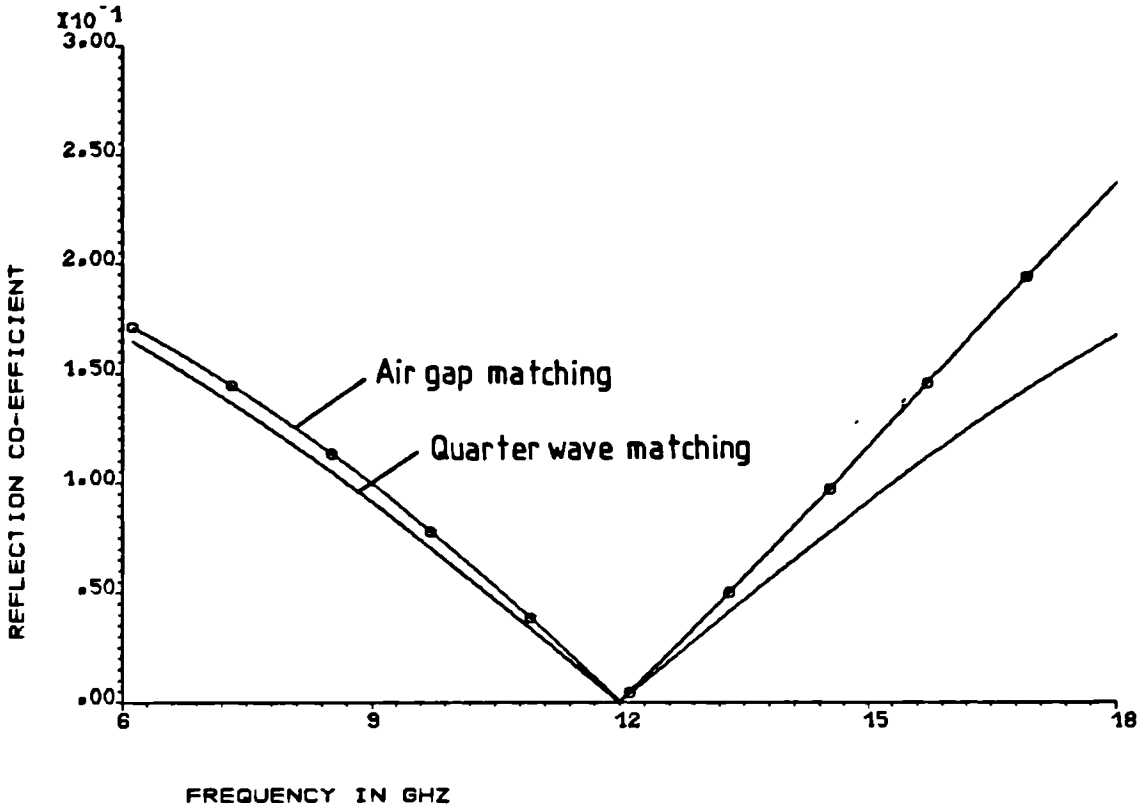

Fig 4.23. Frequency response of the air gap matching layer.

fig(4.23), along with that of a quarter wave matching layer. A pair of matching layers were made and put on the faces of a wedge. The 8-element array was placed in front of the wedge parallel to its first face and the distance between the array and the wedge was varied. The return loss of the array varied as the reflected waves from the wedge faces interfered with the return loss of the array itself. Fig(4.24) shows the return loss due to the variation of distance, with and without a matching layer.

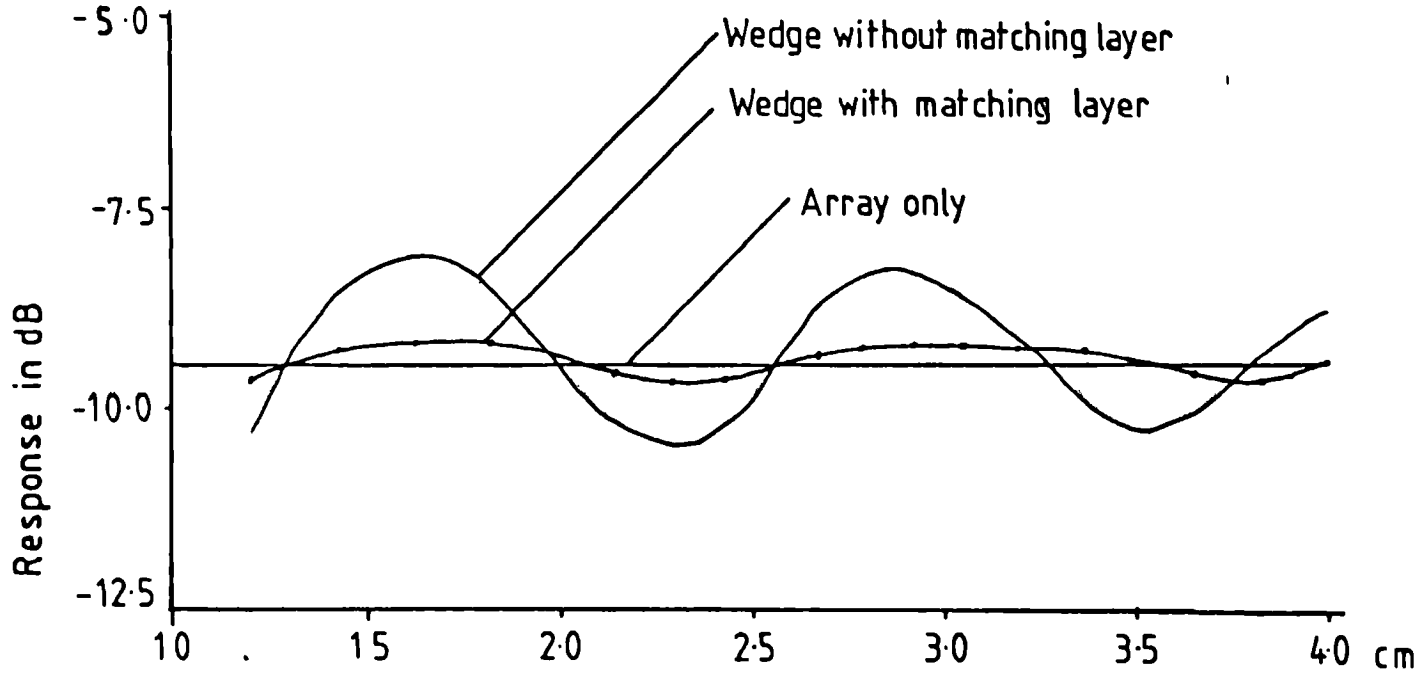

Fig 4.24. Variation of the return loss of the 8-element array for different positions of a wedge.

The reduction in variation of the return loss with the matching layers on the wedge faces can be easily seen. Reflection from face 2 of the wedge emerges at an angle of 39^{o} and very little of it is absorbed by the array. So, the change in return loss is mainly due to the reflection from the first surface. Taking the reflection coefficient for the perspex surface to be -12.6dB, the reflection coefficient with the matching layer is calculated to be -25dB using fig(4.24). The peak of the ripples in the figure corresponds to constructive interference between the reflected waves and the return loss of the array by itself.

4.3.7. Improvement in Radiation Pattern Due to the Matching Layer : Comparison Between Theory and Experiment

The measured radiation pattern showed a great improvement when the matching layer was placed on both the faces of a wedge. The measured pattern of a pair of horns steered by a single wedge is shown in the fig(4.25). When compared to fig(4.9) and (4.10) we can distinctly recognize the improvement in radiation pattern. The variation of sidelobes due to change in position x and y of the wedge is much smaller as the reflection from the wedge faces are reduced. Some more measurements were taken at different frequencies as shown in fig(4.26) and (4.27). A computed result is shown in fig(4.28) for a frequency of

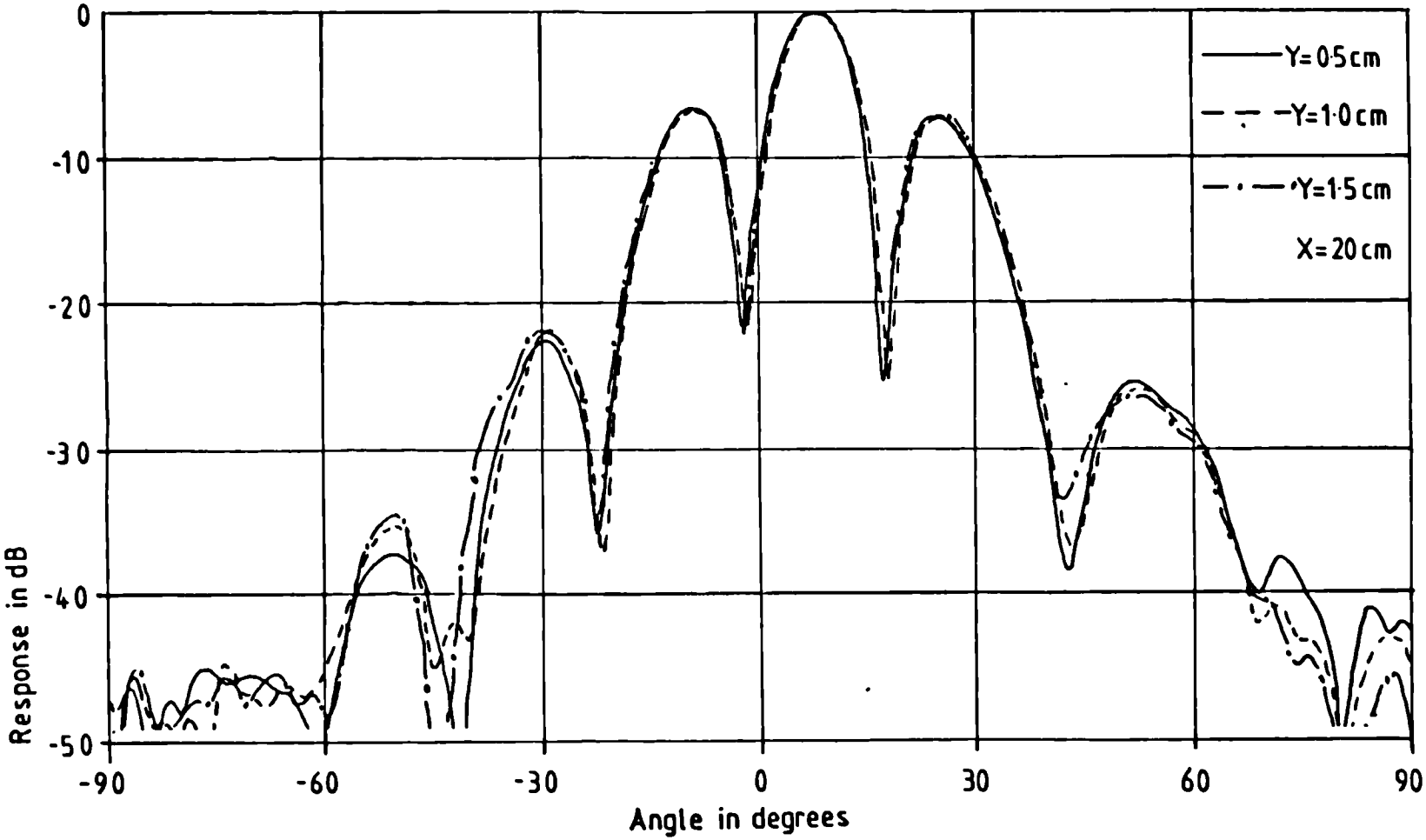

Fig 4.25. Steered radiation pattern of the array of horns at 12.4GHz using a matched wedge.

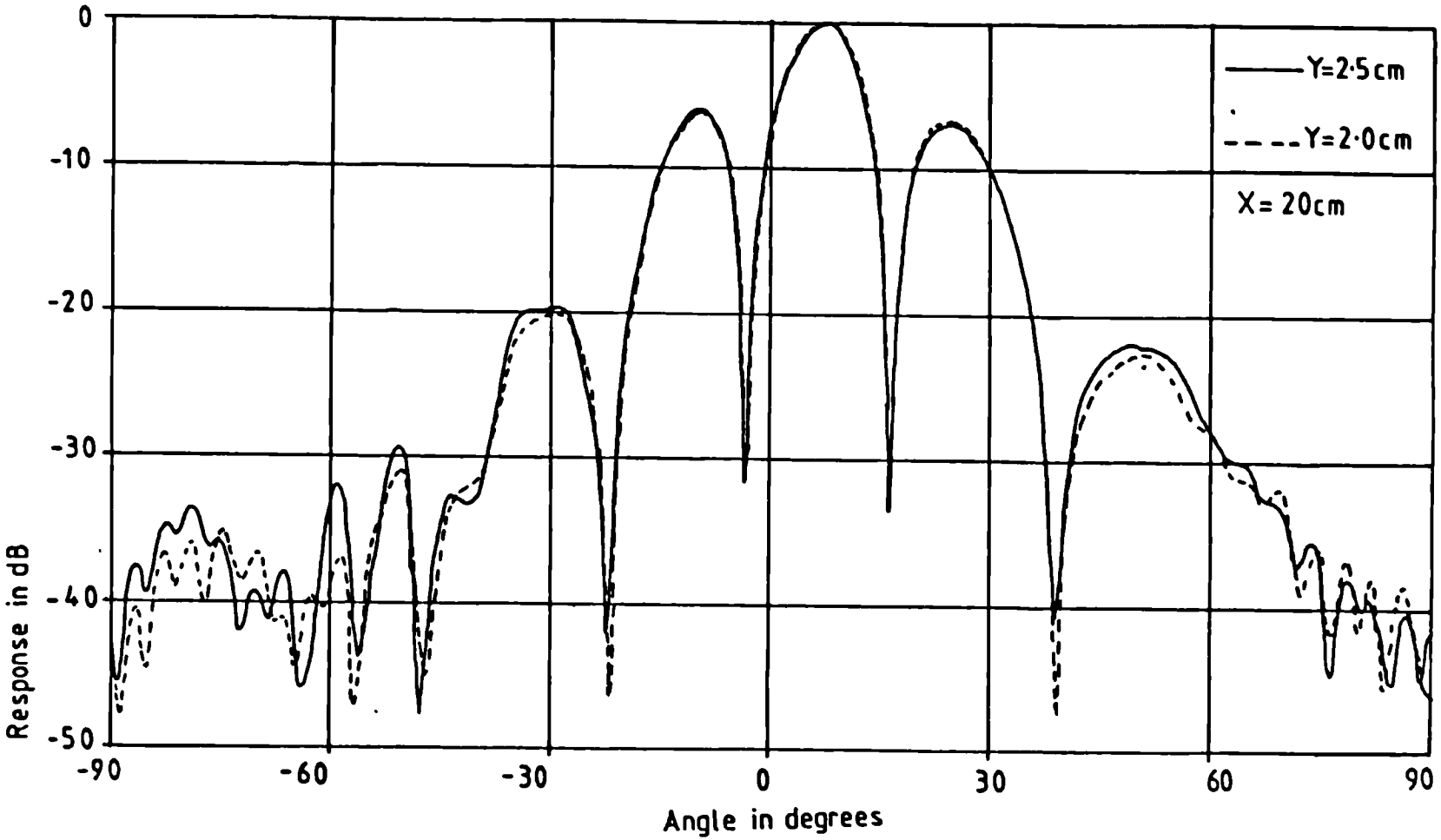

Fig 4.26. Steered radiation pattern of the array of horns at 12GHz using a matched wedge.

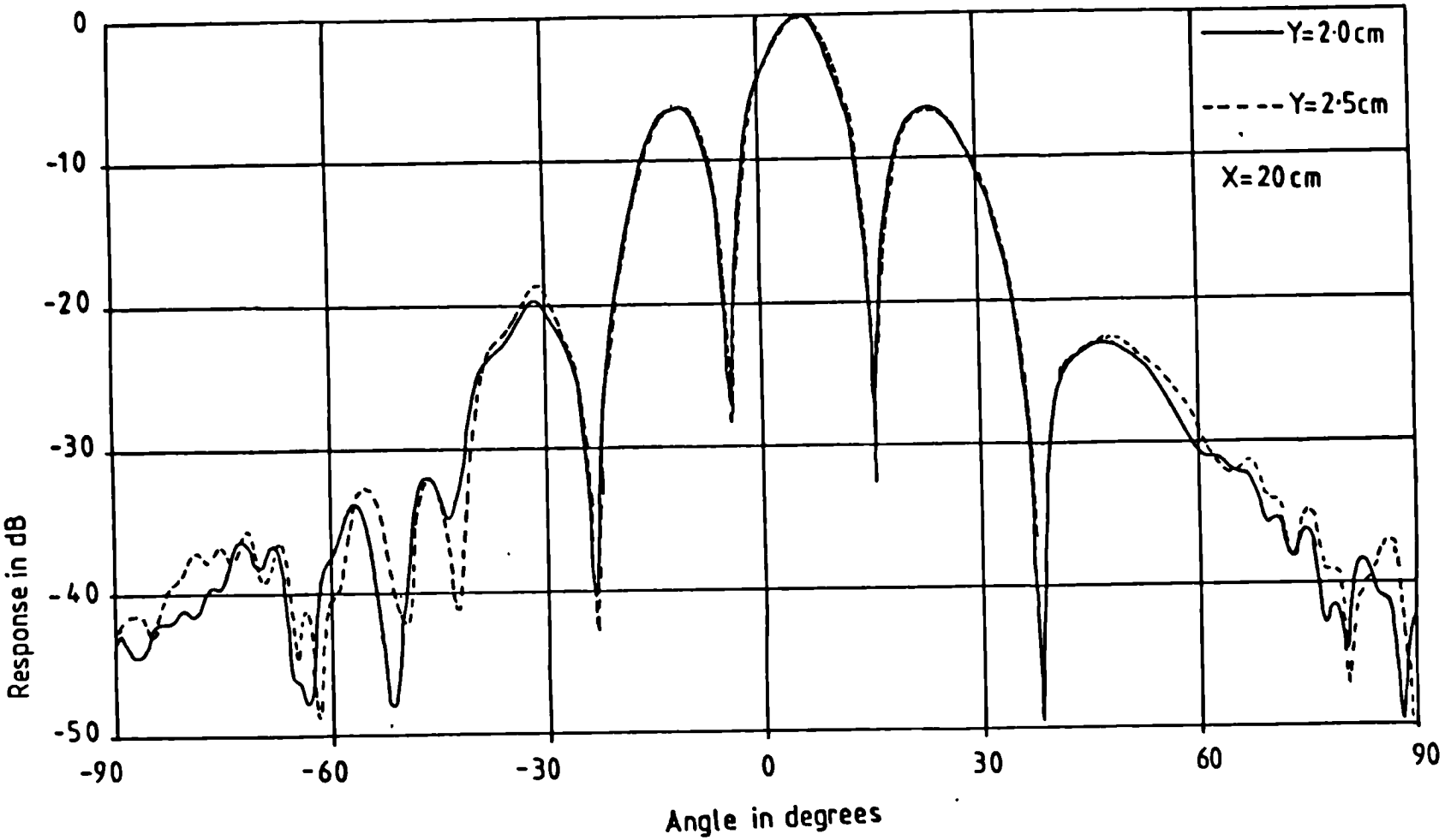

Fig 4.27. Steered radiation pattern of an array of horns at 11.8GHz using a matched wedge.

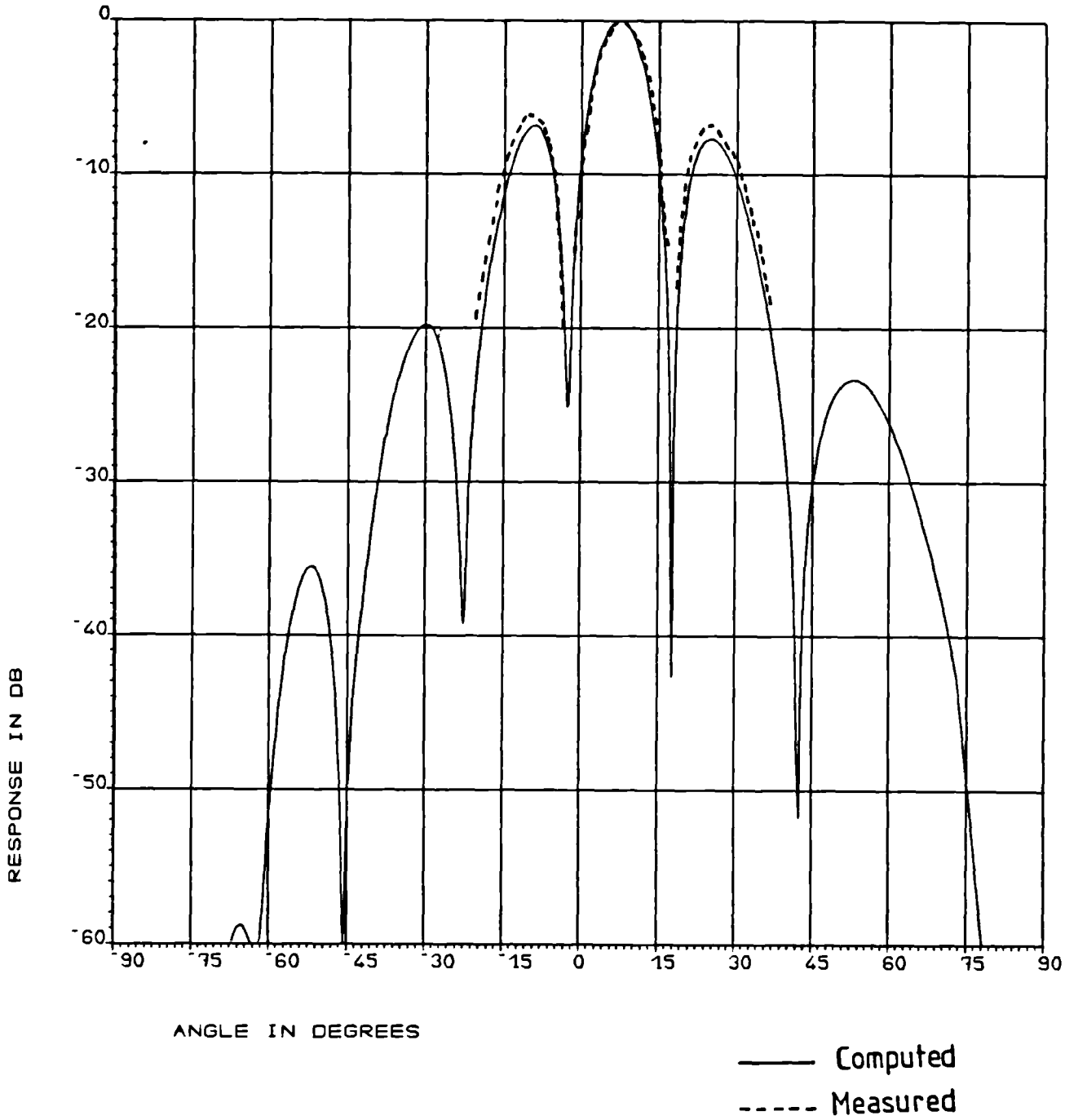

Fig 4.28. Computed radiation pattern of the array of horns steered by a single wedge.

12.4GHz. On the same graph, the average of the measured pattern is plotted, and this agrees quite well with the computed one. Fig(4.29) and fig(4.30) show the measured patterns when two wedges are placed for maximum and no deflection respectively. The far out sidelobes below -20dB level seem to have interfered with the reflected waves and lost their identity as the overall reflection is doubled due to the presence of two wedges. Computed results are shown in fig(4.31) and (4.32) along with a comparison of the measured results. There is reasonable agreement between the computed and the measured results. Table 4.1 shows the tabular form of comparison between the measured and the computed results. The change in sidelobes agree quite well although the absolute values of the sidelobes differ slightly due to the difference in the computed and the measured pattern of the array.

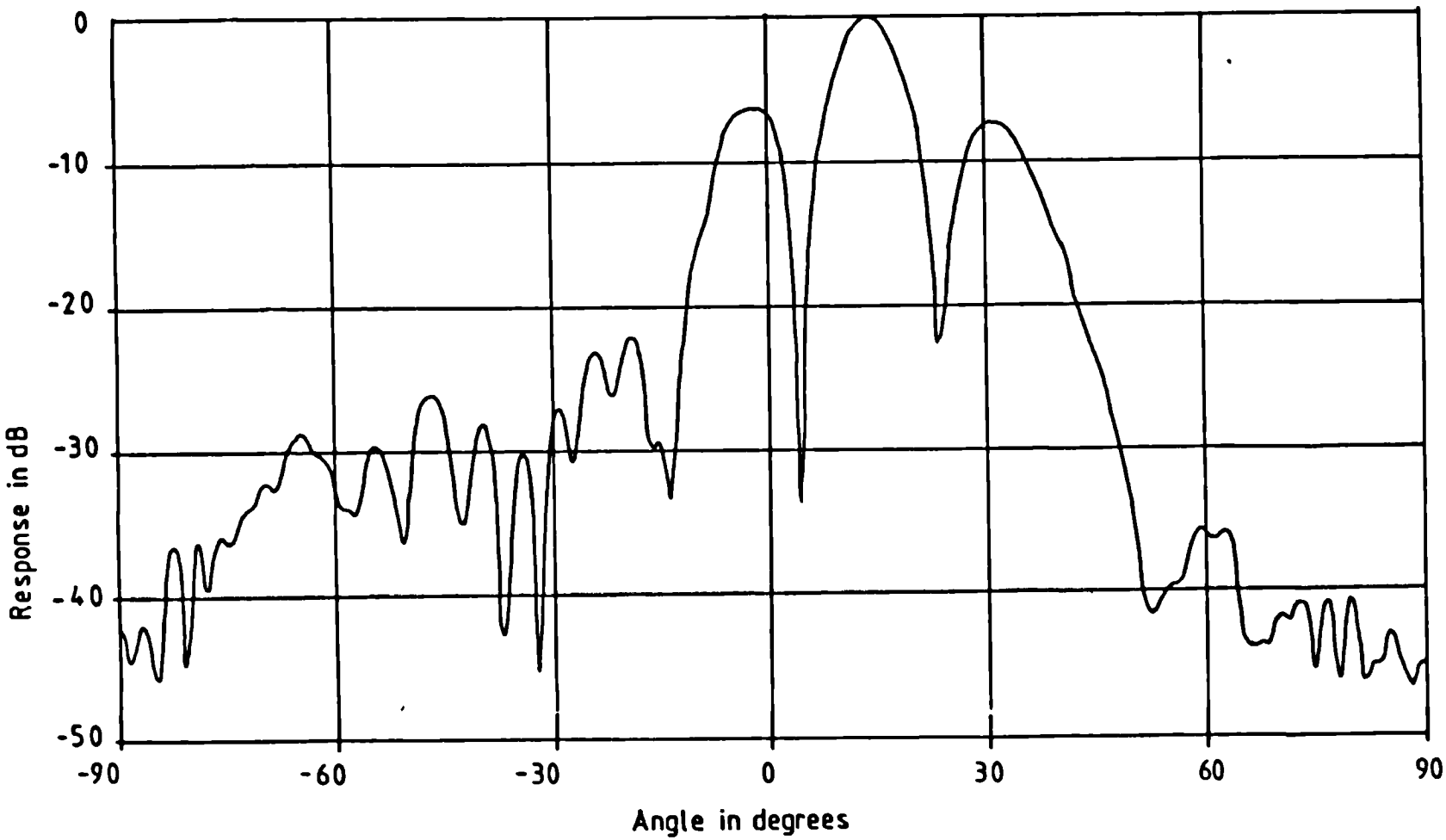

Fig 4.29. Measured pattern with two wedges for maximum deflection, f = 12.4GHz.

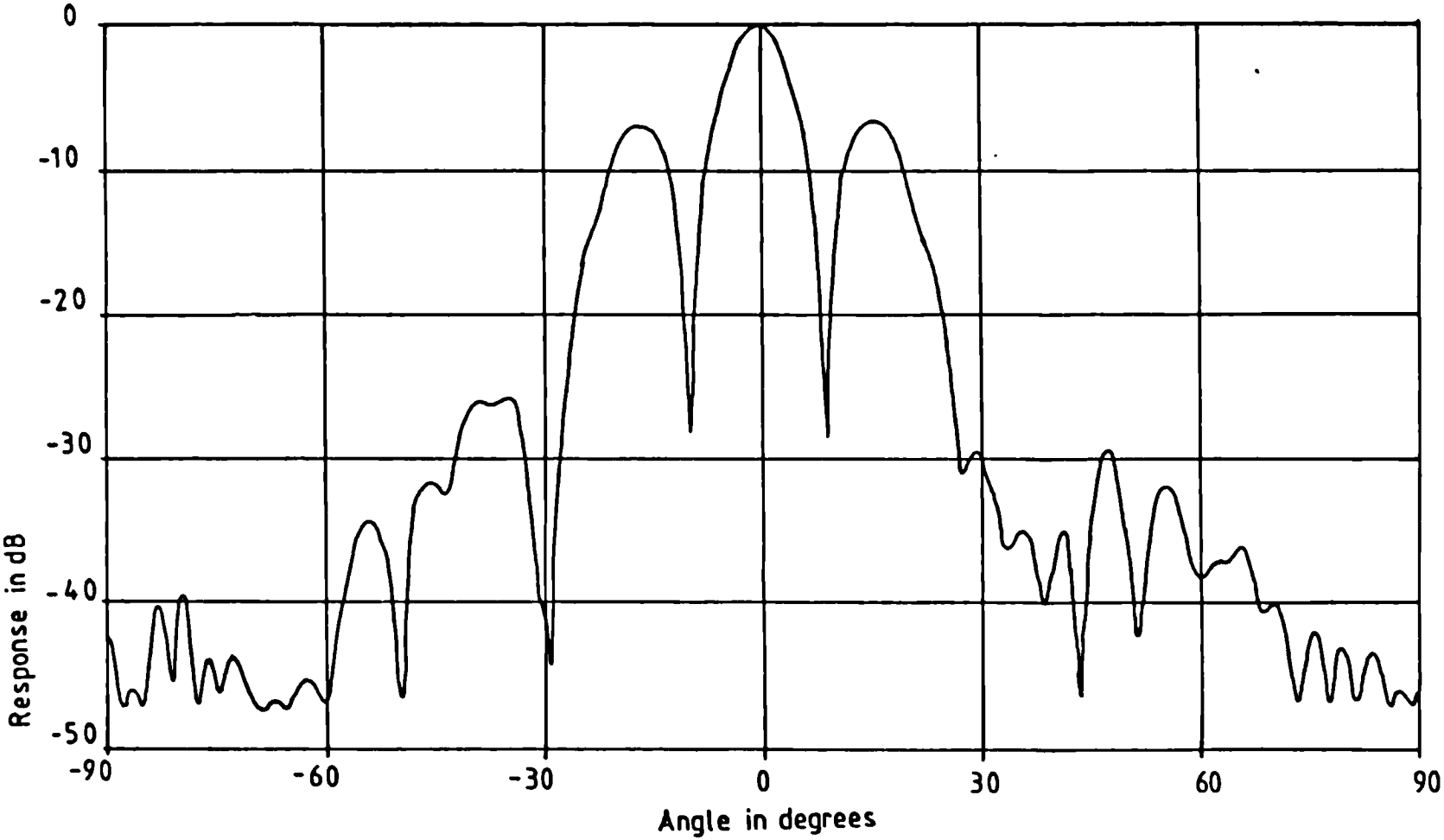

Fig 4.30. Measured pattern with two wedges for no deflection, f = 12.4GHz.

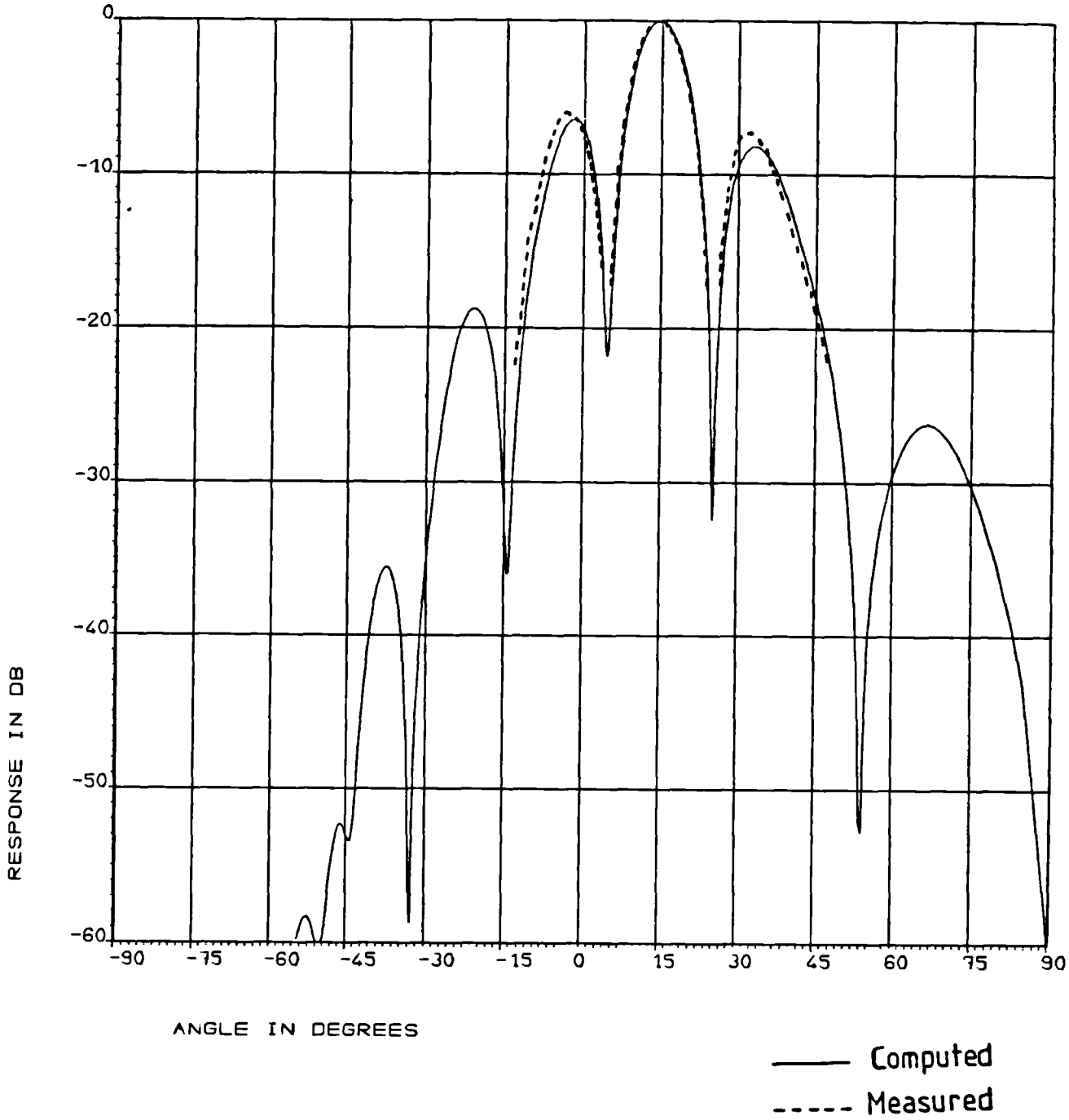

Fig 4.31. Computed pattern of the array of horns steered by two wedges for maximum beam deflection.

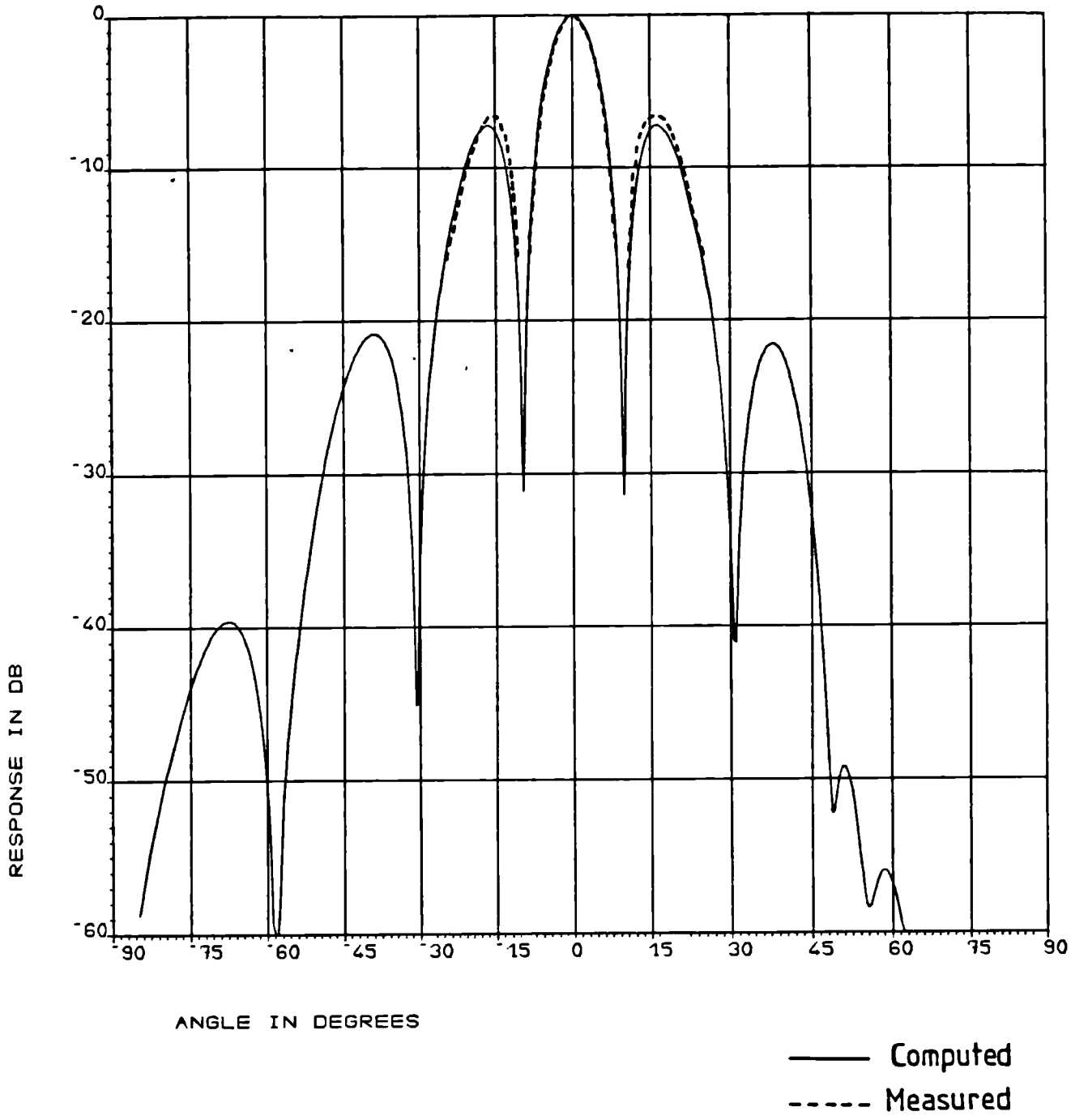

Fig 4.32. Computed pattern of the array of horns with two wedges for no deflection.

* = From unsteered position

	Computed							Measured						
	Beam Pos.	Side lobe						Beam pos.	Side lobe					
		1st RHS			1st LHS				1st RHS			1st LHS		
		pos.	dB	Change dB *	pos.	dB	Change dB *		pos.	dB	Change dB *	pos.	dB	Change dB *
No wedge	0	16.5°	-7.2	-	-16.5°	-7.2	-	0°	16°	-6.5	-	-16°	-6.3	-
1 wedge	7.4°	24.8°	-7.7	-0.5	-9.2°	-6.8	0.4	7.5°	24.5°	-6.8	-0.3	-10°	-6.0	0.3
2 wedge Max. def.	14.6°	33.2°	-8.1	-0.9	-1.8°	-6.4	0.8	14.5°	32.5°	-7.0	-0.5	-2.0°	-5.9	0.4
2 wedges no defl.	0	16.2°	-7.2	0	-16.2°	-7.2	0	0	16°	-6.3	0.2	-16°	-6.4	-0.1

Table 4.1. Comparison between the measured and computed results.

4.4. Discussion

The measured results presented in section 4.3.3 and section 4.3.7 clearly show the importance of matching the wedge faces. A mismatched surface can cause unpredictable behaviour of the sidelobes when the antenna is mounted. In this chapter we have devoted some effort to analyzing the scattering behaviour of an array fed by a corporate feed network. But this behaviour will be quite different for a parabolic dish, as the incident plane waves are converted to spherical waves after being reflected from the dish.

A prominent feature of the overall radiation pattern is the small change in sidelobe levels. The sidelobes on the same side as the beam steering are lowered but they are increased on the other side of the main beam. This difference in sidelobe level is due to two main reasons. Firstly, the reflection co-efficient of the emergence waves changes quite rapidly as the emergence angle is increased. But the situation is different on the other side of the main beam where the reflection coefficient is smaller. Secondly, as the beam is steered, both the main beam and the sidelobes on the steered side of the main beam are affected by their inclination to the wedge face. So, the main beam and the sidelobes become broader but their amplitude is reduced. But the sidelobes on the other side of the main beam are less inclined to the surface, compared to their unsteered position. Hence, the overall

level of the sidelobes normalised to the main beam changes accordingly. However, these small changes in the sidelobes should not have any significant effect on the gain of the system. We can safely neglect the effect of the change in sidelobes, as far as the gain is concerned.

In conclusion, the performance of the airgap matching layer is quite good although not as good as a quarter wave matching section. One of the reason for this is the greater number of reflecting surfaces compared to that of a quarter wave matching layer. But, it could still be a very attractive matching technique as it does not require any third material to make the matching layer.

CHAPTER 5 : DIELECTRIC MATERIALS FOR THE WEDGES

5.1. Introduction

Considerable effort was devoted to the search for a suitable dielectric material for the wedges. Ideally, a light weight, low loss, high dielectric constant material is best suited for the purpose. A low loss dielectric material with reasonably high dielectric constant is quite expensive. A number of other properties were also taken into consideration, like machinability, specific gravity and loss. The data for the dielectric constants and loss tangents presented in this chapter, other than the measured ones, are quoted from von Hippel [29].

5.2 Liquid Dielectric Materials

Liquid dielectric materials are mainly used in high voltage engineering devices like transformers and circuit breakers. These liquid dielectrics are mainly petroleum oils having some additives to improve their performance. Water has a dielectric constant of 55 at 10GHz and 25^{o}C. but the loss tangent is too high (2.56) for any practical use at microwave frequencies near 10 GHz; its performance is best near 100 MHz. Any additives in solution make the loss tangent even higher.

Petroleum oils are low loss dielectric materials at X-band frequencies, but their dielectric constants are low,

ranging from 2.0 - 2.3. Other liquid dielectric materials include organic liquids with similar dielectric constants, but most of them are very lossy. Properties of some liquids of this type are given in table 5.1 below.

Material	Temp °C		Frequency	
			10^8	10^{10}
Methyl alcohol(CH_3OH)	25	ε_r	78	34
		tanδ	380×10^{-4}	2.65
Carbon Tetra-chloride (CCl_4)	25	ε_r	2.17	2.17
		tanδ	$<2\times10^{-4}$	16×10^{-4}
Vaseline	25	ε_r	2.16	2.16
		tanδ	$<4\times10^{-4}$	10×10^{-4}
Styrene	25	ε_r	2.40	2.38
		tanδ	$<3\times10^{-4}$	37×10^{-4}

Table 5.1. Dielectric properties of some liquids.

5.3 Solid Dielectric Materials

There are varieties of solid materials whose dielectric properties depend on their chemical structures. Some of them are plastic-like materials with low dielectric constants and low loss. Most of the good quality high dielectric constant materials are ceramics. Some of the

ceramic materials have dielectric constants as high as 165.

5.3.1. Plastic type dielectric materials

Most of the plastic type dielectric materials are organic compounds like polystyrene and their dielectric constants range from 2.0 to 4.0. Materials like perspex and polystyrene have low loss tangents but their dielectric constants are too low to make large wedges. On the other hand their specific gravities range from 1.2 to 1.5. So, a pair of wedges made from these plastic materials can be very heavy when designed to be used with large antennas such as a 50cm dish. Some measurements were made on perspex to determine the dielectric constant and loss tangent. Barlow and Cullen [30] present different measuring techniques for dielectric constant and loss tangent. The measuring technique is described in appendix III. The dielectric constant and the loss tangent were measured to be 2.59 and 0.0061 respectively. Although the measured loss is not very low, it is considered acceptable for small wedges to produce small deflections. Polystyrene has a similar dielectric constant of 2.2, but is more difficult to machine than perspex.

5.3.2. Ceramic type dielectric materials

Ceramic type dielectric materials are heavy and mechanically strong. Ceramic type materials are normally mixed with plastic type dielectric materials in a definite proportion to obtain a particular dielectric constants of the composite products.

Titanium dioxide (TiO_2) is a well known dielectric material with a dielectric constant of 96 and a loss tangent of 3.4×10^{-4}. It is commercially available in powdered form and has a specific gravity of 4.0. TiO_2 mixed with polystyrene is extensively used in illuminated road signs. The dielectric constants of some samples of TiO_2 mixed in polystyrene were measured. The percentage of the TiO_2 was varied to produce different dielectric constants. Table 5.2 shows some of the results.

% TiO_2	1%	2%	10%	20%	50%
ε_r	2.46	2.56	2.86	3.53	5.57

Table 5.2. Dielectric constants of polystyrene mixed with different proportions of TiO_2.

It was found that the end product became very brittle when TiO_2 was added more than 50% by weight. The dielectric constant even at 50% TiO_2 is not very high compared to the dielectric constant of pure TiO_2. This is because of the high specific gravity which makes 50% by weight of TiO_2 equivalent to only 12.5% by volume. Table 5.3 gives the

dielectric properties of some of the solid materials discussed so far.

Material	Temp °C		Frequency	
			10^8	10^{10}
Polystyrene (commercial)	25	ε_r	2.55	2.54
		tanδ	3.5×10^{-5}	12×10^{-4}
Polyurethane (100% pure)	25	ε_r	2.25	2.25
		tanδ	$<2\times10^{-4}$	4×10^{-4}
Polyvinyl chloride	20	ε_r	2.85	2.84
		tanδ	81×10^{-4}	55×10^{-4}
Aluminium oxide	25	ε_r	8.6	8.6
		tanδ	$<10^{-3}$	14×10^{-4}
Sodium chloride	25	ε_r	5.9	5.9
		tanδ	$<2\times10^{-4}$	$<5\times10^{-4}$
Titanium dioxide	24	ε_r	—	96
		tanδ	—	3.4×10^{-4}
Calcium Titanate	25	ε_r	166.8	165
		tanδ	5×10^{-4}	85×10^{-4}
Phosphate glass	25	ε_r	5.24	5.0
		tanδ	20×10^{-4}	42×10^{-4}
Fused quartz	25	ε_r	3.78	3.78
		tanδ	10^{-4}	10^{-4}

Table 5.3. Dielectric properties of some solids.

5.4 Artificial Dielectric Materials

The molecular theory of dielectric materials expresses the dielectric constant of a material as a function of the polarization of the molecules. Kock [31] extended the molecular concept to be applied to small metallic obstacles. If the metallic obstacles are placed in a rectangular lattice-like structure, they effectively behave as a dielectric material, provided the metallic obstacles are much smaller than a wavelength. Equivalent permittivity and permeability of such a material can be expressed as -

$$\varepsilon_r = \varepsilon_1/\varepsilon_o \quad (1 + \alpha_e N/\varepsilon_1)$$

$$\mu_r = \mu_1/\mu_o \quad (1 + \alpha_m N/\mu_1)$$

$$n = \sqrt{\mu_r \varepsilon_r} = \text{Refractive index}$$

where ε_r , μ_r = permittivity and permeability of the artificial dielectric material.

ε_1 , μ_1 = permittivity and permeability of the base material

α_e , α_m = electric and magnetic polarization

N = no. of obstacles/ unit volume

However, Clausius-Mossoti relation for metallic sphere gives more accurate results. Useful information and analysis on artificial dielectric materials are provided by Jasik [32] and Collin [33]. It was found that the maximum dielectric constant achievable using metallic

spheres was about 1.7. The reason is the magnetic polarization by the spheres that reduces the overall propagation delay. Kock [31] avoided the magnetic polarization by using thin metal discs placed parallel to the electric and magnetic fields. Different types of thin metallic obstacles can be used as shown in fig(5.1). Circular and rectangular discs can be used for any arbitrary polarization of the incident waves; however the metal strips shown in fig(5.1c) can only be used for one polarization. The typical dimensions of the discs or the widths of the strips should be less then $\lambda/10$ to get a good frequency response. So far, we have discussed only the delay structures for the artificial dielectrics. But it is possible to increase the phase velocity, instead of decreasing it, by using right type of metallic structures [34]. Fig(5.2) shows two different structures. Fig(5.2a) shows parallel plates, the electric field being parallel to the plates, which effectively behave like rectangular waveguides and produce fast waves. The situation in the case of metal rods is similar. Any wedge made from a fast wave structure will deflect the beam as shown in fig(5.3), which is opposite to the direction for dielectrics having $\varepsilon_r > 1.0$.

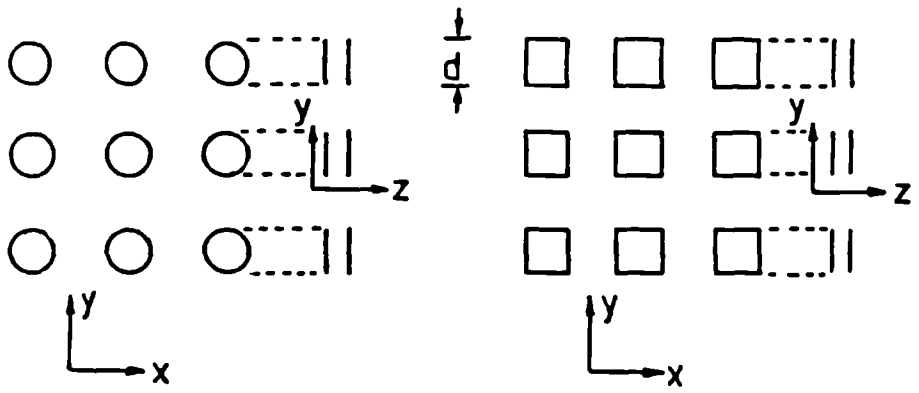

z-Direction of propagation

$\alpha_e = \frac{2}{3} d^3 \varepsilon_1$ $\qquad$ $\alpha_e = 1{\cdot}032\, d^3 \varepsilon_1$

(a)

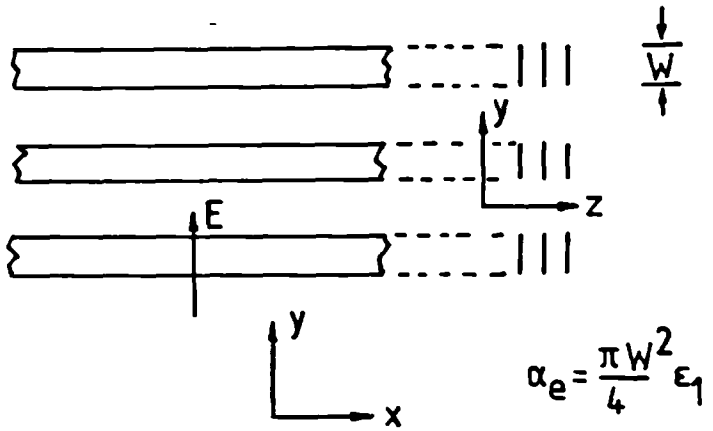

(b)

Fig 5.1. Different metallic obstacles for artificial delay dielectrics ($\varepsilon_r > 1$).

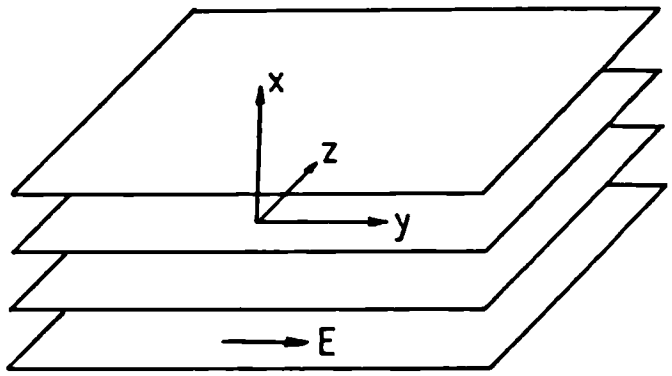

(a)

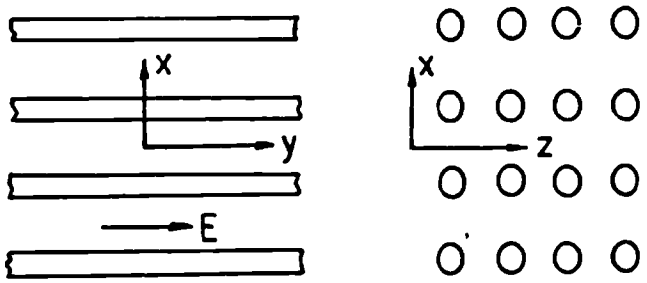

(b)

Fig 5.2. Two different metallic structures for artificial dielectrics having $\varepsilon_r < 1$.

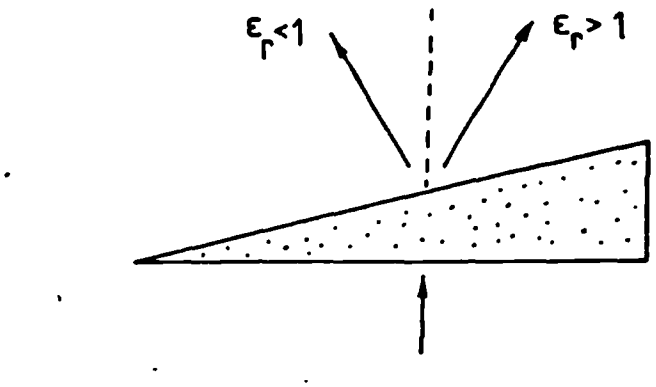

Fig 5.3. Direction of beam steering due to a dielectric wedge having $\varepsilon_r < 1$.

5.5 A Wedge Made of Artificial Dielectric Material

A wedge was made from artificial dielectric material using metal discs inside polyurethane (expanded) sheets. Twelve thin layers of polyurethane each having dimensions of 22.86cmx11.43cmx0.22cm were cut out from a block. Small depressions of 3.2mm diameter were made on each of the sheets. The separation between the depressions were 4.23mm. These dimensions were chosen considering the limitations of our machine shop. When assembled, all the twelve sheets of polyurethane form a brick-like structure. If the block is cut into two, two identical wedges would be obtained as shown in fig(5.4). Placing the metallic discs inside the depressions of the polyurethane layers would have left a certain amount of polyurethane

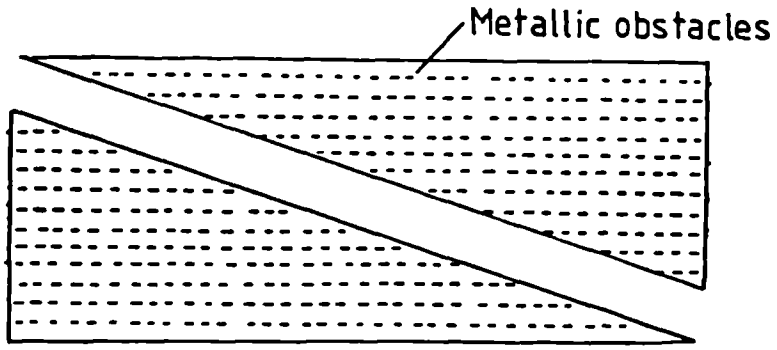

Fig 5.4. Two identical wedges made from a block of artificial dielectric material.

between the metallic layer and the slanting wedge surface. Considering the phase of the emergence wave due to a plane wave incident on face 1, a stepped phase distribution will be obtained as shown in fig(5.5). So, any matching layer placed on the second wedge face cannot match properly because of the ployurethane left in between the matching layer and the metallic layer. Considering this factor, a stepped structure as shown in fig(5.6) was built up by making one polyurethane layer smaller than the previous one. The width of the steps was 1.8cm i.e., 0.72λ at 12GHz. Metallic discs of 3.2mm diameter were placed in the depressions and the wedge was built up. The dimensions of the metal discs and their separations were chosen to produce a dielectric constant of 4.74. Perspex layers were then placed on the stepped face and on the plane face of the wedge to reduce reflection. The final structure is

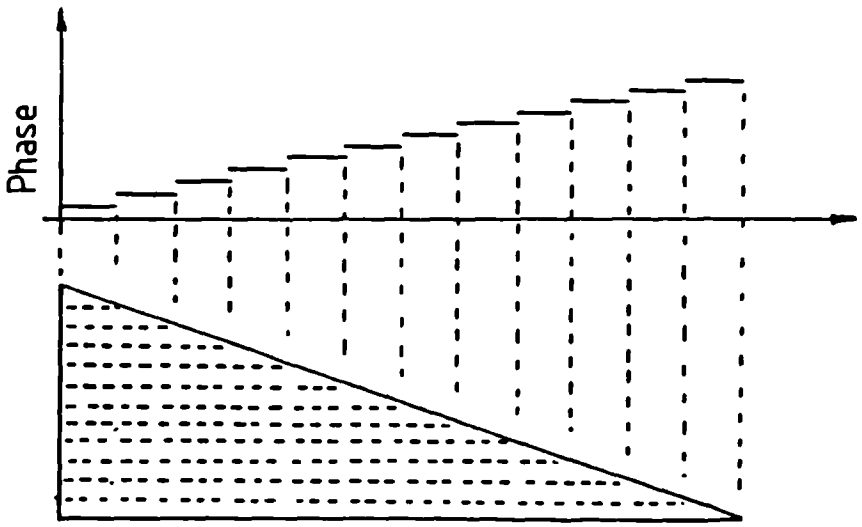

Fig 5.5. Phase distribution on the projected aperture of the emergence face of the wedge made from artificial dielectric material.

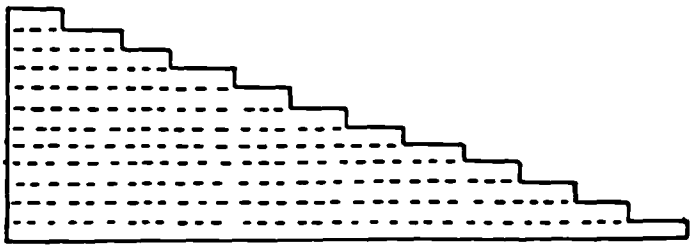

Fig 5.6. Stepped structure of a wedge made from artificial dielectric material.

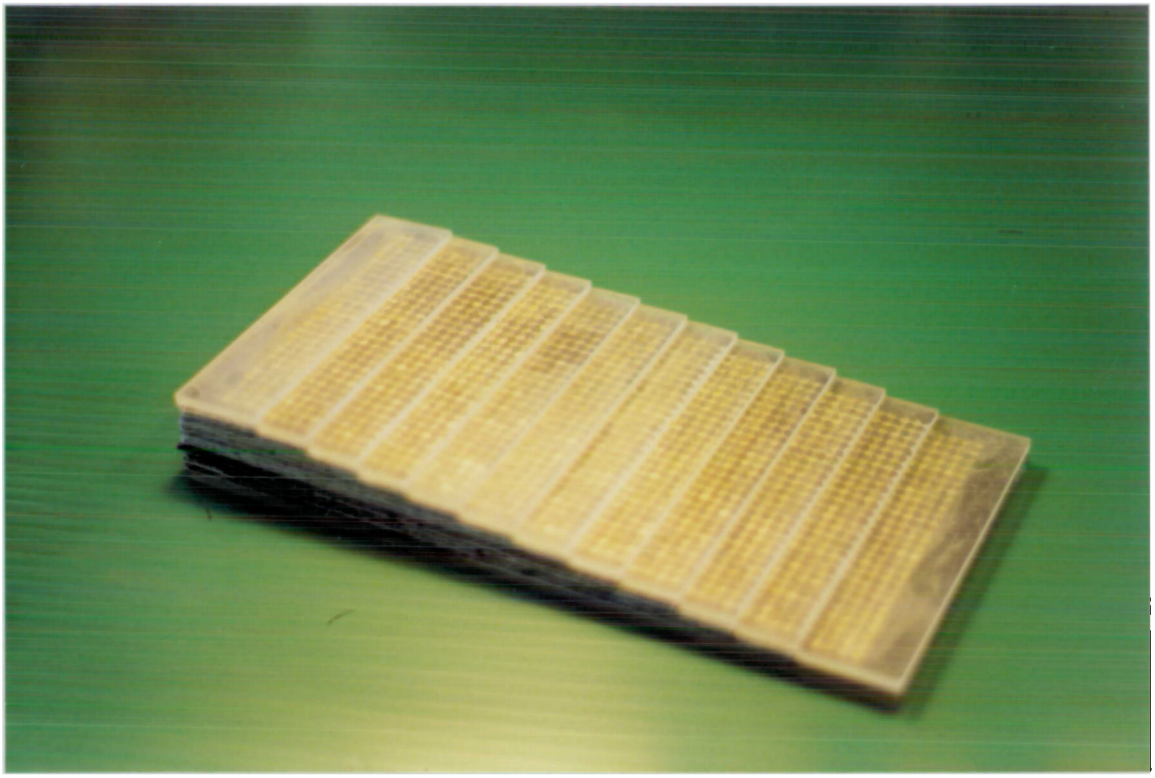

Fig 5.7. A stepped wedge made from artificial dielectric material with perspex layers on its faces.

shown in fig(5.7). Measurements were taken using this wedge in front of the array of two horns, as discussed in section 4.3.5. Fig(5.8), (5.9), (5.10) show the measured patterns for three different frequencies of 12.4, 12.0 and 11.5 GHz respectively. Beam steering angles of 5.0°, 4.5° and 4.0° were obtained which correspond to dielectric constants of 3.24, 2.9 and 2.62 respectively. The dielectric constants achieved were smaller than the designed value. There may be a number of reasons for this. The thickness of the metal discs was 0.25mm, which cannot be taken as very thin. This might have polarized the magnetic field which in turn reduced the overall propagation delay. A second possibility is the

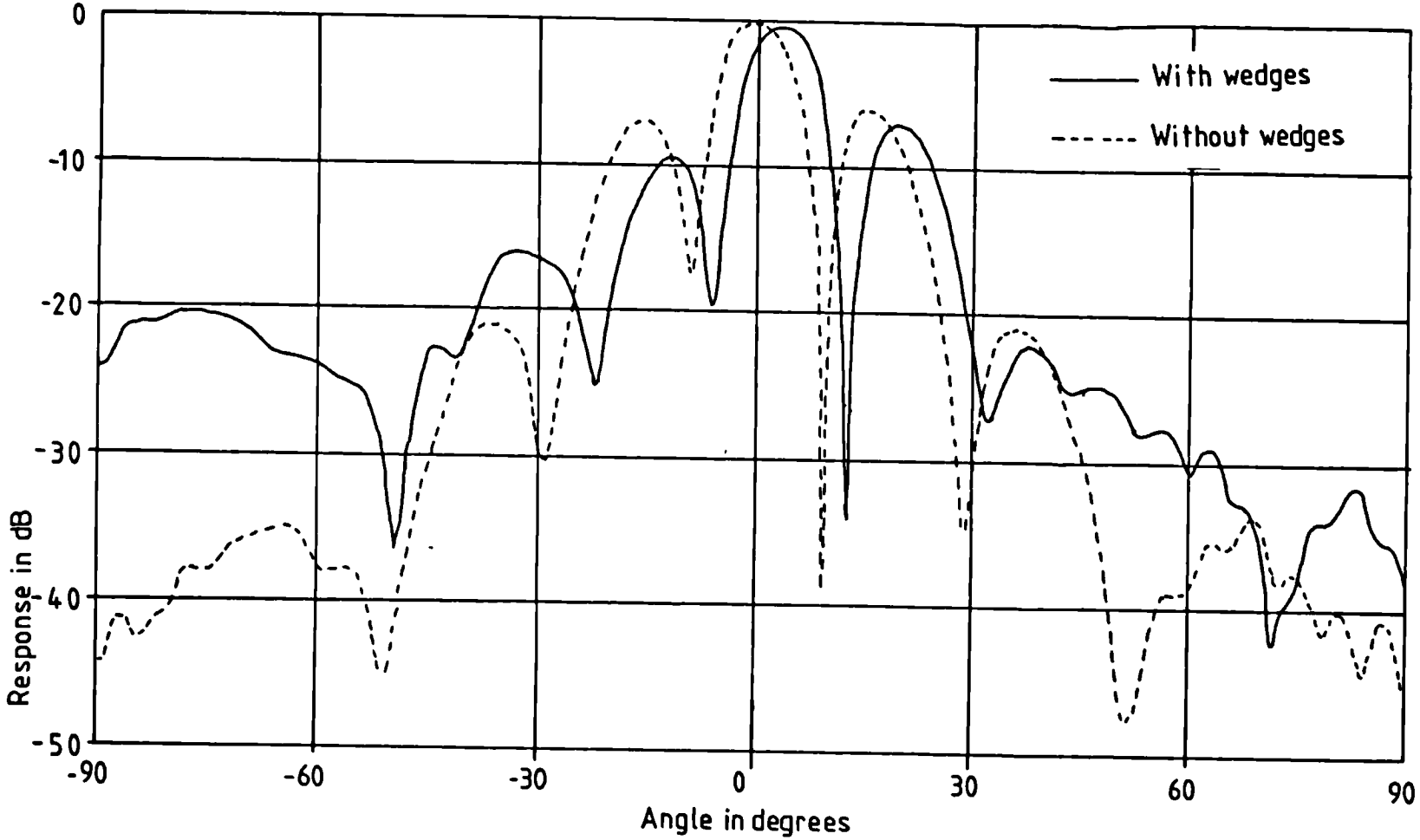

Fig 5.8. Radiation pattern of a pair of horns steered by the artificial dielectric wedge at 12.4GHz.

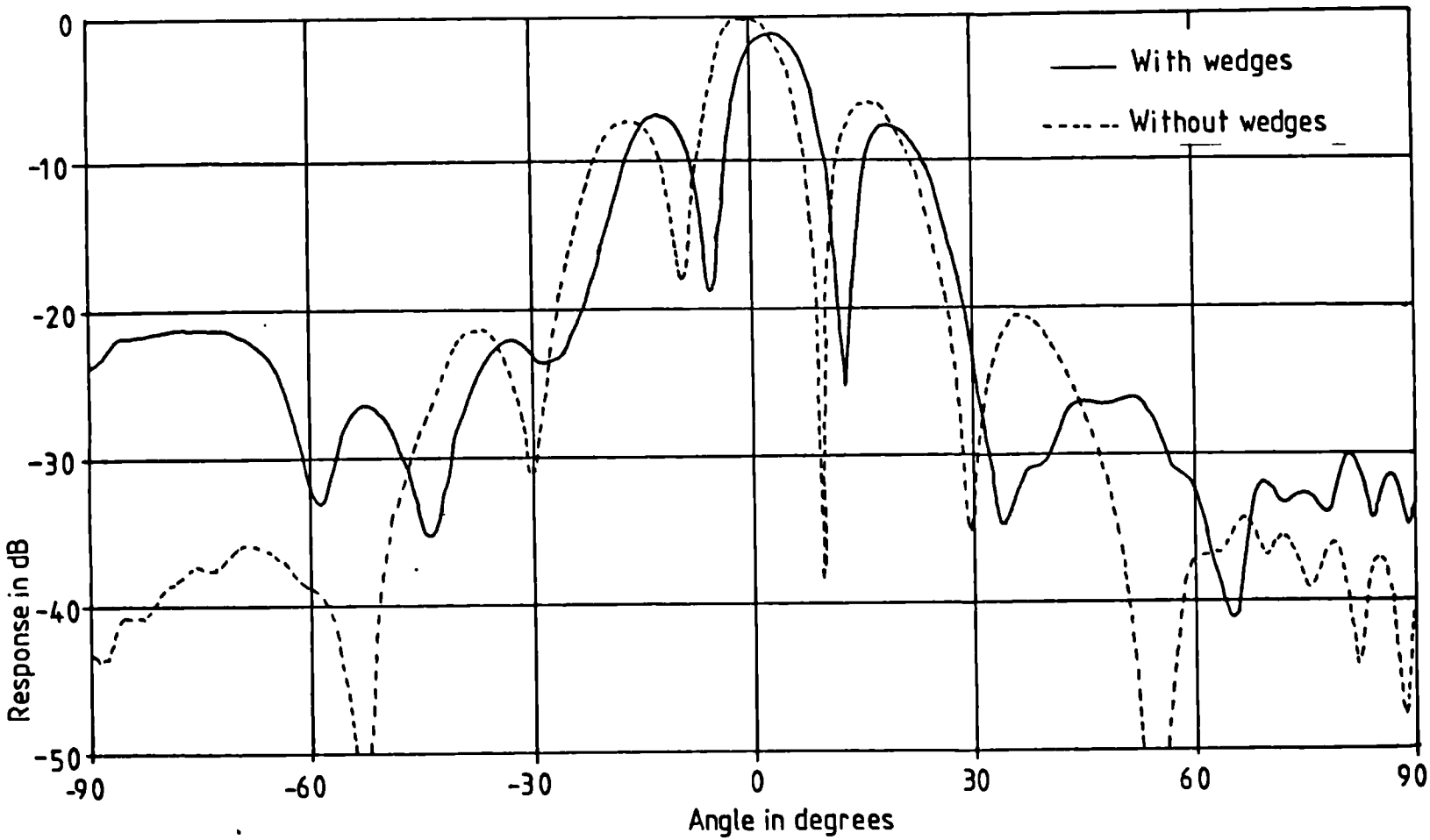

Fig 5.9. Radiation pattern of a pair of horns steered by the artificial dielectric wedges at 12GHz.

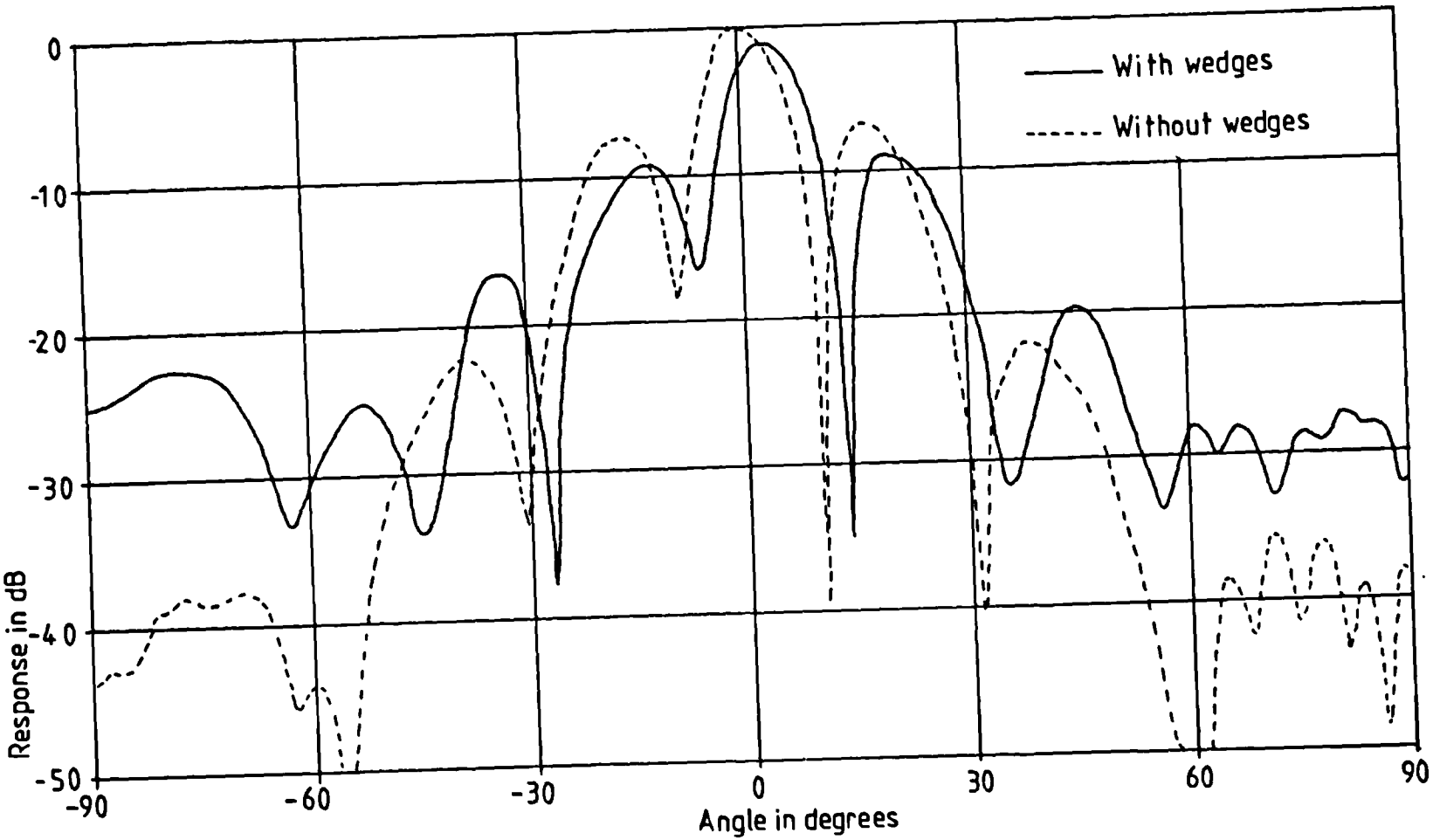

Fig 5.10. Radiation pattern of a pair of horns steered by the artificial dielectric wedge at f = 11.5 GHz.

insufficient accuracy of the formulae used, as they require diameters less than $\lambda/10$, which is not true for the metal discs used.

The sidelobes at large angles, especially opposite the direction of beam steering, tend to increase as the beam is steered. They are the grating lobes resulting from the step-like structure of the wedge. There seems to be some loss involved as can be seen by the reduction in power in the main beam. But this reduction in power level could be the resultant effect of reflection from the wedges and the return loss of the horns, in addition to the loss inside the material. Brass discs were used instead of copper ones, as the brass sheets are easier to punch.

5.6 Discussion

The dielectric materials discussed in this chapter, other than the artificial dielectrics, are quite heavy and can make the weight of the wedges unacceptable from the mounting point of view. Solid materials with high dielectric constants can be used by stepping the wedges as a weight reduction scheme; this is discussed in section 6.2 . Measurements with artificial dielectrics look quite promising. Making them manually is a tedious time-consuming task. Hence, any development of a fabricating system can make the dielectric constants high at a very low cost. More care should be taken in making

the wedges, so that the steps shown in fig(5.6) are smaller then $\lambda/2$ to avoid grating lobes for a moderate angle of beam steering. This can be done by making the layers of the base materials thinner or by making the wedge angle larger than a certain value.

CHAPTER 6 : Some Practical Considerations

6.1 Introduction

Mathematical relations of the radiation pattern of the wedge antenna system have been developed in chapter 4. However, this do not take into consideration some other important aspects such as the effect of loss in the dielectric material of the wedges and the generation of cross polar components, which are discussed here. Besides the loss in the dielectric, there will be a reduction in gain as the beam is steered; this is discussed in sec(6.5). This chapter also discusses the possibility and consequences of stepping the wedges to reduce the weight and volume. Some analysis is done to determine the size of the wedge needed in relation to the size of the antenna aperture. All these discussions have great practical importance from designer's point of view.

6.2 Weight and Volume

The weight of a pair of dielectric wedges for beam steering purposes depends on the dielectric constant of the material. For the same angle of beam steering, a higher dielectric constant results in lower wedge volume. If we consider a pair of dielectric wedges of radius r and wedge angle Ω, then the volume of a single wedge will be-

$$= 1/2.\pi . r^2 2r . \tan\Omega = \pi . r^3 . \tan\Omega \quad ...(6.1)$$

Hence the weight of a single wedge is -

$$= \pi . r^3 . \tan\Omega \ . S \qquad \text{.....(6.2)}$$

where S = specific gravity of the dielectric material

From eqn(6.2) we can see that the weight is smaller when both Ω and S are small. But most dielectric material with high dielectric constants are ceramic type materials and have high values of specific gravity. Hence the possibility of getting both high dielectric constant and low specific gravity is quite remote, unless artificial dielectric materials are used (sec 5.4). However, it is possible to reduce the weight of the wedges by stepping them as shown in fig(6.1). The height of the steps are chosen such that they correspond to a phase difference of 2π for the adjacent waves in the dielectric and in air. The technique is widely used in stepped dielectric lenses [35]. Using this technique, it is possible to use a low dielectric constant material to obtain a substantial beam steering angle without making the wedges too heavy. There is, however, a lower limit to the volume of the wedges corresponding to the dielectric constant of the material. The smallest thickness of the wedge corresponds to a phase difference of 2π at the steps. For materials of lower dielectric constant the thickness is greater. The height of the steps has some adverse effects on the overall radiation pattern. The steps produce shadows on the

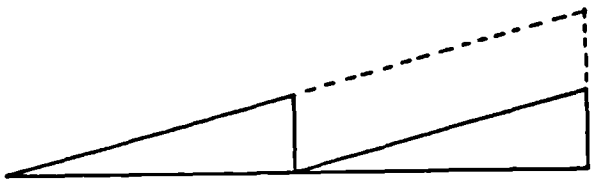

Fig 6.1a. A stepped dielectric wedge.

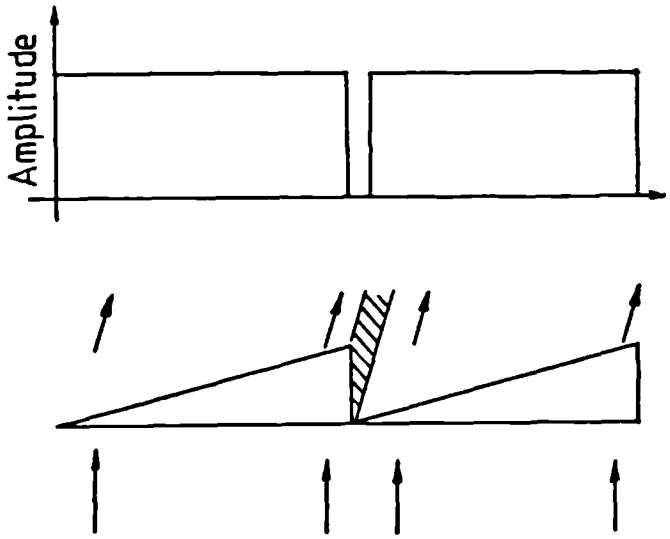

Fig 6.1b. Shadowing effect due to the stepping of the wedge.

aperture plane as shown in fig(6.1b) and cause higher sidelobes in the radiation pattern. The effect is obviously stronger for materials of lower dielectric constant, as they require higher steps on the wedge. Although the shadows produced by the steps are not well defined, we can still get reasonable results assuming sharp shadows [36]. Hence the radiation pattern worsens with increasing number of steps. Fig(6.2) shows the radiation pattern of a 12λ rectangular aperture steered by 15.5^{o} using a single wedge

i) having no steps

ii) having one step

iii) having two steps.

The patterns were computed using eqns(4.4a) and (4.4b) by taking into consideration the actual phase shift at the steps for each of the individual angular spectra. The abrupt phase shift at the steps were positive while computing the wedge aperture and negative while computing the radiation pattern. We can easily see the deterioration of the radiation pattern with the increasing number of steps. In the case of a circular aperture, it may be wiser to use two steps instead of one, because a single step will run across the diameter producing the maximum possible length of shadow.

So far, we have discussed only the effect of shadowing. There is another important effect of the steps. It is possible to make the step height correspond to 2πphase

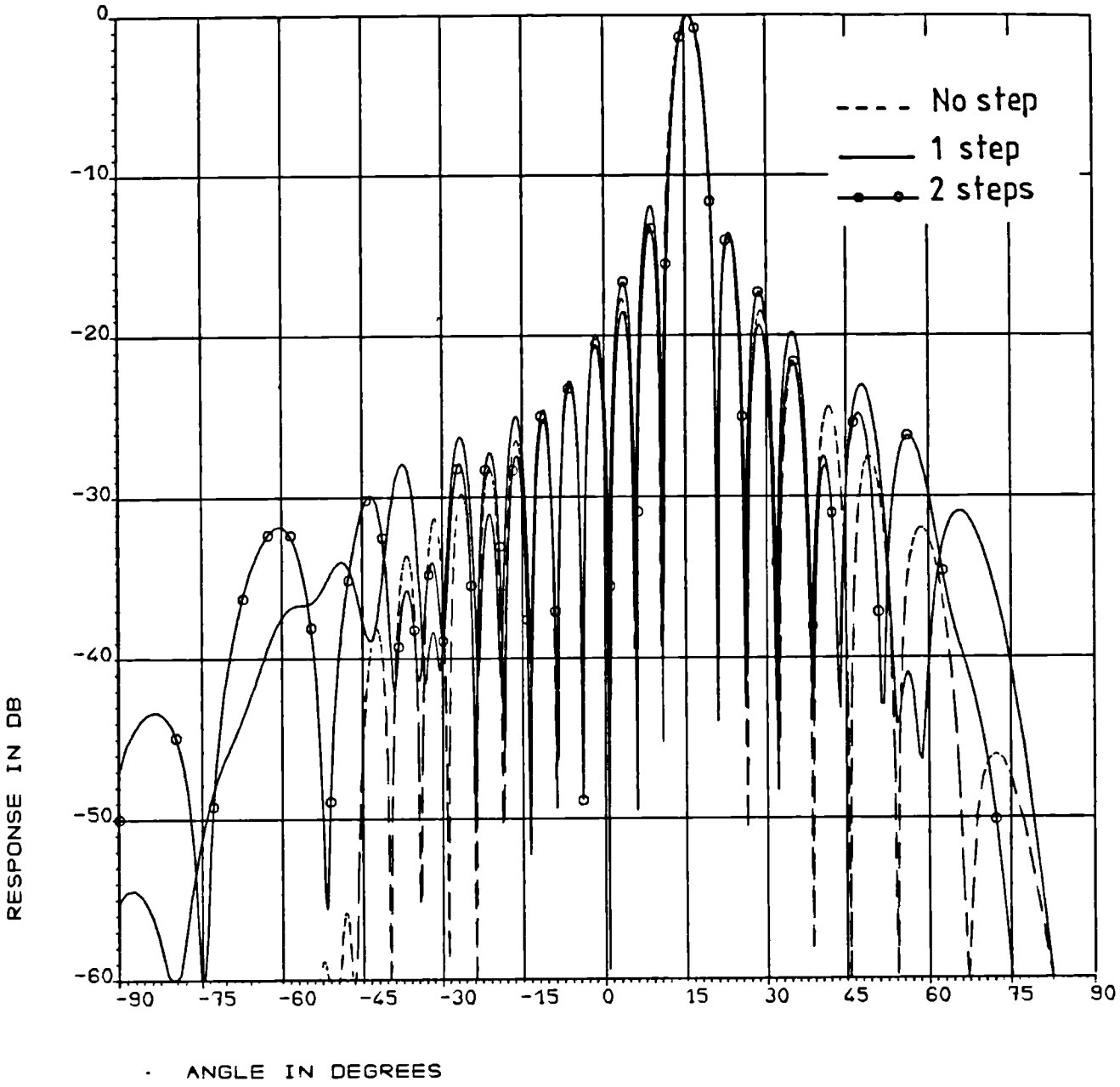

Fig 6.2. Degradation of the radiation pattern due to stepping of the wedge.

difference only at a single frequency and a certain angle of incidence or emergence of the waves. So, any change in frequency or change in the angle of incidence or emergence will disturb this condition. It has been shown that the bandwidth of the stepped system reduces to 25/n percent, where n is the number of steps [37]. In our scheme of beam steering, both the frequency and the angle of incidence or emergence may vary, which makes the situation worse. Considering all these factors, the number of steps should be optimized to produce the best overall performance of the wedges.

6.3. Effect of Loss in The Wedges

The propagation of electromagnetic waves in a lossy medium is discussed in section 3.6 . The amplitude of a plane wave is reduced as the wave propagates through a medium. The thickness of the dielectric wedge considered varies with position. So, a plane wave incident on the dielectric wedge emerges with an amplitude taper. The portion of the plane wave passing through the thicker end suffers more reduction in amplitude compared to the thinner end of the wedge. If α_d is the attenuation factor of the wedge material, then the amplitude at the emergence face will have an $e^{-\alpha_d x}$ taper, as shown in fig(6.3). So, we need to take into consideration this change in amplitude distribution while using the relations in section 4.2 to evaluate the radiation pattern.

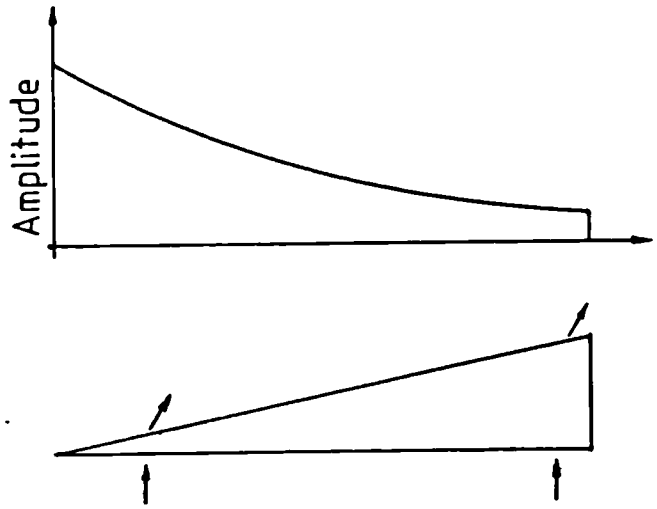

Fig 6.3. Exponential amplitude taper on the wedge aperture due to the attenuation of the wedge material.

Fig(6.4) shows the radiation pattern of a 12λ aperture for two aperture illuminations, one with uniform amplitude distribution and the other with an exponential taper of $e^{-.072x}$ (here x is expressed in wavelengths). This attenuation factor corresponds to a maximum taper of -10dB at the thickest edge of the wedge. Comparing the patterns, we can see that there is very little change in pattern other than the slight increase in sidelobes and the filling in of the nulls. Although, there is no substantial change in the radiation pattern, there will be an overall reduction of gain. This reduction in gain can be minimized by stepping the wedges, as discussed in section 6.2 which reduces the overall thickness of the wedges. The amplitude pattern on the wedge face will look like a periodic exponential

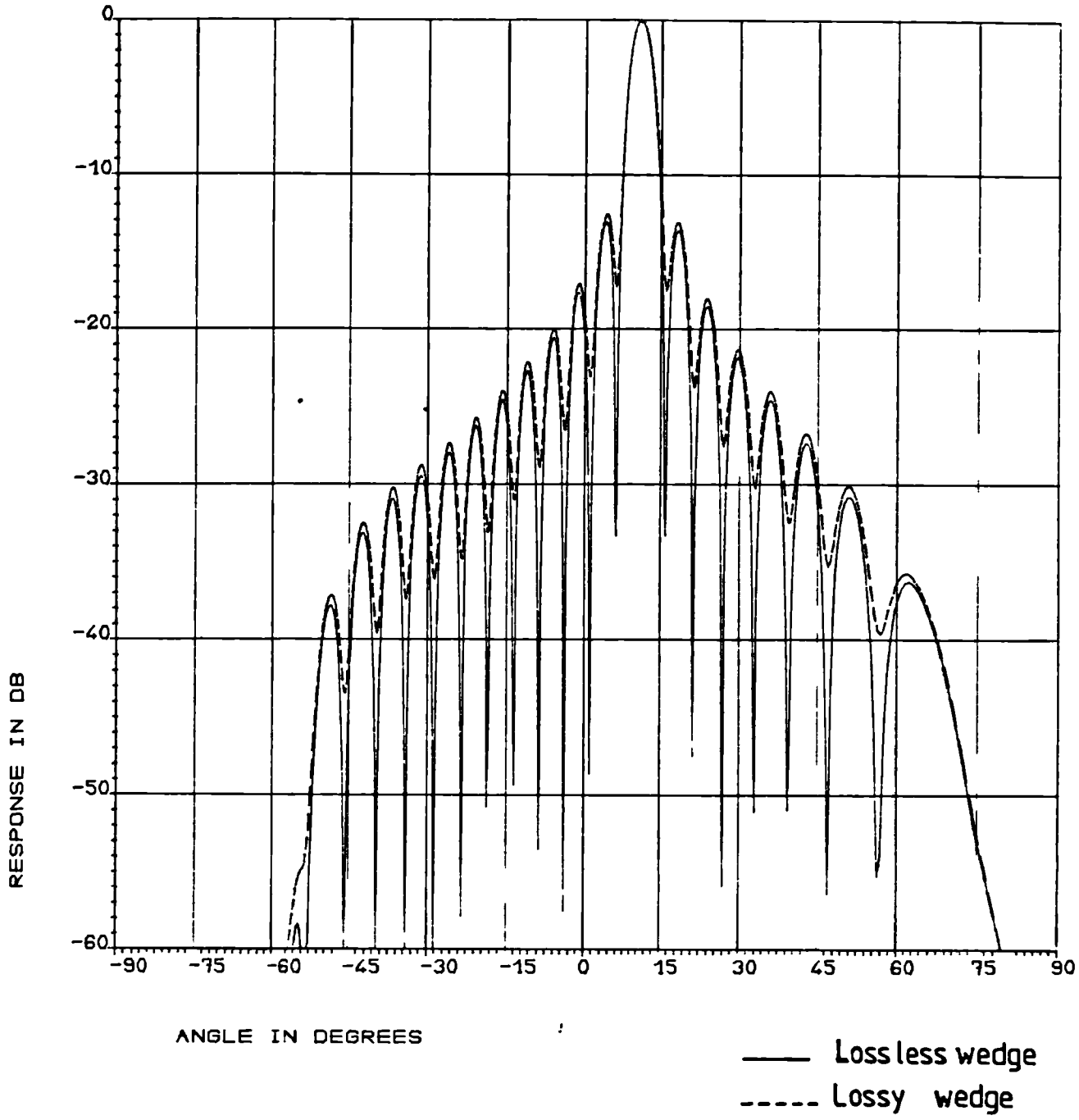

Fig 6.4. Radiation pattern of a lossy wedge compared to that of a loss free wedge.

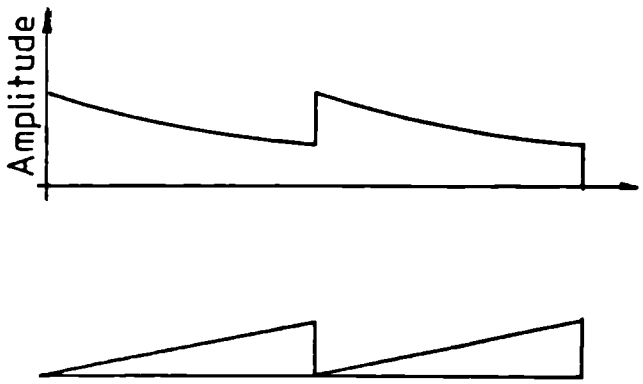

Fig 6.5. Amplitude distribution on the face of a lossy wedge having steps.

function as shown in fig(6.5). This should not change the overall radiation pattern by a great deal when compared to the stepped wedges with negligible losses, because the radiation patterns of the individual stepped segments do not change appreciably due to loss.

6.4 Matching layers for the dielectric wedges

The importance of a matching layer has been discussed in section 4.3.3 . There are different techniques of matching the dielectrics, and these have different responses as a function of frequency and angle of incidence. In this section we shall be discussing the general behaviour of the matching techniques applied to

our beam steering mechanism.

The arrangement of the wedges is chosen as shown in the fig(6.6). Hence the first face of the first wedge is parallel to the aperture plane. This ensures normal incidence of the waves from the antenna and a constant emergence angle of the main beam from the second face of

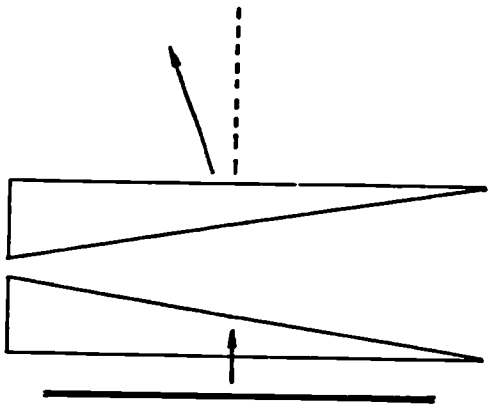

Fig 6.6. A wedge-antenna system for beam steering.

the first wedge. So, the faces of the first wedge can be matched quite effectively as the incidence or the emergence angles do not change. But the situation is quite different for the second wedge. The incidence angle at the first face of the second wedge can vary from $\theta+\Omega$ to $\theta-\Omega$ depending on the relative position of the second wedge with respect to the first one. Here θ is the deflection angle for the first wedge and Ω is the wedge angle.

Similarly, the emergence angle of the second wedge can vary from 0^{o} to a maximum deflection of θ_{o}. Hence we may attain the best performance by designing the matching layer corresponding to an angle which is approximately midway between the maximum and the minimum of the beam deflection angle. For small deflection angles, such an optimization may not be of great importance, as the performance of the conventional matching layers may be quite satisfactory over the required range of frequency and beam steering angle.

6.5 Reduction in gain due to beam steering

The antenna gain is reduced as the beam of the antenna is steered from the boresight. This is due to the reduction in the projected area of the antenna aperture. In our scheme of beam steering, the wedges are placed in the near field of the antenna. The aperture distribution is not very much changed on the emergence face of the first wedge except that the aperture size is increased by a factor of $1/\cos\Omega$, where Ω is the wedge angle. The situation is illustrated in fig(6.7). If the beam is steered by an angle of θ_1 from the boresight, it makes an angle of $(\theta_1+\Omega)$ with the emergence face of the wedge, reducing the gain by a factor of $\cos(\theta_1+\Omega)$. Hence, there is an overall reduction of gain by a factor of $\cos(\theta_1+\Omega)/\cos^{2}\Omega$, considering the increased projected area on the face of

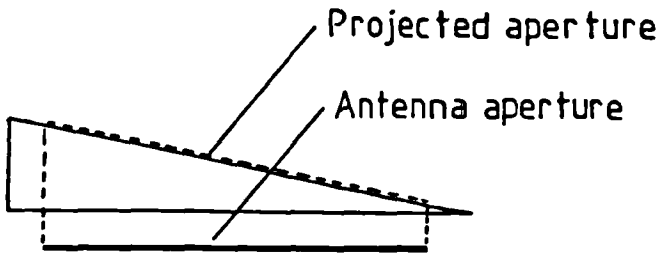

Fig 6.7. Increase in amplitude area due to the projection of the antenna aperture on the wedge aperture.

the wedge. The relation for the radiation from the wedge, developed in section 4.2 was used to check and confirm the validity of this reduction in gain. Fig(6.8) shows the computed gain for $\varepsilon_r = 10$ using eqn(4.4) and the gain computed using the cosine rule. They are very nearly the same. When two wedges are used as shown in fig(6.6) the gain changes by $\cos\theta$. But for fig(6.9) it changes by $\cos(\theta + \Omega)$. This shows an interesting possibility of compensating the gain as the beam is steered, when the wedge has a dielectric constant less than unity. This is possible if waveguide-like structures are used to make the wedges.

Besides the obliquity factor, there will be other small losses involved - like spill over losses and losses due to reflections. However they should be quite small. So, the overall loss of the antenna is dominated by the loss in the dielectric material and loss due to the reduction in

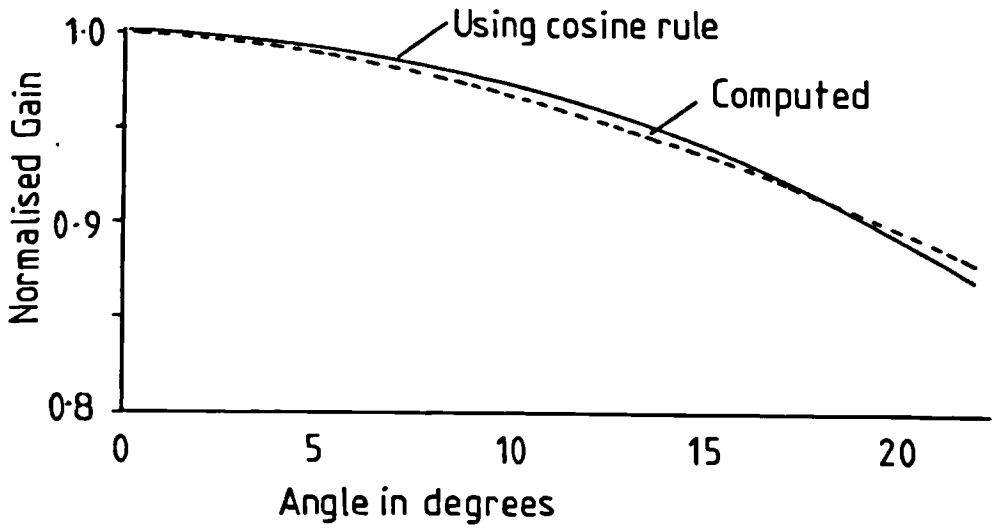

Fig 6.8. Reduction in gain due to beam steering by a single wedge.

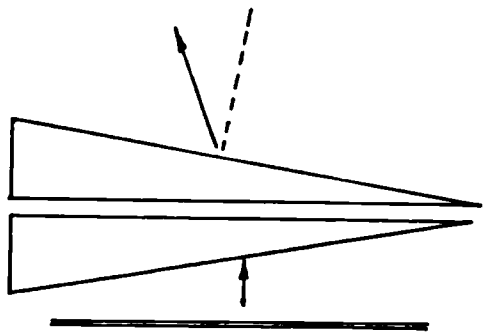

Fig 6.9. Wedge-antenna system with the first face of the first wedge being oblique to the antenna aperture.

the projected aperture as the beam is steered. Fig(6.10) shows a plot for the computed value of gain vs. the steering angle. The curve is very nearly the cosine curve of the steering angle. The discrepancy observed is due to the loss due to reflection.

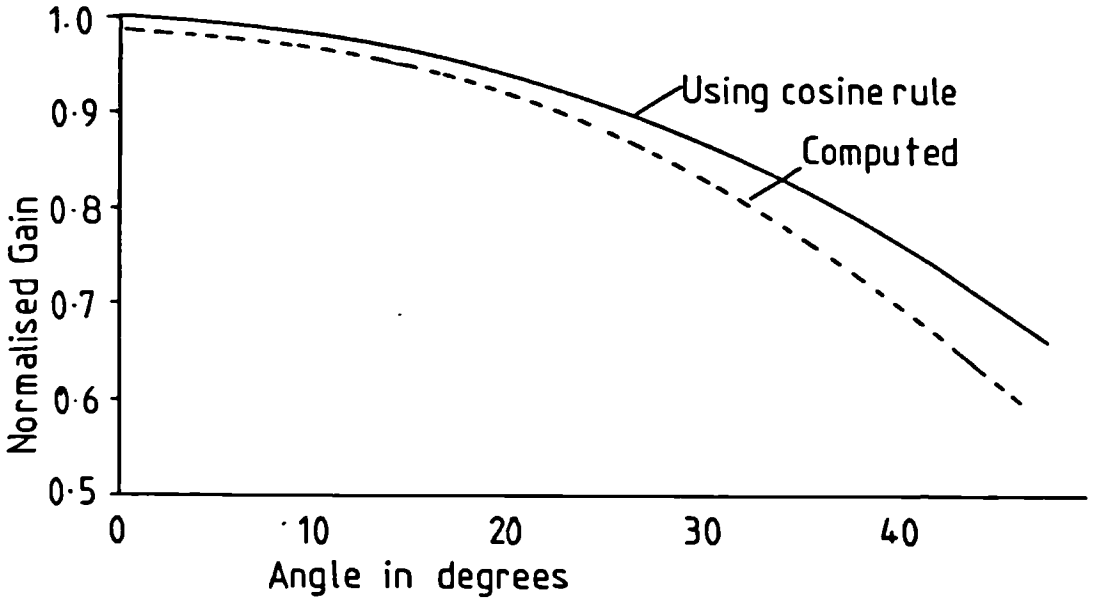

Fig 6.10. Reduction in gain due to beam steering using two wedges.

6.6 Size of the wedges in relation to the size of the antenna

The relation developed in chapter 4 to predict the overall radiation pattern takes into consideration the dimensions of the wedge aperture. It is easy to understand that the wedges should not be smaller than the antenna, because, otherwise, they will block a portion of the aperture. The amplitude distribution in the near field remains approximately the same as the amplitude distribution of

the antenna. But there will be a shift of the overall amplitude pattern depending on the phase tilt on the aperture. The situation is illustrated in fig(6.11). Fig(6.11a) shows the amplitude distriution for an aperture having uniform phase. Fig(6.11b) shows the shift in the amplitude distribution towards the direction of the main beam when there is a phase tilt on the aperture. The situation when the waves emerge from the first wedge is similar. The main beam is tilted and there is a lateral shift in the amplitude pattern as the waves travel from the antenna to the emergence face of the second wedge. This lateral shift in the amplitude pattern requires that the size of the wedges should be made larger, so that they can intercept the majority of the amplitude distribution.

We can calculate the amount of shift in the amplitude pattern approximately, using simplified assumptions. There is almost no shift in pattern inside the first wedge as the main beam is steered after the waves emerge from it. So, the significant amount of shift occurs in the space between the first and the second wedge. There will be some shift inside the second wedge depending on the dielectric constant of the wedge material. If r is the radius of the wedges and Ω is the wedge angle, then the thickness of the wedge at its thickest end is $2.r.\tan\Omega$. Considering the wedges are placed as shown in the fig(6.9), the minimum possible distance between the

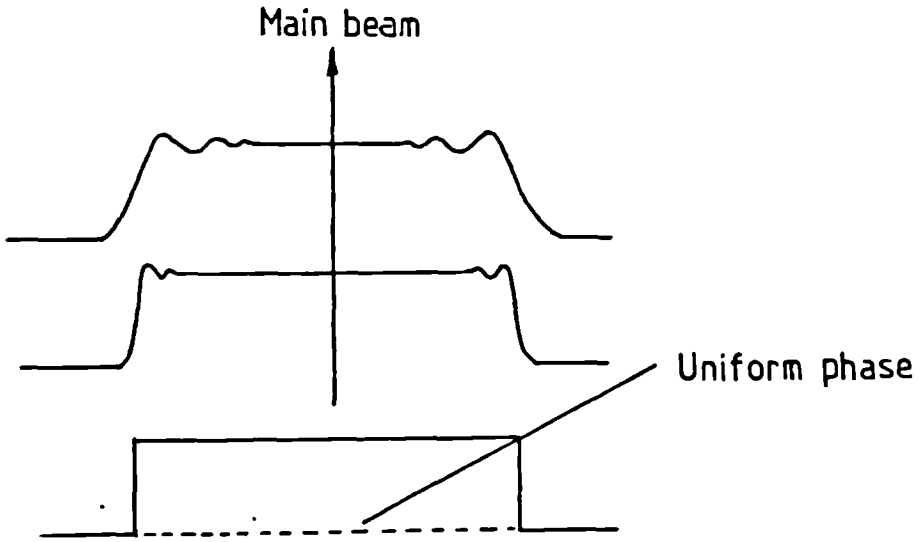

Fig 6.11a. Amplitude distribution at a distance from an aperture having uniform phase.

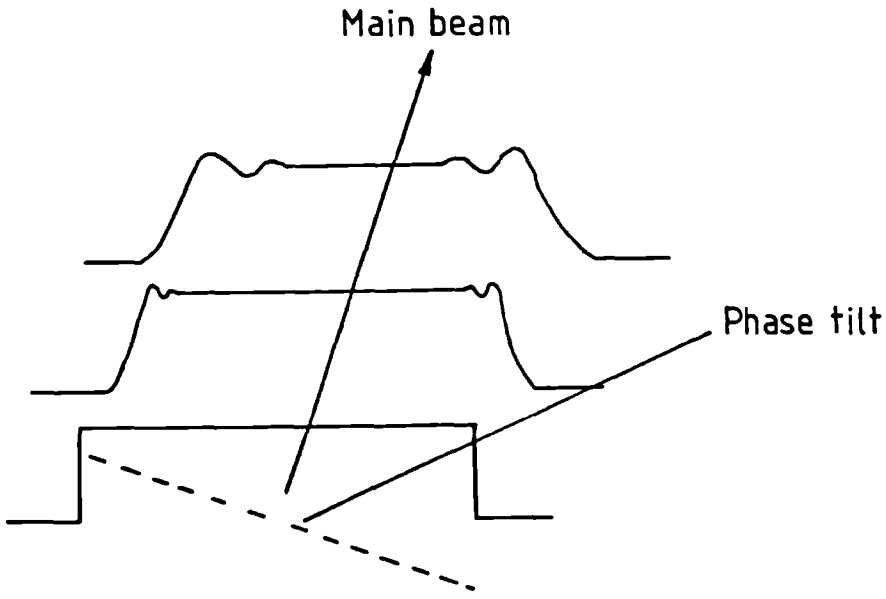

Fig 6.11b. Lateral shift in amplitude distribution at a distance from an aperture having a phase tilt.

centres of the second face of the first wedge and the first face of the second wedge is $2.r.\tan\Omega$. If ε_r is the dielectric constant of the wedge material, then the emergence angle of the main beam from the first wedge is

$$\theta_1 = \sin(\sqrt{\varepsilon_r}\sin\Omega) - \Omega \qquad \ldots. \quad (6.3)$$

and the shift in pattern $\Delta_1 = 2.r.\tan\Omega \ .\tan\theta_1$

The angle inside the second wedge is -

$$\theta_2 = \sin^{-1}(\sin(\theta_1 - \Omega)/\sqrt{\varepsilon_r}) + \Omega \qquad \ldots(6.4)$$

Hence the shift inside the second wedge $\Delta_2 = r.\tan\Omega \ .\tan\theta_2$, since the thickness of the wedge is $r.\tan\Omega$ at the centre.

Hence the total shift $\Delta = \Delta_1 + \Delta_2 \qquad \ldots.(6.5)$

For higher dielectric constant material Δ_2 will be much smaller than Δ_1 . Fig(6.12) and fig(6.13) show the amplitude distribution of a 12λ uniformly illuminated aperture for a single and a double wedge. We can see the shift in the amplitude pattern in fig(6.13). Computing the shift from equation (6.5) we can see that the amplitude pattern is reduced quickly beyond the computed radius of 6.9λ . Evaluating the size of the wedge from eqn(6.5) needs an approximate diameter of the wedges. This can be taken to be equal to the size of the antenna. The radius of the wedge should be increased by the amount of shift of the pattern.

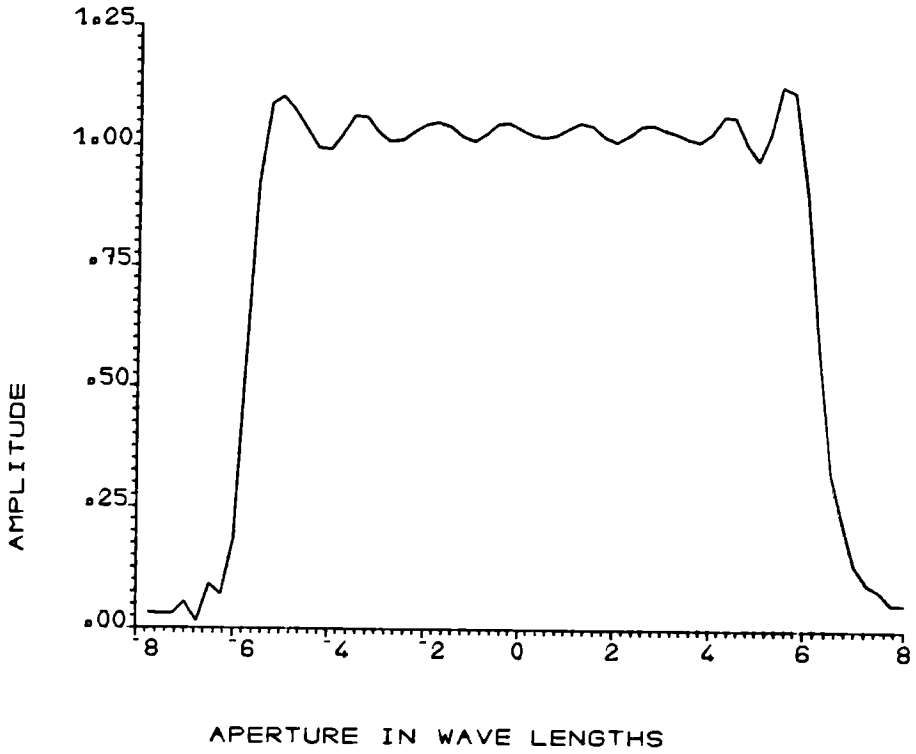

Fig 6.12. Amplitude pattern on the emergence face of the first wedge.

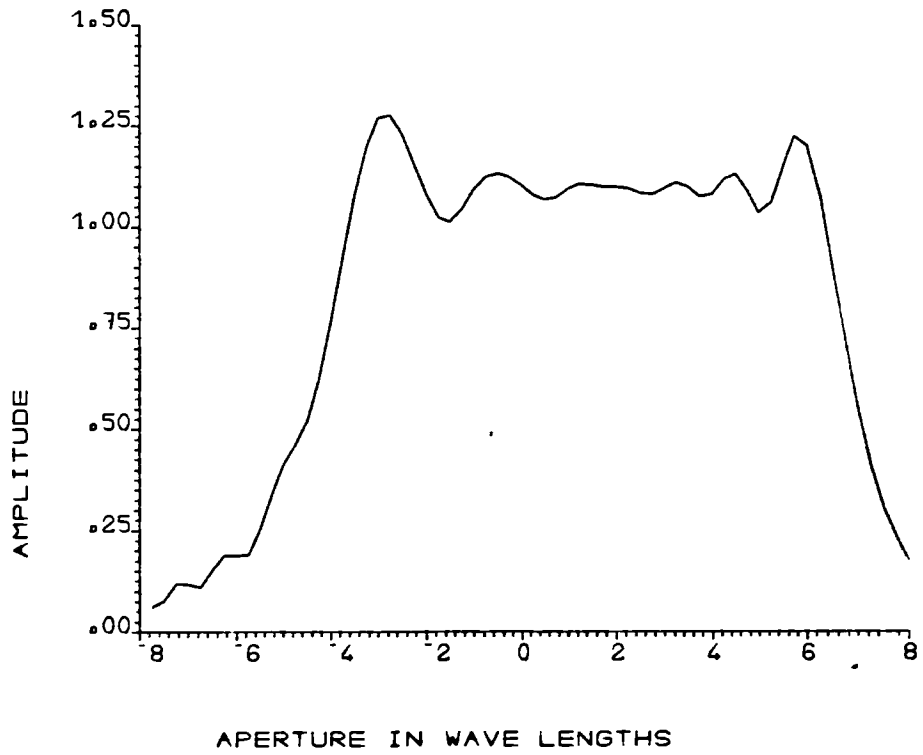

Fig 6.13 Amplitude distribution on the emergence face of the second wedge.

6.7 Generation of Cross-polarization

It has been discussed in section 3.2 that when the incidence angle is different than normal, the wave impedances are different for different polarizations. Hence the reflection co-efficient at a dielectric interface can be different depending on the polarization of the incident wave. Any wave incident at an angle ψ with an arbitrary polarization can be resolved into two components, one having polarization in the plane of incidence and the other normal to the plane of incidence. Due to the difference in reflection co-efficients, the transmitted components of the waves change their amplitudes and phase differently and thus cause the direction of polarization of the overall transmitted wave to change. However, when the incident wave is polarized in the plane or perpendicular to the plane of incidence, there will be no change in polarization.

6.7.1 Linear Polarization

Let an incident plane wave have unit amplitude and the electric field make an angle ψ with the plane of incidence. Hence the components of the electric field in the planes parallel and perpendicular to the plane of incidence are $\cos\psi$ and $\sin\psi$ respectively.

Let $T_1 e^{j\sigma_1}$ and $T_2 e^{j\sigma_2}$ be the complex transmission functions for the total electric fields for the two

components discussed above. So, the transmitted waves are $\cos\psi\, T_1 e^{j\phi_1}$ and $\sin\psi\, T_2 e^{j\phi_2}$ respectively. Therefore, the cross polar component of the emergence wave can be calculated by taking the contribution of these components of the incident wave in a direction perpendicular to the direction of the incident polarization.

The cross polar component -

$$C.P. = (\cos\psi\, T_1 e^{j\phi_1}) \cdot \sin\psi - (\sin\psi\, T_2 e^{j\phi_2}) \cdot \cos\psi$$
$$= \sin\psi \cdot \cos\psi \cdot (T_1 e^{j\phi_1} - T_2 e^{j\phi_2}) \quad ....(6.6)$$

For a certain angle of incidence, $T_1 e^{j\phi_1}$ and $T_2 e^{j\phi_2}$ are constants. Hence differentiating C.P. with respect to polarization angle ψ , we find the angle of maximum cross polar generation. This angle is 45°. When the transmitted fields are calculated for a dielectric interface, they are real quantities. But the overall transmitted field becomes complex when there is a third layer of dielectric medium in between, for example a quarter wave matching layer.

6.7.2 Circularly Polarized Waves

For the sake of analysis, let us split up the circularly polarized wave into two components, one parallel and the other perpendicular to the plane of incidence and having a phase shift of 90 degrees. Let the incident electric field be resolved into two components of equal amplitude -

$$\bar{E}_i = \bar{a}_1 + j\bar{a}_2$$

where $\bar{a}_1$ and $\bar{a}_2$ are unit vectors in the direction parallel and perpendicular to the plane of incidence respectively. So, after transmission, they have complex amplitudes $T_1 e^{j\phi_1}$ and $T_2 e^{j\phi_2}$ respectively.

$$\bar{E} = (\bar{a}_1 T_1 e^{j\phi_1} + \bar{a}_2 T_2 e^{j\phi_2})$$

$$= \frac{(T_1 e^{j\phi_1} + T_2 e^{j\phi_2})}{2} (\bar{a}_1 + j\bar{a}_2) + \frac{(T_1 e^{j\phi_1} - T_2 e^{j\phi_2})}{2} (\bar{a}_1 - j\bar{a}_2)$$

From the above expression we can separate out the cross polar component -

$$C.P. = (T_1 e^{j\phi_1} - T_2 e^{j\phi_2})/2 \qquad .....(6.7)$$

If we compare this cross-polar term to the linear cross-polar term, we would find that they are same for $\psi = 45^\circ$ i.e., the maximum cross-polar component for linear polarization is the same as that of the circularly polarized wave for the same angle of incidence. So, the diagrams presented in this chapter are computed for circular polarization only. Fig(6.14) shows the cross polarization for two different dielectric material, $\varepsilon_r = 2$ and $\varepsilon_r = 100$, in the presence of a matching layer for normal incidence from air. Maximum cross polarization occurs for an incidence angle of 90°. The maximum value of cross

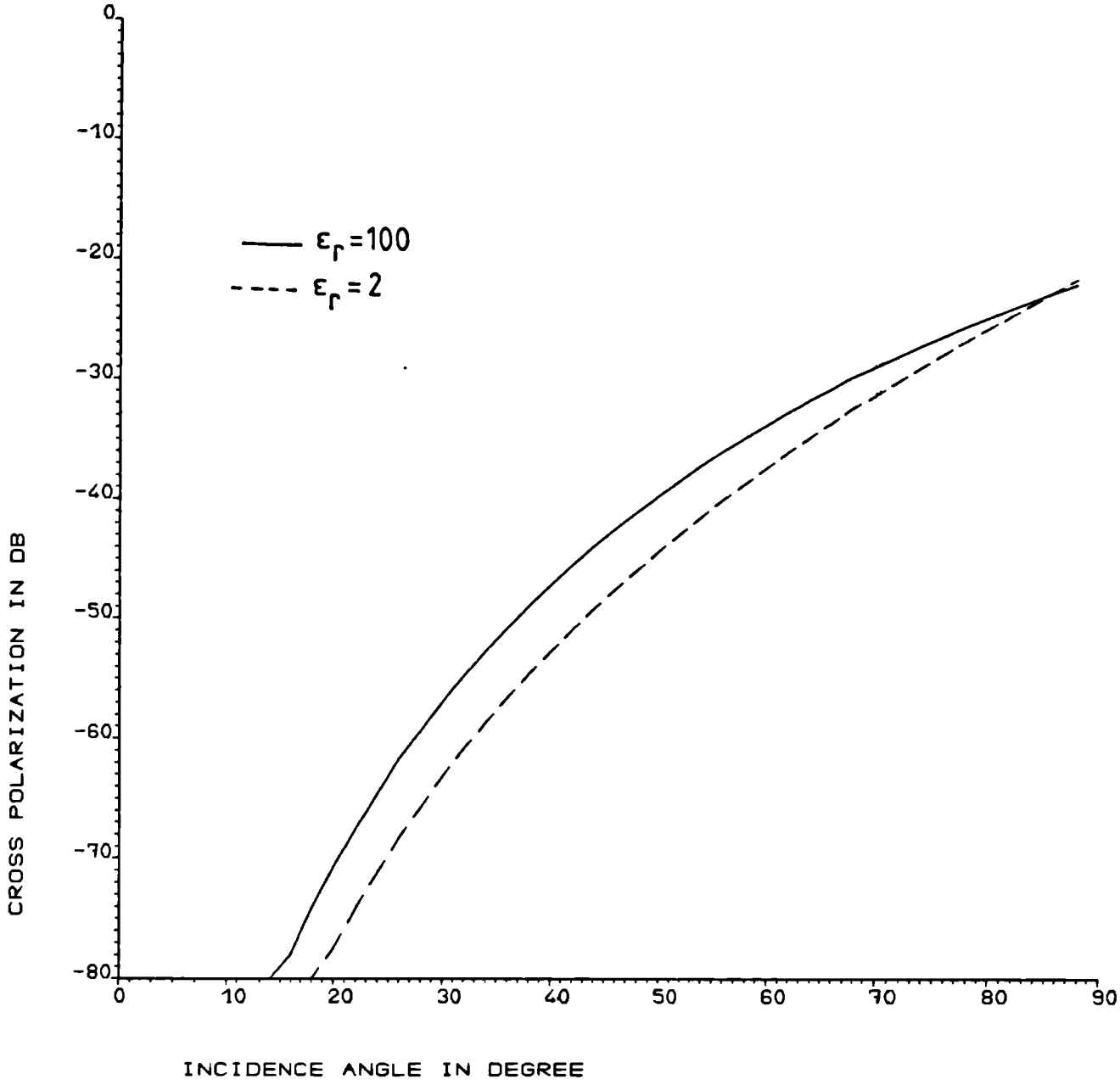

Fig 6.14. Generation of cross polarization at a dielectric interface matched for normal incidence.

polar component is about -20dB. For small incidence angles, cross polarization is very small. Fig(6.15) and fig(6.16) show cross polarization for the same two media, but matched for TE and TM waves respectively, for an incidence angle of 30^{o}. Although the response is similar at large incidence angles, the cross polar components are higher at smaller angles. This is due to the difference in reflection co-efficient between the TE and TM components of the incident waves (fig(3.4), (3.5), (3.6)). When the incidence angle is near 30^{o}, one of the constituent polarizations of the incident wave has very small reflection compared to the other polarization. So, the cross polarization is dominated by the component having the higher reflection co-efficient. For ε_r =2, there is a dip on the curve near 30^{o}, but the dip is absent when ε_r=100.This is due to the higher values and the greater differences of reflection co-efficients for the TE and TM waves when ε_r =100, which can be seen in fig(3.5) and fig(3.6).

Comparing all the figures for the cross-polarisation, we can safely conclude that cross-polarization is quite low for incidence angles $<30^{o}$.

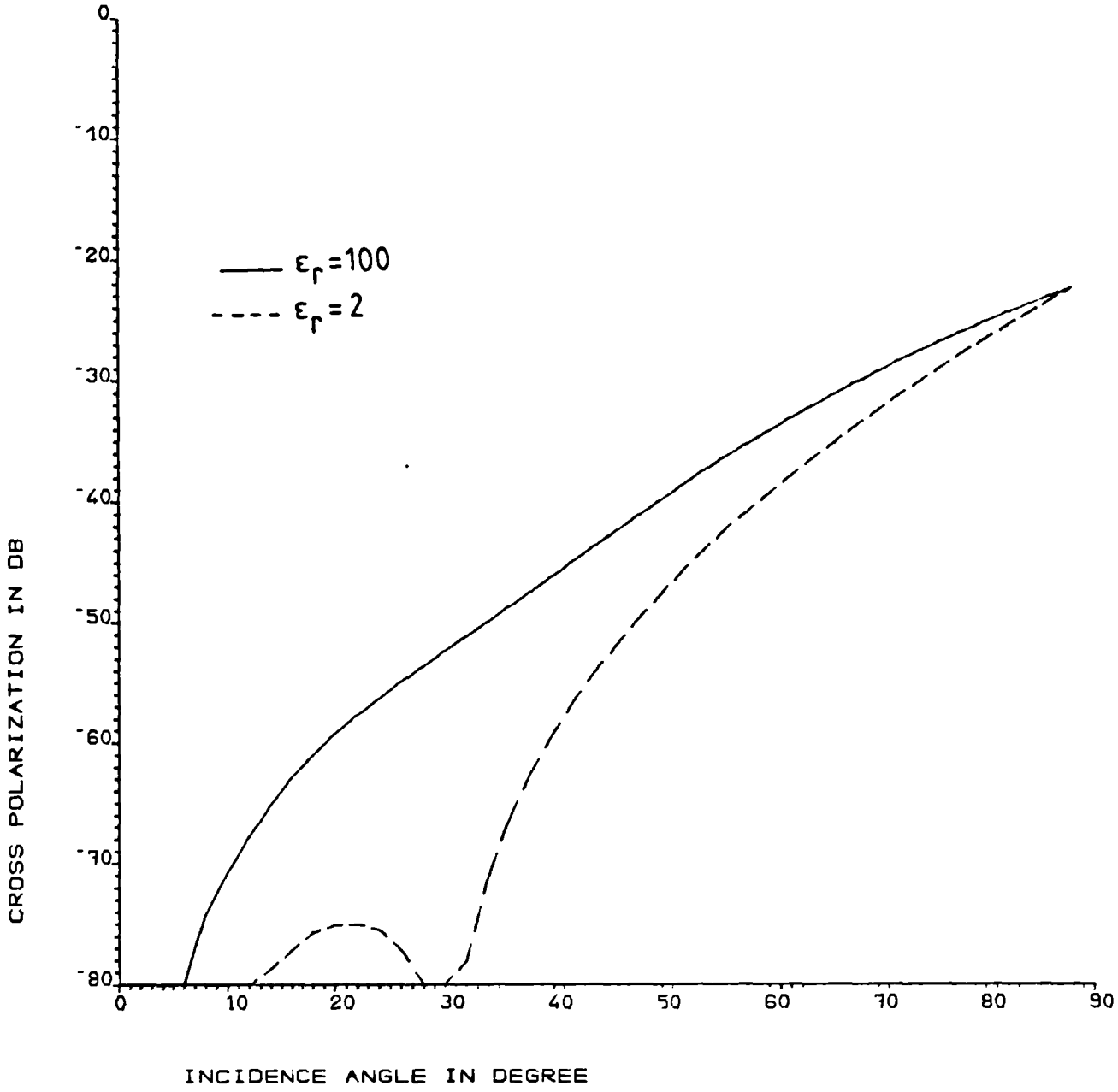

Fig 6.15. Generation of cross polarization at a dielectric interface matched for TE waves at an incidence angle of 30^{o}.

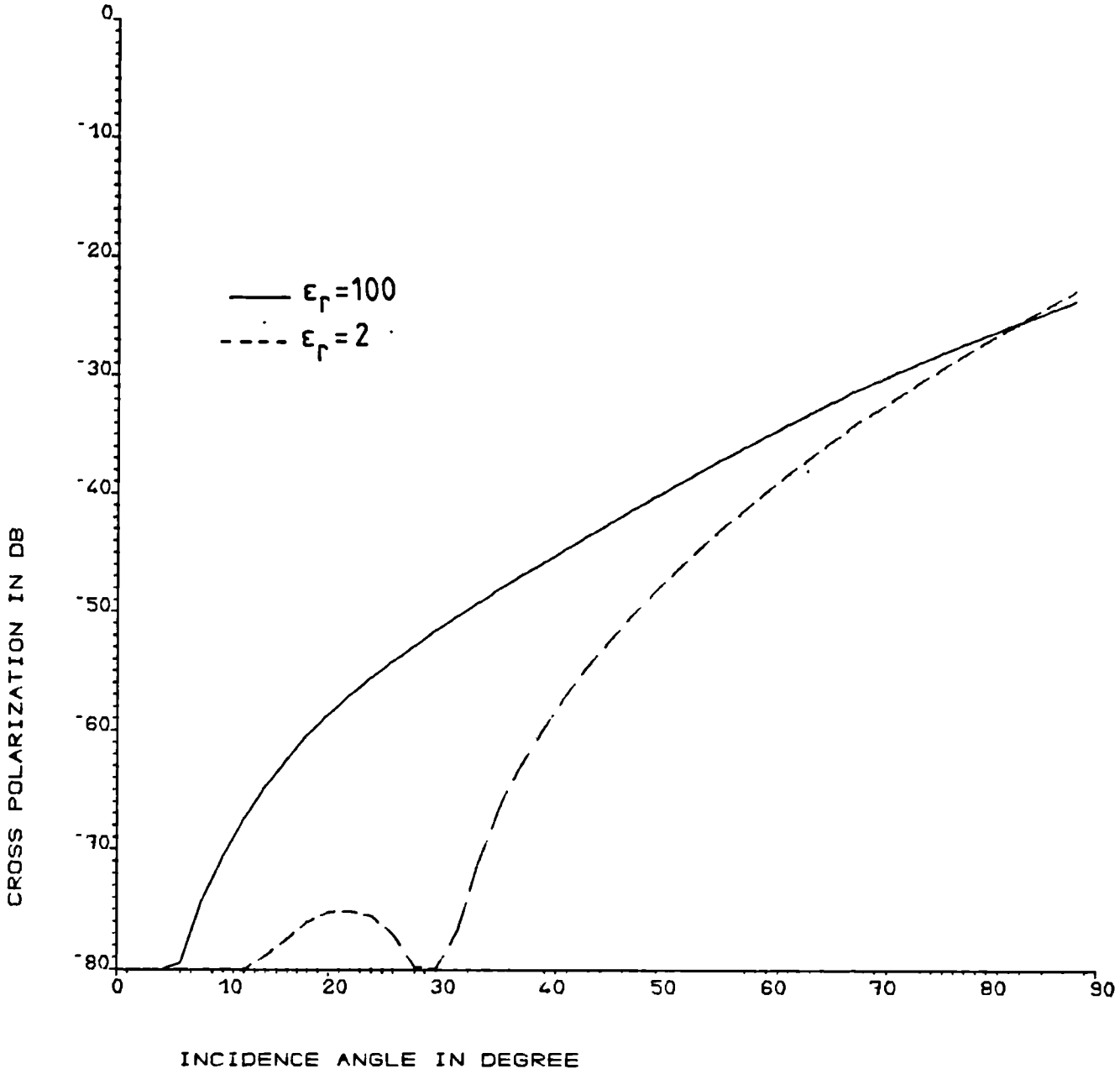

Fig 6.16. Generation of cross polarization at a dielectric interface matched for TM waves at an incidence angle of 30^{o}.

6.7.3 Experimental Investigation

An experimental investigation was made to measure the cross polar performance of the wedges. From the discussions in section 4.6.1, we can see that the generation of the cross polar components depends on the polarization angle of the incident wave with respect to the dielectric interface. Theoretically, no cross polarization should be present for a polarization angle of 0^{o} or 90^{o}. Maximum cross polarization occurs at a polarization angle of 45^{o}. So, we used an array of a pair of horns tilted by 45^{o} to obtain the direction of electric field 45^{o} to the horizon to measure the worst possible polarization for that pair of wedges. A schematic diagram is shown in fig(6.17). The dimensions of the horns are

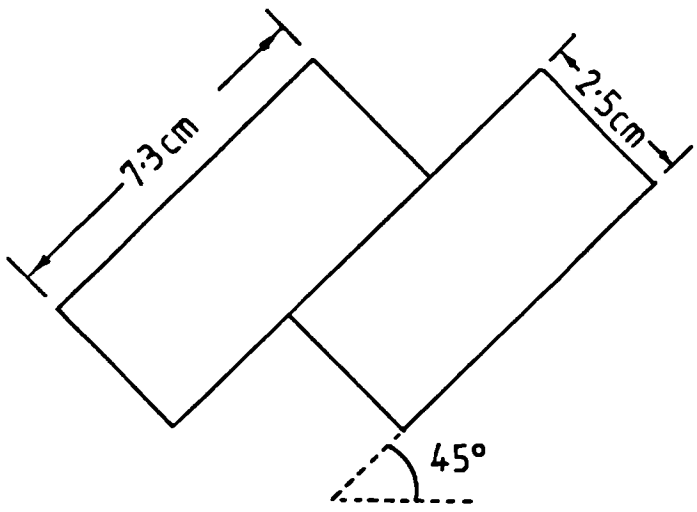

Fig 6.17. Tilted horn to produce a polarization angle of 45^{o} with the horizon.

also shown in the figure. The cross polar pattern of the array was measured with and without a perspex wedge, and the results are shown in fig(6.18). The radiation pattern of the array on its own is also shown on the same plot for comparison. We can see that there is no significant change in the level of cross polarization in the case when the wedge is used. This is an expected result as we can conclude from the computed cross polarization for different dielectrics (fig(6.14),(6.15),(6.16)) that the cross polarization is very small even for a large amount of beam steering ($<30^{o}$).

6.8 Discussion

Different important aspects of the beam steering technique using dielectric wedges have been studied in this chapter. Weight and volume of the wedges seem to be two of the most important aspects of the scheme as far as the commercial usage is concerned. Stepping is a practical way of reducing the weight, but there is a consequent deterioration of the radiation pattern. This deterioration is smaller for a reasonably high dielectric material ($\varepsilon_r > 4$) as the height of the steps will be smaller than a wavelength. Although stepping of the wedges degrades the radiation pattern, the loss inside the material will be reduced. So, there may not be an overall penalty for stepping the wedges depending on the loss factor of the material used. Hence for a system like

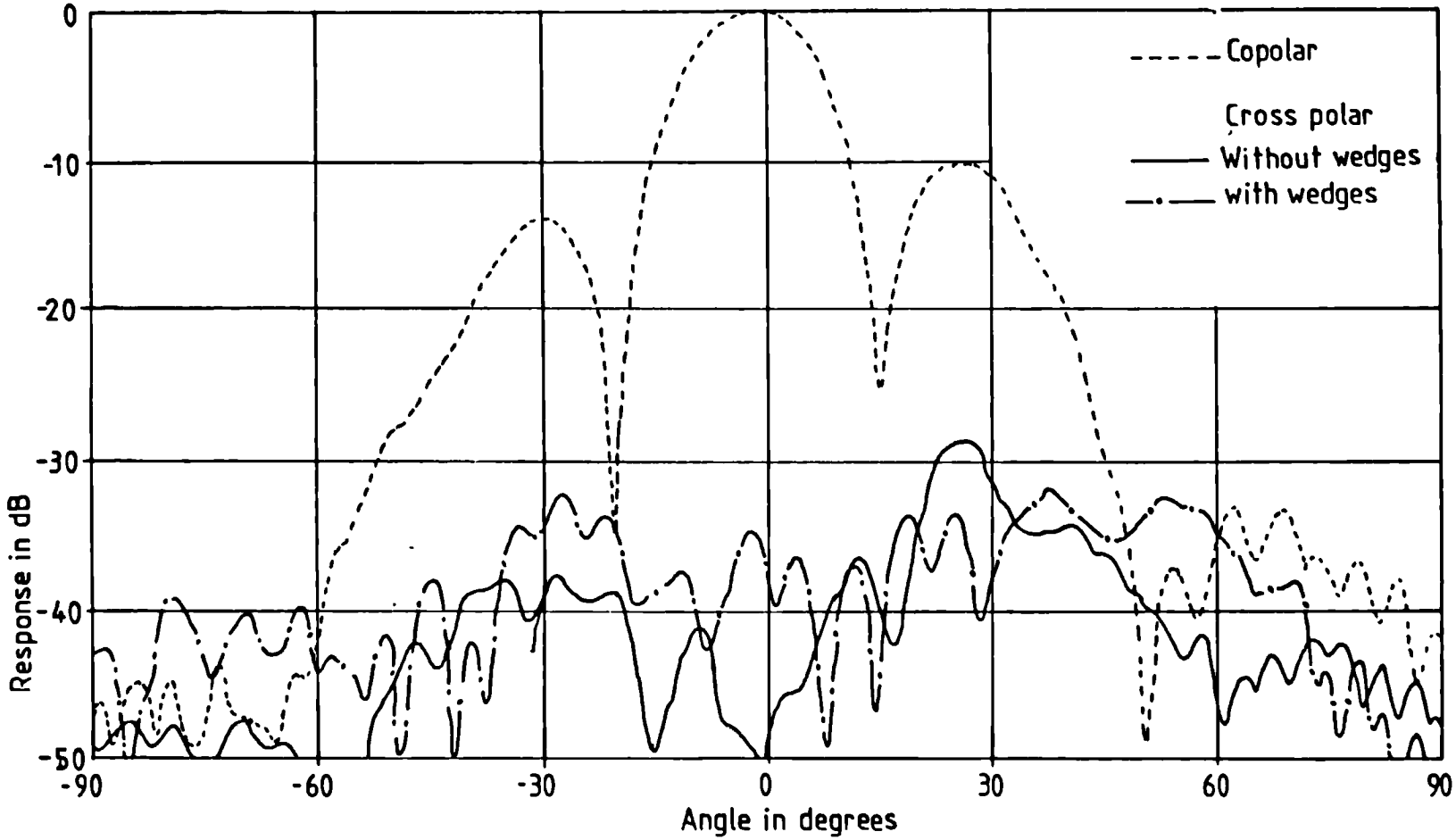

Fig 6.18. Measured cross polar pattern due to a single wedge.

DBS, where the bandwidth requirement is not very high (<7%), stepping the wedges is a practical proposition.

The analysis in section 6.6 has shown that the size of the wedges should be made slightly larger than the size of the antenna to be used. The diameter of the wedges should be, generally, 2-3 wavelengths larger than the size of the antenna. This ensures a minimal loss of power without increasing the size of the wedges by a large amount. In case of large antennas, such as a 50cm dish, the size of the wedges can be made equal to the size of the antenna without any appreciable loss. However, it is still important to take the wedge angle and the amount of beam steering into consideration to find out the amount of shift in the aperture distribution discussed in section 6.6.

Reduction in the gain of the antenna in this technique is mainly dependent on the loss inside the wedge material. Hence a good dielectric material can make the loss negligible. Although the loss due to the inclination of the main beam appears unavoidable, some improvement can be achieved by using artificial dielectrics with dielectric constants less than unity. In that case, the wedges can be placed as shown in fig(6·9) and the deflection of the main beam is such that it increases the projected area on the wedge face. But a similar situation is not possible when the dielectric constant is greater than 1.

Detailed analysis of the cross polarization is performed in section 6.7. It is evident from the computed results (fig(6.11),(6.12),(6.13)) that the cross polarization does not vary by any significant amount (<5dB) for different dielectric materials. The cross polarization is nearly -60dB for an incidence angle of 30^{o}. From the computed and the experimental results we can safely conclude that the effect of cross polarization can be neglected for any steering angles less than 30^{o}.

CHAPTER 7 : Essentials of Wedge Design

7.1 Introduction

The dimensions of the dielectric wedges are determined mainly by the maximum beam steering requirements. For the same maximum achievable beam steering angle we can have different dimensions of the wedges, depending on the dielectric constant of the material. Once the wedge is made, it is important to know the position of the beam when the wedges are placed at any arbitrary relative position. All thses involve quite complicated mathematical computations which may be difficult for both the user and the designer. Hence, some charts are provided in this chapter to facilitate the design and use of the wedges.

7.2 Deflection of the main beam in relation to the wedge angle and the dielectric constant

The maximum deflection of the main beam by a pair of wedges is dependant on the wedge angle Ω and the dielectric constant ε_r of the wedge material. Placing the first wedge with its first face parallel to the antenna aperture, the deflection by the first wedge is

$$\theta_1 = \sin^{-1}(\sqrt{\varepsilon_r}\sin\Omega) - \Omega \qquad \text{.....(7.1)}$$

This deflected beam is incident on the second wedge at an angle of $\theta_1 - \Omega$, as shown in fig(7.1), and enters the

second wedge at an angle of θ_2 where

$$\theta_2 = \sin^{-1}(1/\sqrt{\varepsilon_r} \sin(\theta_1 - \Omega)) \quad .....(7.2)$$

Hence the overall deflection on leaving the second wedge is

$$\sin\theta_o = \sqrt{\varepsilon_r} \sin(\theta_2 + \Omega) \quad .....(7.3)$$

Substituting θ_2 in terms of θ_1 and the θ_1 in terms of Ω, the final expression is obtained in terms of Ω and ε_r.

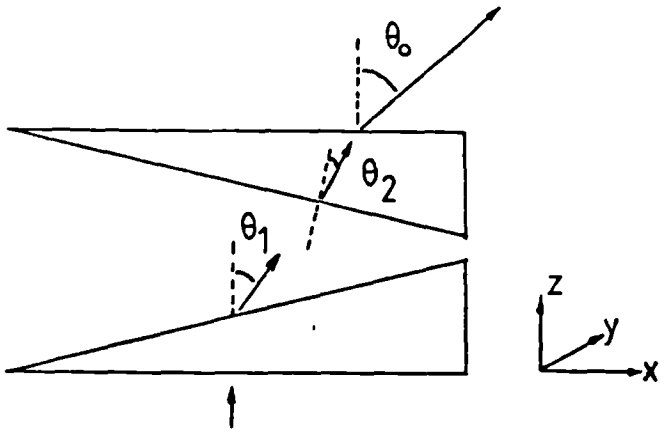

Fig 7.1. Incidence and emergence angles for the wedges in a wedge-antenna system.

Once the values of Ω and ε_r are found, it is not very difficult to calculate the maximum beam deflection θ_o. But when the maximum deflection is known, it is not easy to find out a suitable combination of Ω and ε_r . So, a chart is provided in fig(7.2) which plots wedge angle Ω vs. the dielectric constant for different values of maximum beam deflection angle θ_o. When the value of maximum beam deflection is decided, there are an infinite number of combinations of Ω and ε_r for a given value of maximum beam deflection angle. From the designer's point of view it is also important to know the emergence angle of the main beam from the first wedge for the design of a suitable matching layer. This can be calculated from eqn(7.1).

7.3 Designer's Chart

The beam deflection angle can be varied by the rotation of the dielectric wedges relative to each other. It is simpler from the user's point of view to know the beam position in terms of azimuth and elevation. Before going into more detail about the determination of azimuth and elevation, beam steering behaviour of the wedges should be studied in more detail.

Let us define the reference axis of the wedges by joining the two points on the face of the wedge, where the thickness of the wedges are minimum and maximum respectively, as shown in fig(7.3). The positive

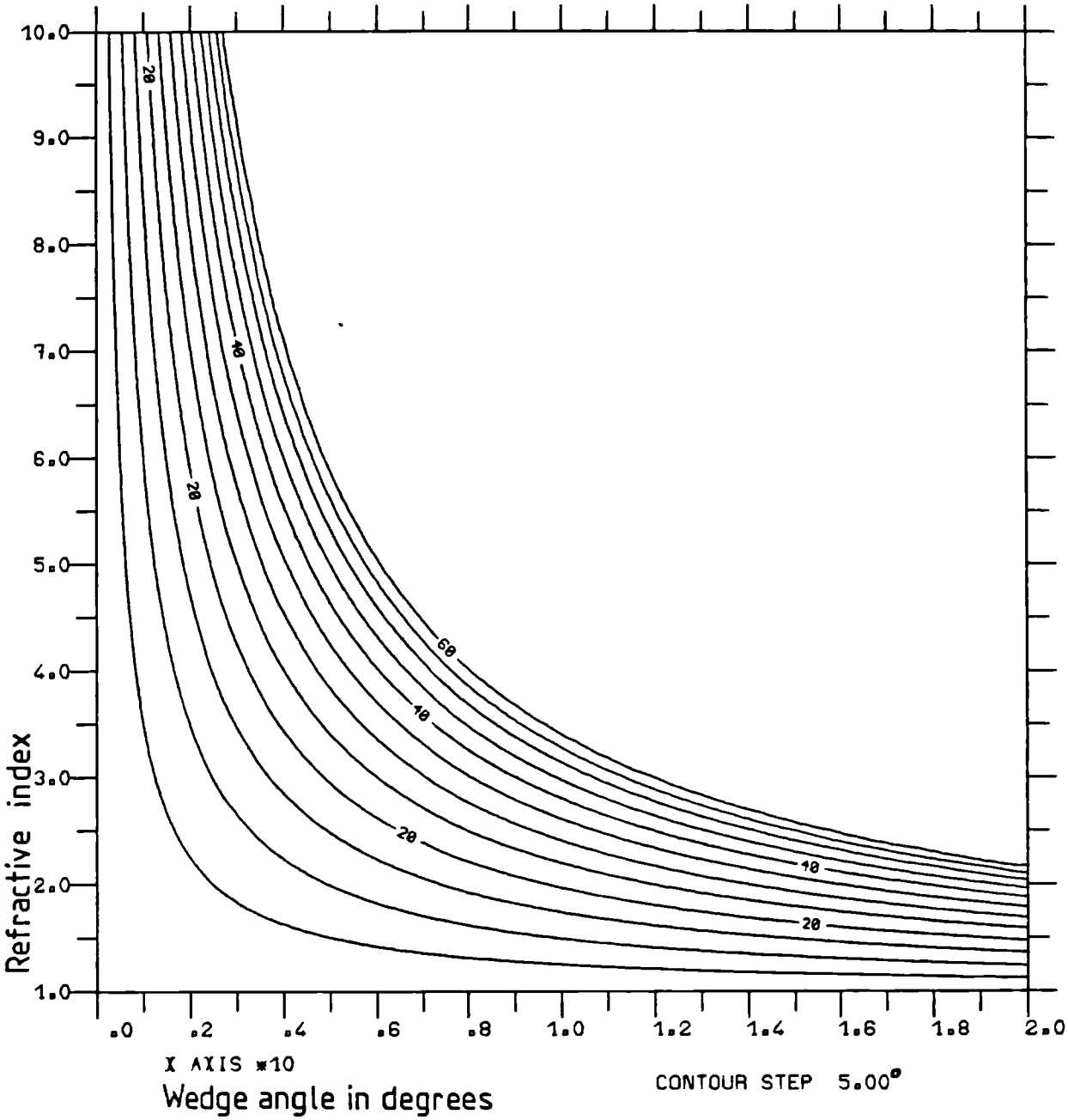

Fig 7.2. Plot for maximum beam steering angle of a pair of wedges for different wedge angles and refractive index.

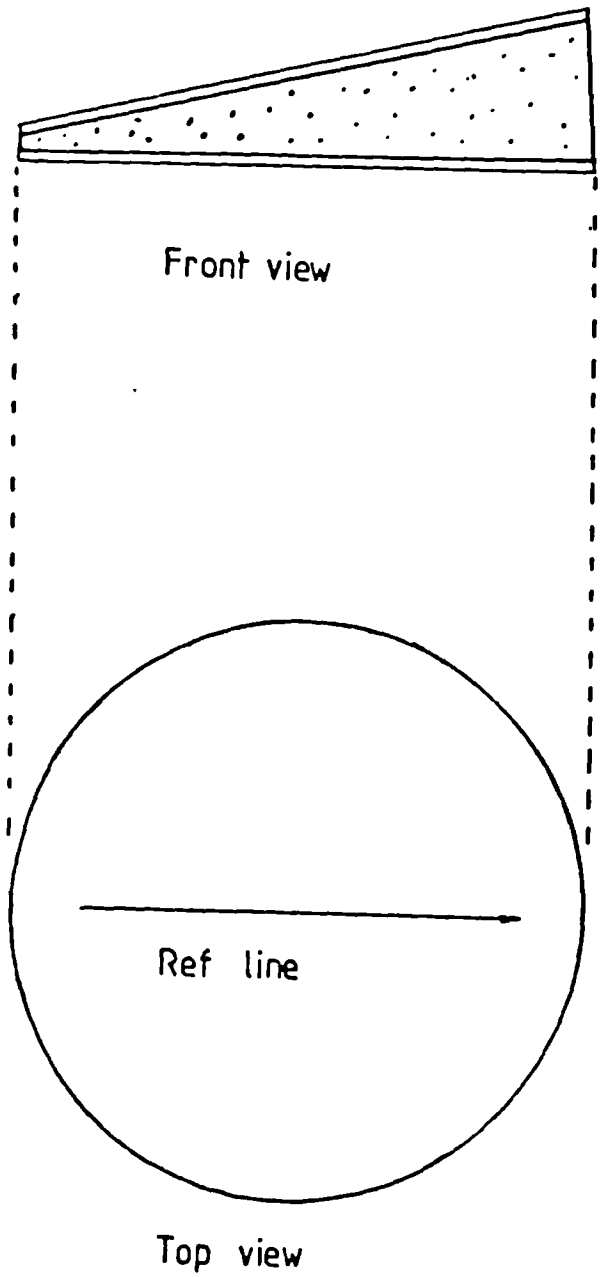

Fig 7.3. Reference axis for measuring the angular position of the wedges.

direction is from the thinner to the thicker edge of the wedge. The position of a wedge is specified by the angle between the horizontal plane and the reference axis of the wedges. Hence the 0^{o} position of both the wedges corresponds to the maximum deflection of the beam in the horizontal plane.

The deflection of the main beam is defined by $(\theta,\emptyset)$; where θ and $\emptyset$ are the angles of the spherical co-ordinate system. Hence θ is the angle made with the z-axis. $\emptyset$ is the angle between the x-axis and the projection of the main beam on the x-y plane. Using these defined co-ordinates, fig(7.4) shows the angle $\emptyset$ of the main beam for

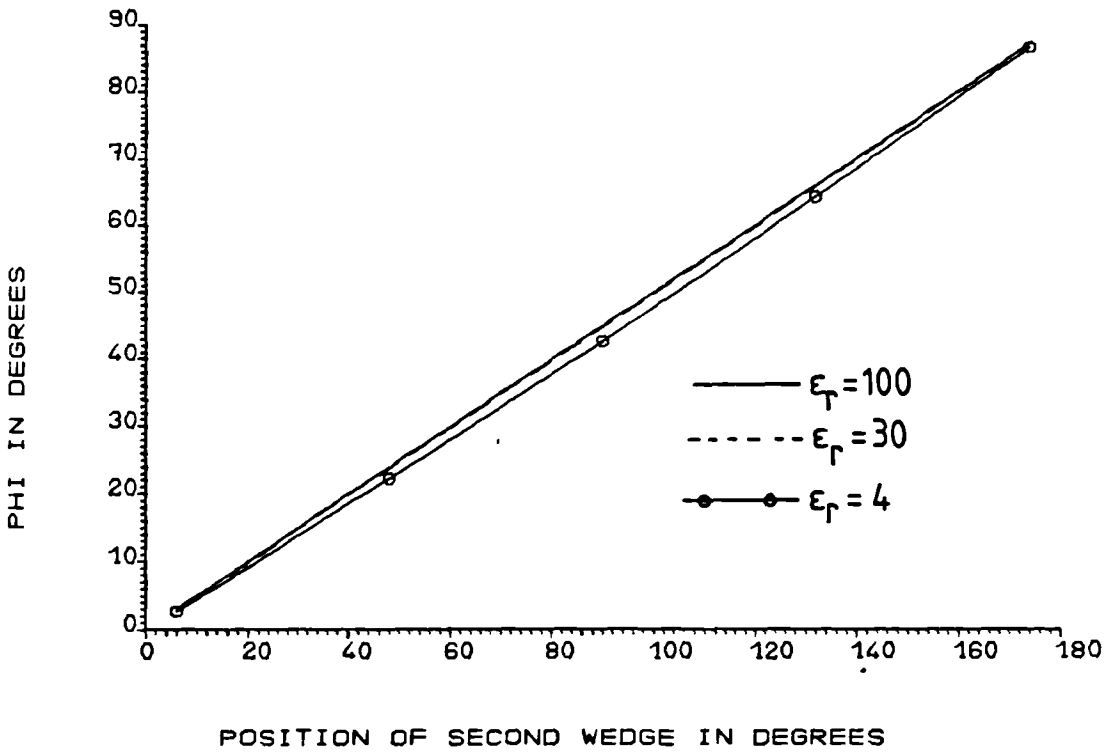

Fig 7.4. Variation of $\emptyset$ for different positions of second wedge keeping the first wedge at 0^{o}.

different angular positions W_2 of the second wedge, keeping the first wedge at 0^o. The figure shows the variation of Ø for different dielectric materials but having the same maximum deflection of 50^o. Values of Ø for all the curves are very nearly $W_2/2$. From this figure it is difficult to determine the deviation of the individual curves from the $W_2/2$ position. The deviation of the curves is plotted in fig(7.5). Lower values of dielectric constant result in higher values of Ω for the same beam deflection angle. So, the value of sinΩ deviates more from its linear nature causing a larger angle of deviation from

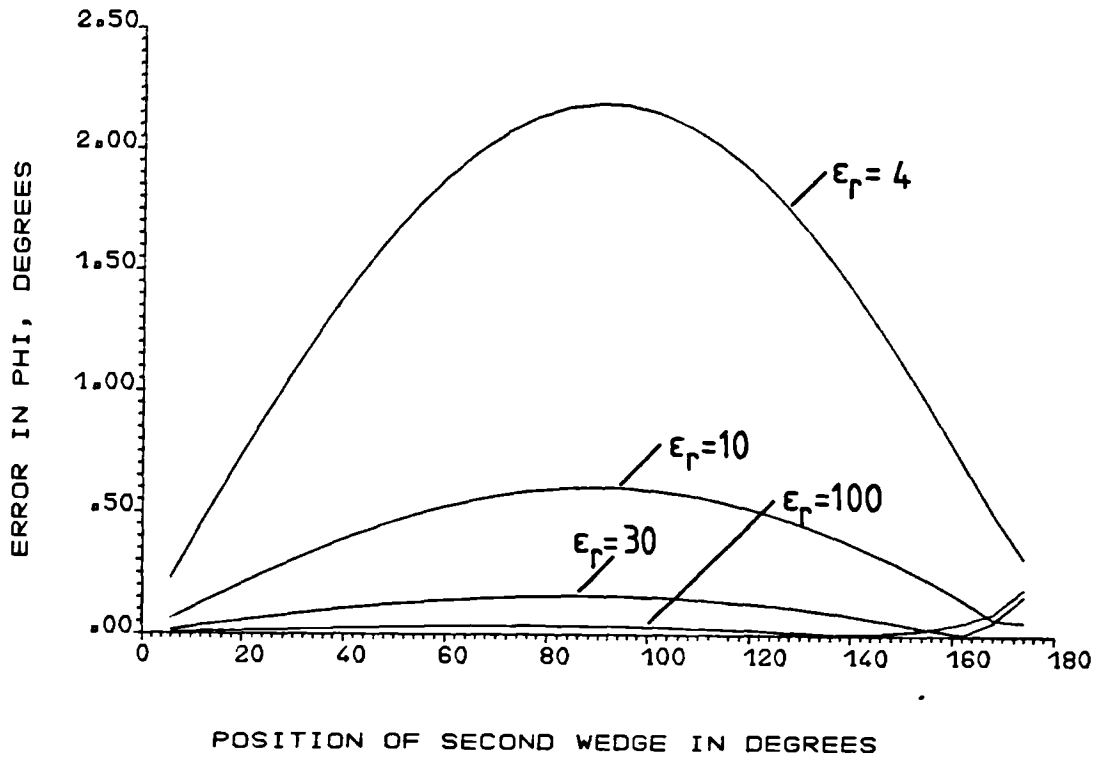

Fig 7.5. Deviation of Ø from $W_2/2$ position for different positions of the second wedge keeping the first wedge at 0^o.

$W_2/2$ position. Hence the dielectric constants are chosen such that the value of Ω never exceeds 20^o. Moreover, a wedge angle $\Omega > 20^o$ does not seem to be a practical proposition, because the wedges will become too thick.

Let us define θ_o to be the maximum deflection angle for any arbitrary position of the wedges. Fig(7.6) shows the curves for θ with respect to W_2 and fig(7.7) shows the deviation of θ from the mean value, for different dielectric materials. From figs (7.6) and (7.7) it can be

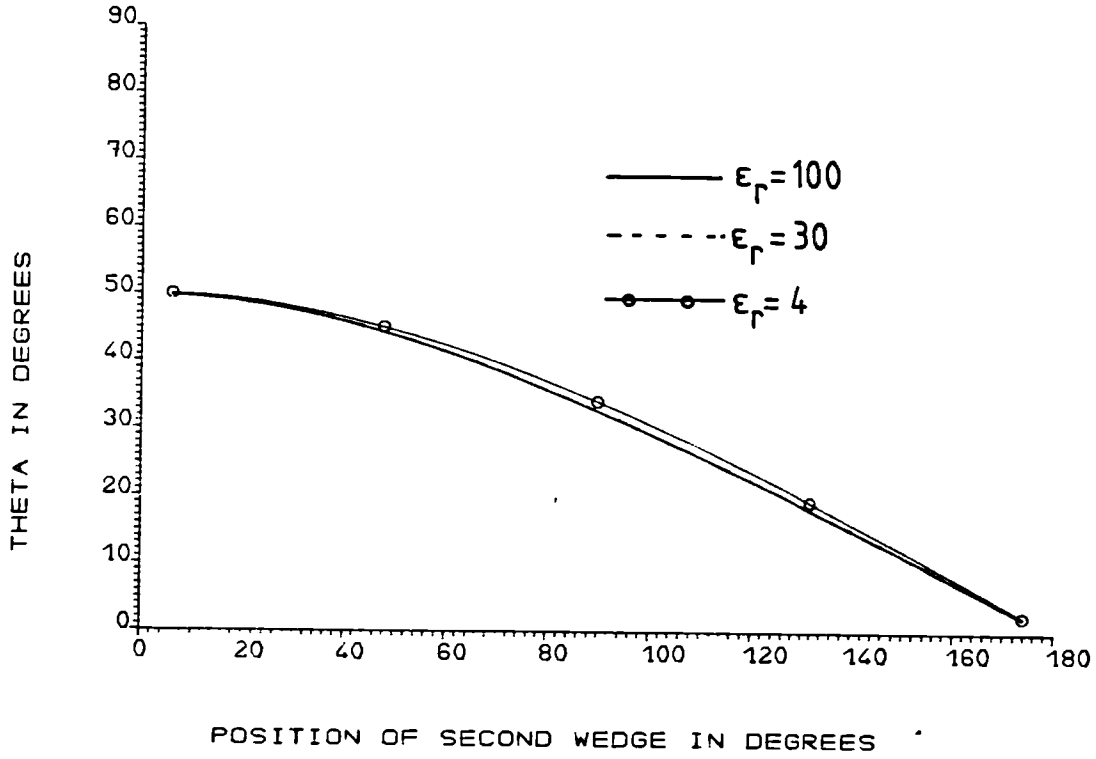

Fig 7.6. Variation of θ for different positions of second wedge keeping the first wedge at 0^o.

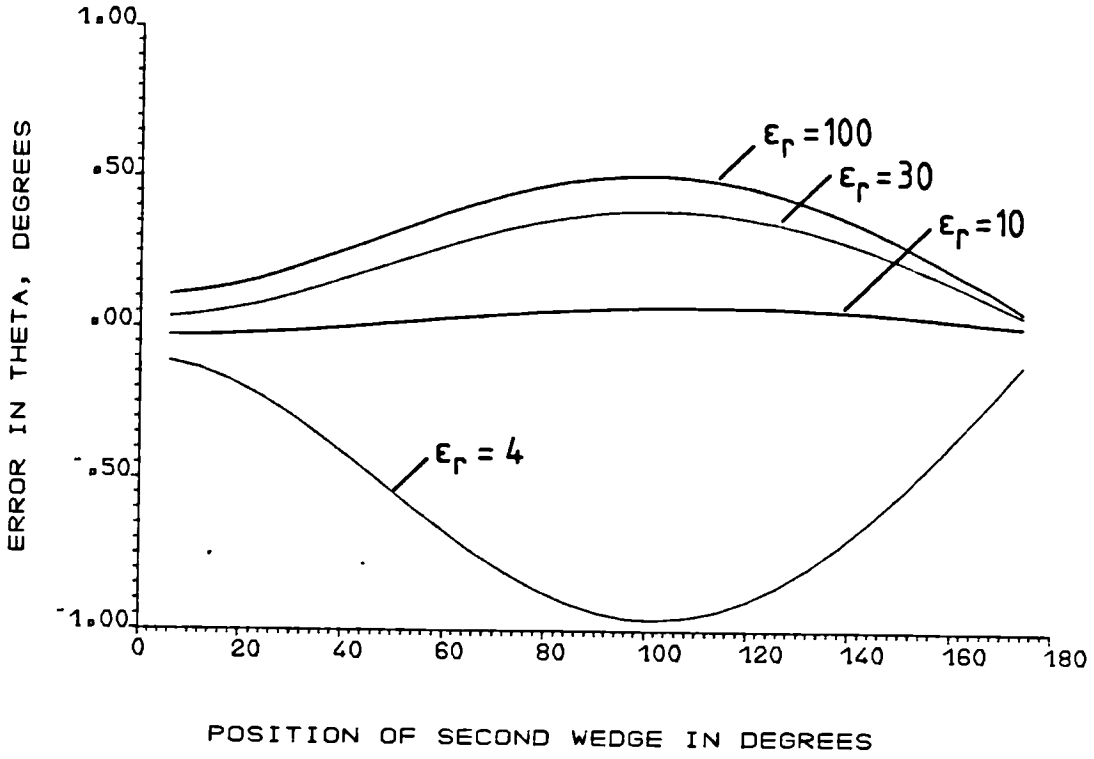

Fig 7.7. Deviation of θ from the mean value for different positions of second wedge keeping the first wedge at 0^o.

seen that the beam deflection behaviours are approximately the same for the wedges having different dielectric material but the same beam deflection angle. To study the beam deflection behaviour for different θ_o but the same ε_r, θ was normalised with respect to θ_o, the maximum beam deflection angle. Fig(7.8) shows the plot of normalised θ for different values of θ_o for ε_r = 10. The curves differ slightly for different θ_o. Using figures (7.6) ,(7.7) and (7.8) it can be concluded that it is possible to represent the beam steering behaviour of a group of wedges having different dielectric constants but similar values of θ_o by

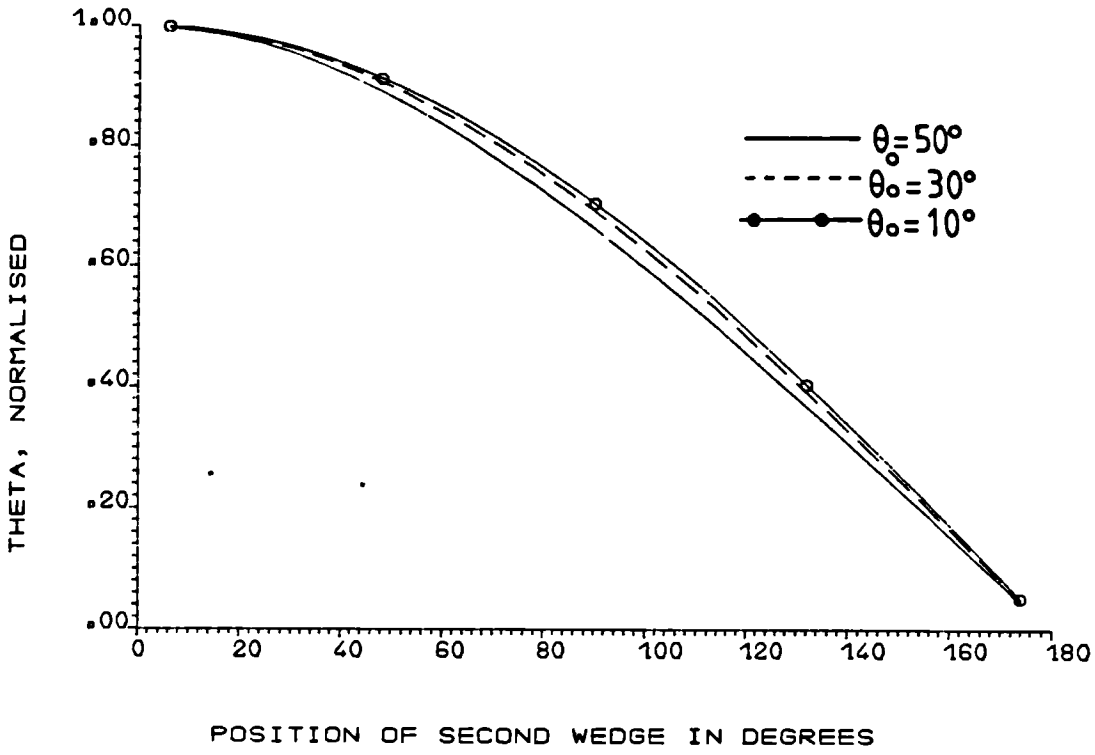

Fig 7.8. Variation of θ for different position of second wedge, normalised to the maximum steering angle θ_0 for $\varepsilon_r = 4$.

a single curve with negligible error. Hence the average of the curves for ε_r=100 and ε_r=4 for different values of θ_0 are taken to represent all the curves within that range of θ_0. Ranges of θ_0 were chosen such that the maximum pointing error does not exceed 1^o.

Azimuth and elevation curves are presented in figures(7.9), (7.10) and (7.11) , normalised as the percentage of θ_0 for different wedge positions W_1 and W_2. These three figures represent the three different ranges of θ_0; $\theta_0 = 0^o$ to 25^o, $\theta_0 = 25^o$ to 40^o and $\theta_0 = 40^o$ to

50^{o}. Hence using figures (7.9), (7.10), (7.11), we can determine the normalised value of azimuth and elevation for the wedge positions W_1 and W_2.

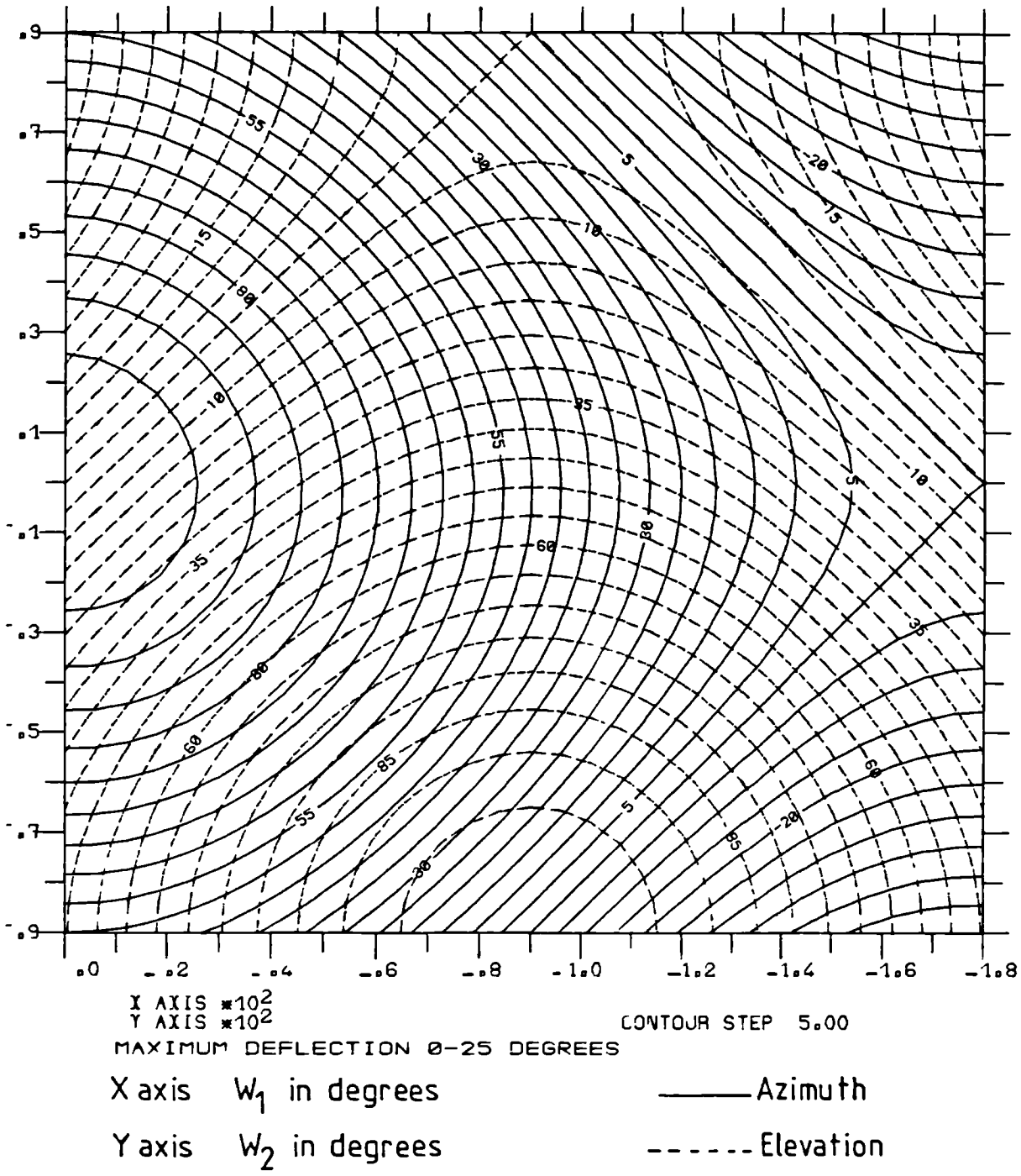

Fig 7.9. Normalised azimuth and elevation of the main beam for different positions of the wedges, for maximum beam steering angle ranging from 0 - 25°.

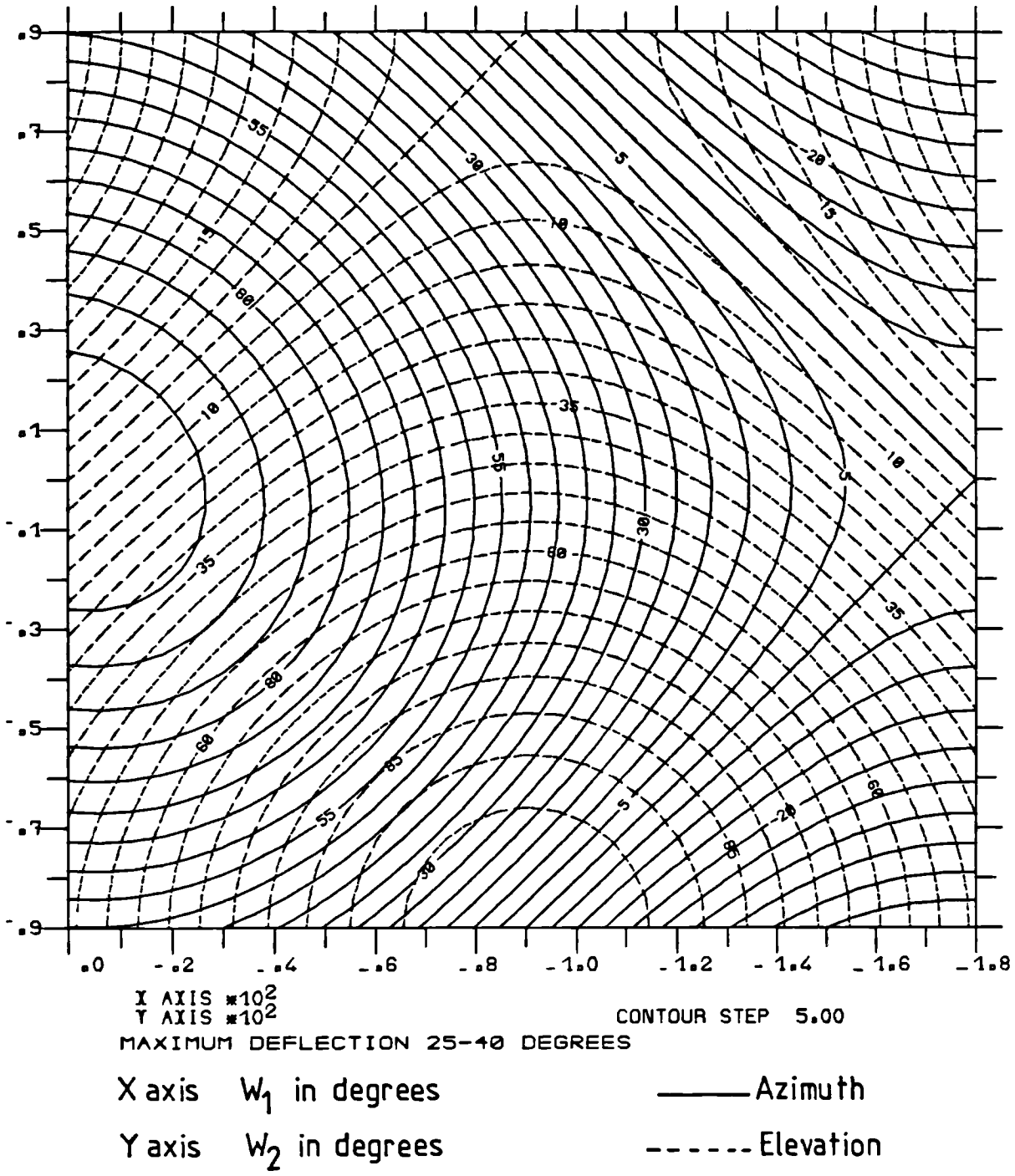

Fig 7.10. Normalised aziuth and elevation of the main beam for different positions of the wedges, for maximum beam steering angle ranging from 25^{o} - 40^{o}.

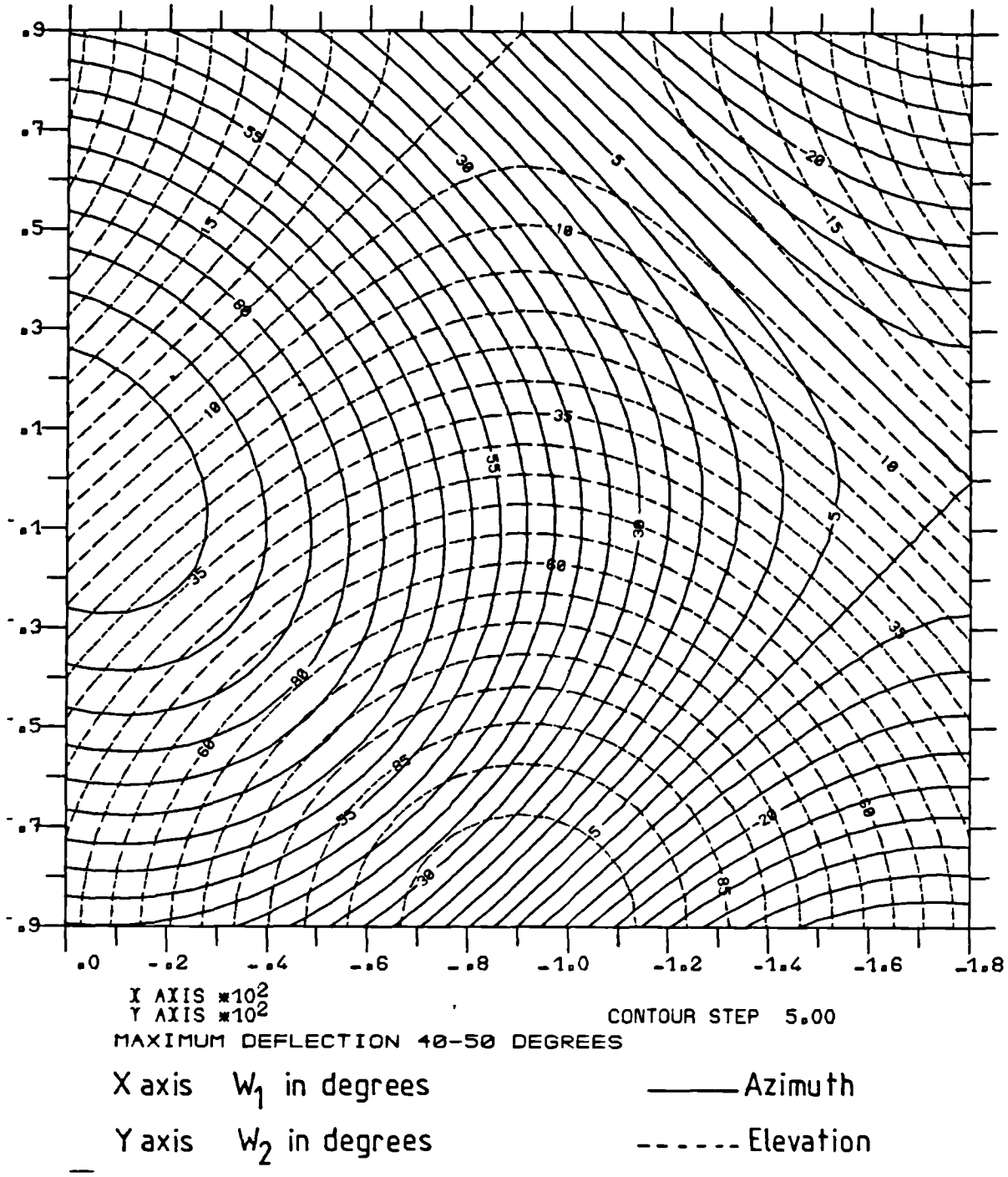

Fig 7.11. Normalised azimuth and elevation of the main beam for different positions of the wedges, for maximum beam steering angle ranging from 40° - 50°.

CHAPTER 8 : Measurements with Circular Wedges

8.1. Introduction

A mathematical analysis of dielectric wedges has been presented in chapter 4 and some experimental investigation was also made using a pair of rectangular wedges. These rectangular wedges were used to obtain some quick results to justify the theory. However, rectangular wedges have the disadvantage of allowing only two deflection angles - one for the maximum steering angle and the other for no steering of the main beam. In this chapter, results are presented for circular wedges using a parabolic dish as the antenna. Two pairs of such wedges were made, one from Titanium dioxide (TiO_2) and the other from a solid block of perspex. The experiment with the TiO_2 was not very successful, producing extremely bad results. But the pattern for the perspex wedge were quite good and a comparison between theory and experiment is presented.

8.2. Wedges Filled with Titanium Dioxide

Titanium dioxide (TiO_2) is considered as a high quality dielectric material at microwave frequencies. Pure TiO_2 has a dielectric constant of 96 and a loss factor $\tan\delta = 0.00034$. TiO_2 is extensively used for making illuminated road signs. It is also used to make high dielectric constant material by mixing with some

other plastic-like base material. So, the possibility of using TiO_2, which normally comes in powdered form, was explored to make the wedges. TiO_2 powder was packed manually inside a waveguide section and the dielectric constant was measured. Three different samples were tried, and all of them produced approximately the same results (4.71, 4.73, 4.68). It suggested that there will be no appreciable change in the density of the powders when packed manually. The nature of the powder is such that usage of vibrations for packing did not prove very sucessful. So, a perspex frame was made in the shape of a wedge and the powder was packed into the wedge manually. The perspex frame used had a thickness of 0.39cm, which corresponds to a quarter of a wavelength at 12GHz, to reduce the reflections. Although the dielectric constant of perspex does not have the right value to match perfectly, still it could reduce the reflection considerably (about -22dB). Fig(8.1) shows a schematic diagram of the wedge. The dimensions shown in the figure correspond to a wedge angle of 9.16°. The array of a pair of horns, as described in section 4.3.5, was used to measure the steered pattern. The results are shown in fig(8.2). The angle of steering obtained corresponds to a dielectric constant of 4.84 for the wedge material. It can also be seen that there is a reduction of 2dB in the main beam but very little variation in sidelobes as the position of the wedge is changed with respect to the

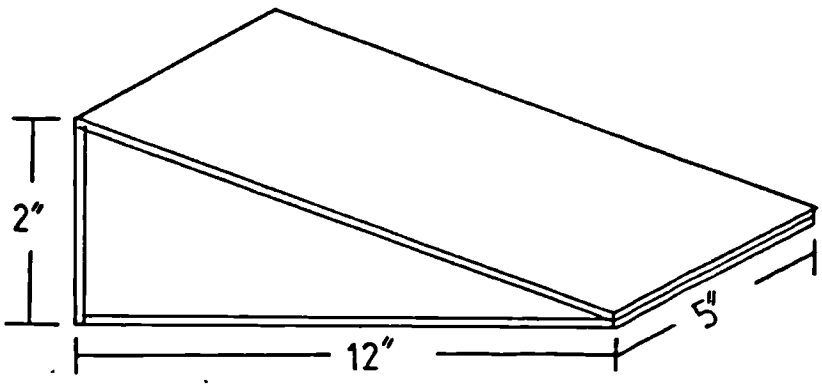

Fig 8.1. Rectangular perspex frame for the TiO_2 filled wedge.

antenna array, which confirms that the reflections are small. At the same time, there is almost no distortion in the steered pattern. This shows that the dielectric constant is reasonably uniform throughout the wedge. Otherwise, any irregularity in the packing density would have resulted in nonuniformity in the dielectric material causing phase distortion on the wedge face. This would have resulted in a radiation pattern with high sidelobes. But such effects are not present. The reduction in gain is thought to be due to loss inside the TiO_2.

Considering these factors, two large perspex frames for the wedges, each 78cm in diameter, were built as shown in fig(8.3). The thickness of the perspex frames was made 3/4 of a wavelength instead of a quarter of a wavelength, to

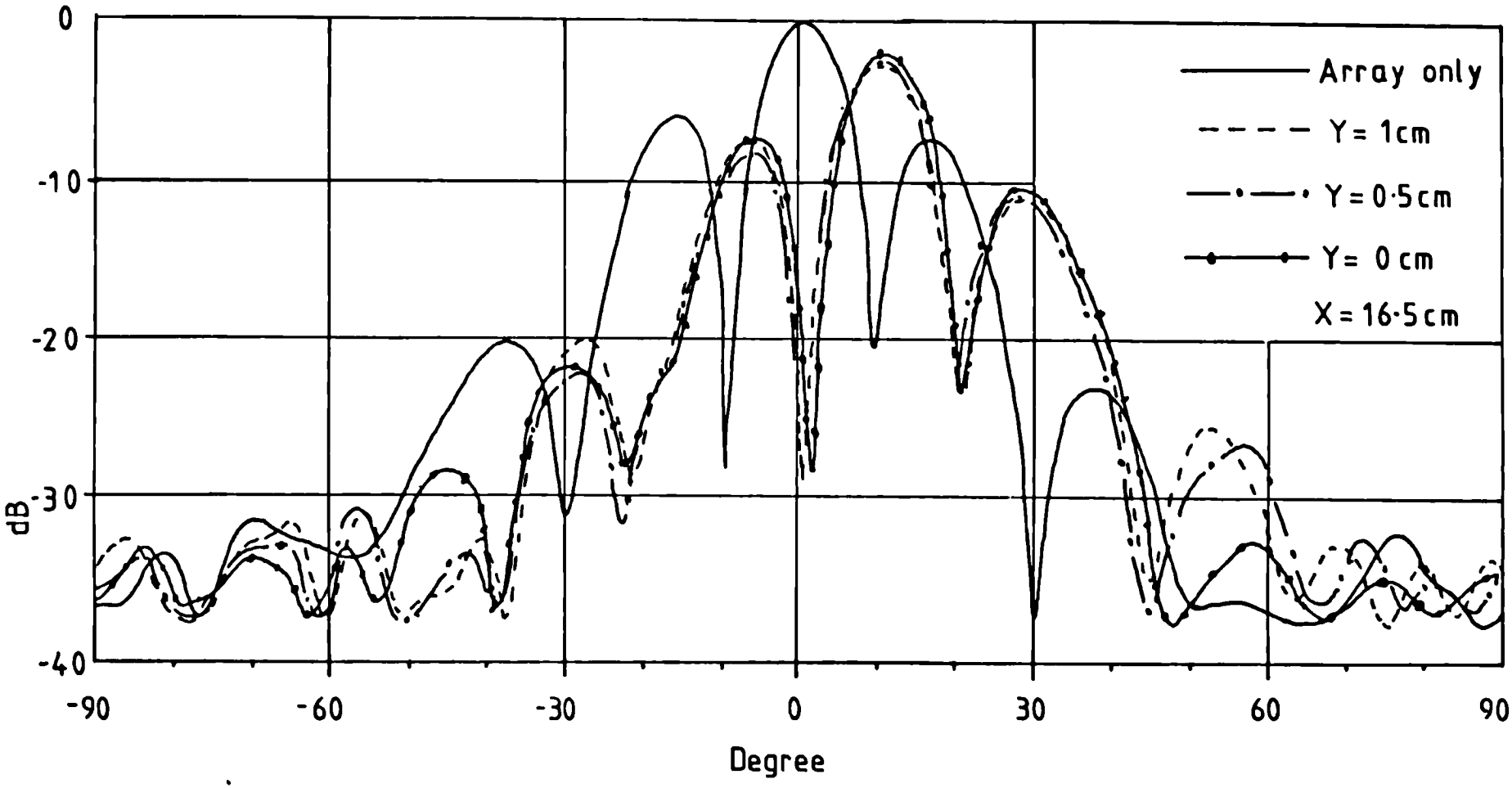

Fig 8.2. Pattern of the array of horns steered by a TiO_2 filled rectangular wedge for different wedge positions.

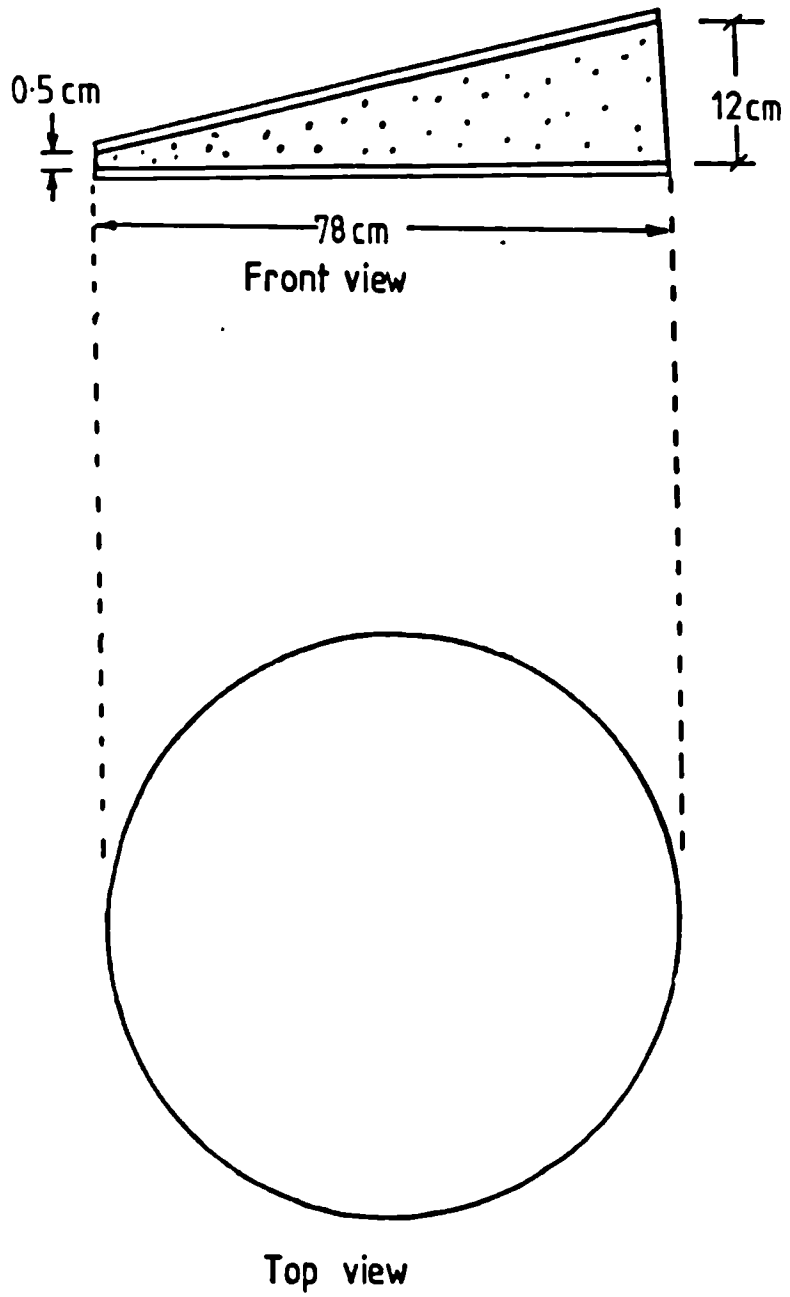

Fig 8.3. Schematic diagram for the TiO_2 filled wedge.

make them mechanically strong. This increase in thickness, however, causes a reduction in the bandwidth of the matching layer. Both the wedges were packed manually and then placed inside a wooden frame, so that they can be rotated easily. The overall weight of the frame and the wedges was very high (100kg) and was quite difficult to handle. A 62cm dish was used behind the wedges. Fig(8.4) shows the radiation pattern of the dish on its own. Fig(8.5) shows the steered pattern using a single wedge. There is some degradation of the pattern, accompanied by a loss of gain of about -6dB. The beam steering achieved was 10^{o}. But when used with both the wedges, the patterns appeared extremely bad, as shown in fig(8.6) and (8.7). The gain was reduced by as much as 16dB and in most of the cases the sidelobes were within -8 to -10dB of the main beam.

The deterioration of the radiation pattern seems to be due to nonuniform packing of the TiO_2 powders. Loss inside the TiO_2 powder and the deterioration of the radiation pattern are responsible for the unacceptable reduction in gain. The TiO_2 ordered was supposed to be 98% pure containing only a small amount of impurities. This 2% impurity seems to have a great impact on the loss factor of TiO_2. Although lossy TiO_2 powder reduces the gain, the pattern would have remained approximately the same (section 6.3) if there had been uniform packing of the material. Considering the amount of

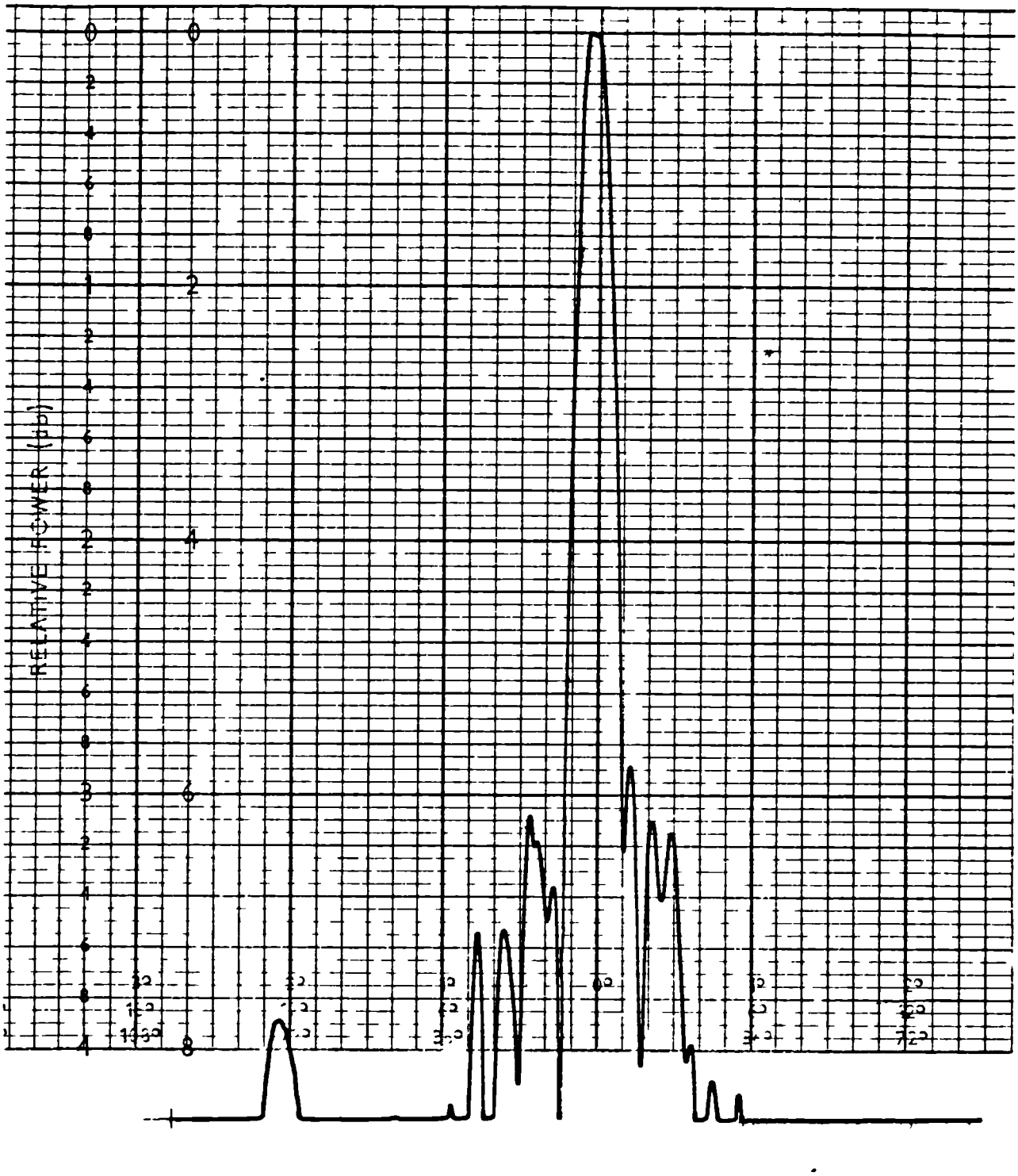

Fig 8.4. Radiation pattern of a 62cm parabolic dish.

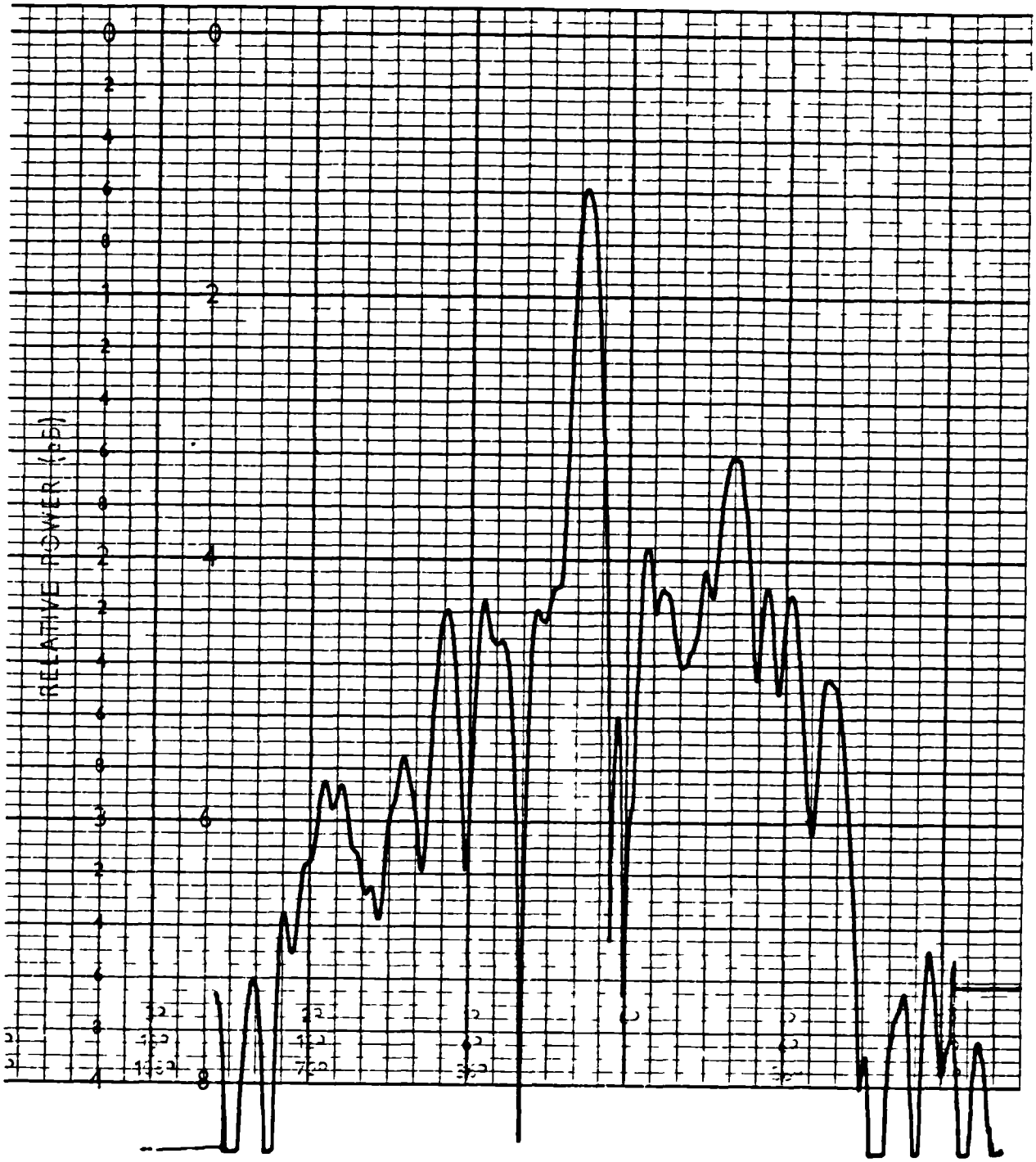

Fig 8.5. Steered pattern of the 62cm parabolic dish using one wedge.

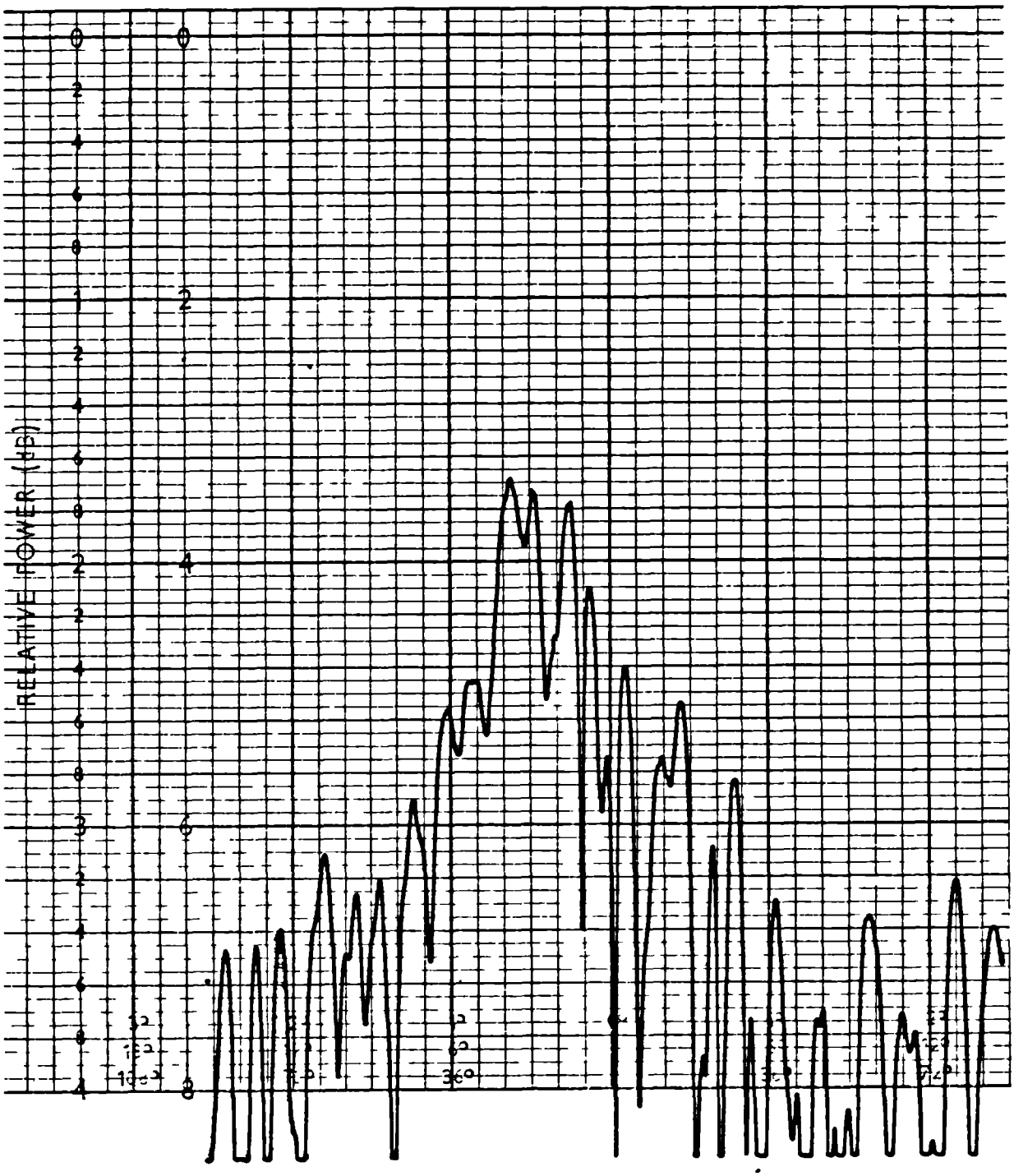

Fig 8.6. Radiation pattern of the 62cm dish steered by a a pair of TiO_2 filled wedges for $\theta_o = 20^o$.

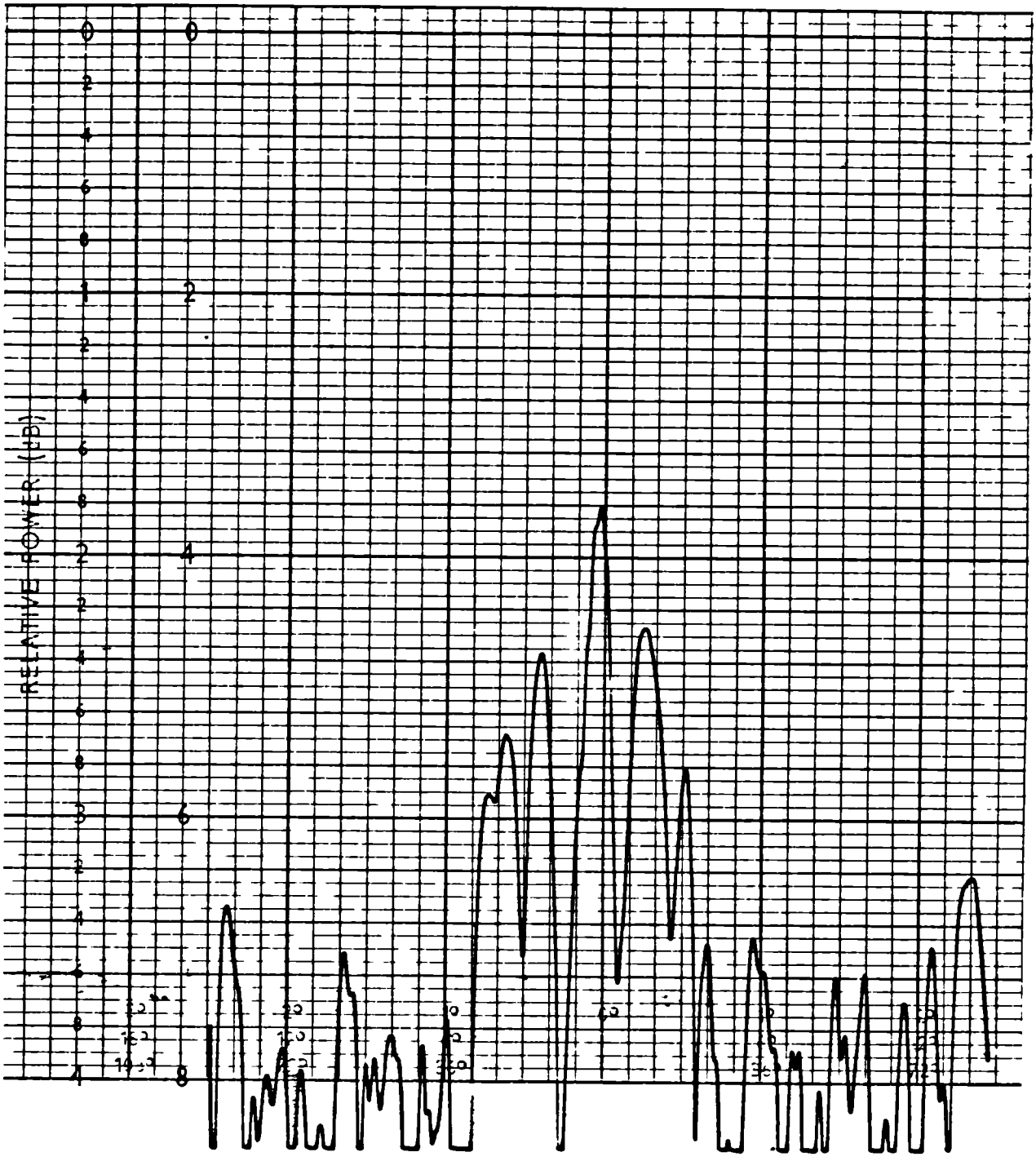

Fig 8.7. Radiation pattern of the 62cm dish steered by a pair of TiO_2 filled wedges for $\theta_o = 0$.

nonuniformity involved, further investigation of the wedges was abandoned and no more effort was made to improve the uniformity of packing material inside the wedges.

8.3. A Pair of Perspex Wedges

As the experiment with TiO_2 filled wedges did not produce good results, a pair of perspex wedges with circular faces were made from a solid block of perspex. The dielectric constant of perspex was measured to be 2.59, as mentioned earlier, which limits the amount of steering achievable by a pair of wedges if their weight is not to be unacceptably high. Perspex has a specific gravity of 1.2. So, a pair of large wedges would be much too heavy like the TiO_2 filled wedges. Considering these factors, a pair of wedges 36cm in diameter was designed, with a wedge angle of 12.53°. A photograph of the pair of perspex wedges is shown in fig(8.8). A pair of wedges of this type were designed to produce an overall deflection of 16° from boresight which was read from the chart in fig(7.2). Air gap matching layers (section 4.3.6) were used on all four faces to reduce reflections. The air gap matching layer on all the faces were identical and were designed for best matching at normal incidence. As the beam steering angle was not very large, separate matching layers were not designed for different faces, because of the broadband performance of the matching layer (section 4.3.6).

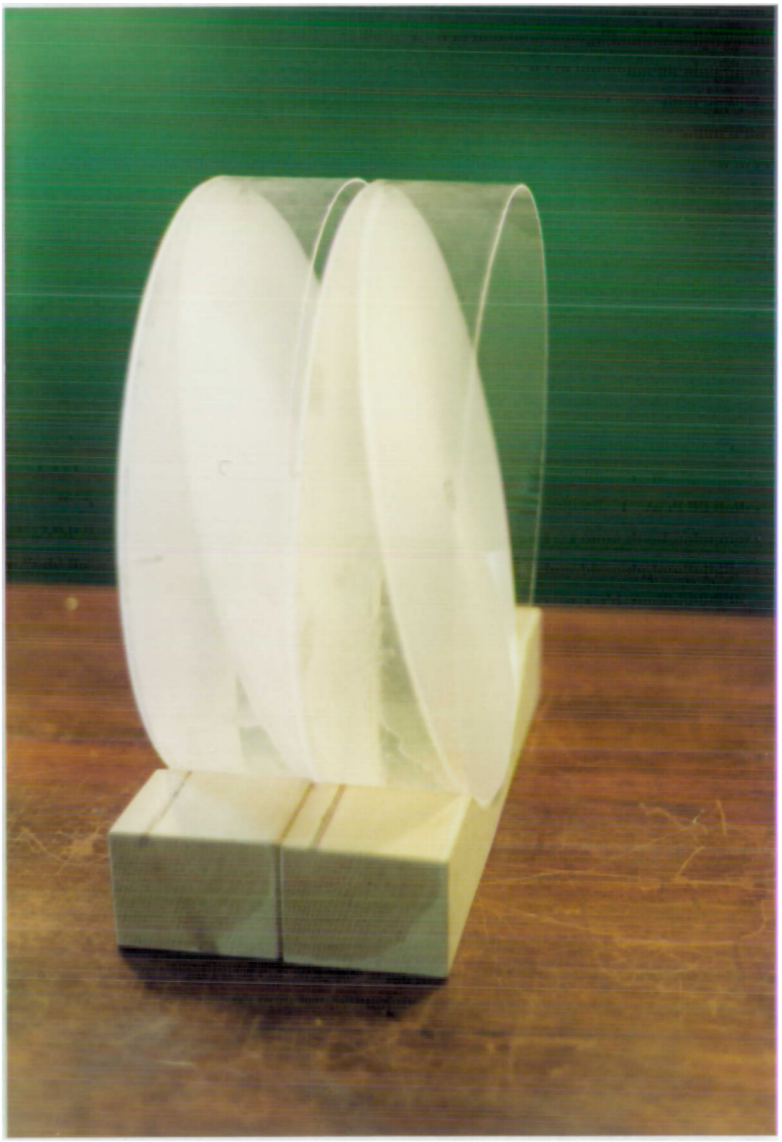

Fig 8.8. A photograph of the pair of perspex wedges.

A 30cm dish having a f/D =0.25, fed by an open ended waveguide flared out in the shape of a horn in the E-plane, was used with the wedges. The horn was 2.0cm in the H-plane and 2.5cm in the E-plane, having a flare length of 2cm. The horn angle was measured to be 90^{o}. Fig(8.9) shows the frequency response of the dish and fig(8.10) shows its measured radiation pattern in the E-plane at 12 GHz. The computed radiation pattern is shown in fig(8.11). The -3dB beamwidth is 8^{o}, which agrees well with the measured result. However, there are no distinct nulls between the sidelobes. This could be due to the wide angle and the small size of the horn flares, which modify the aperture phase and amplitude distribution of the feed. The computation was based on a cosine amplitude distribution in the H-plane and a uniform amplitude with quadratic phase factor due to the flare in the E-plane. Large flare angles in the E-plane make the electric field cylindrical, which changes the tangential component of the aperture field [22]. However, the sidelobes at these low levels are not very important parameters, so long they do not increase to an unacceptable value after the beam is steered. Earlier computed results (section 4.3.7) show that there should not be any marked change in the sidelobe levels.

First the steering of the beam was measured using a single wedge, and the result is shown in fig(8.12). The beam is

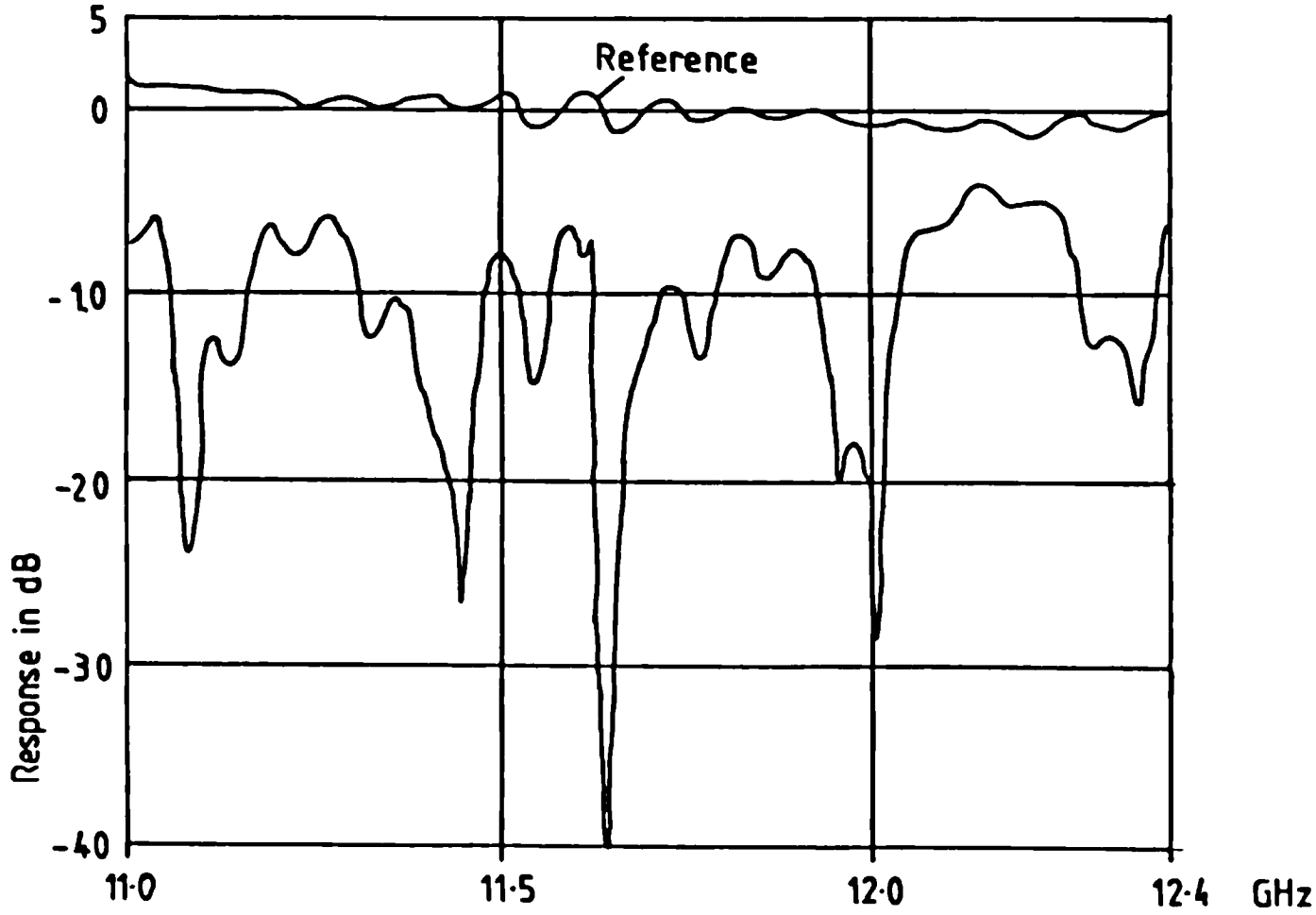

Fig 8.9. Frequency response of the 30cm parabolic dish.

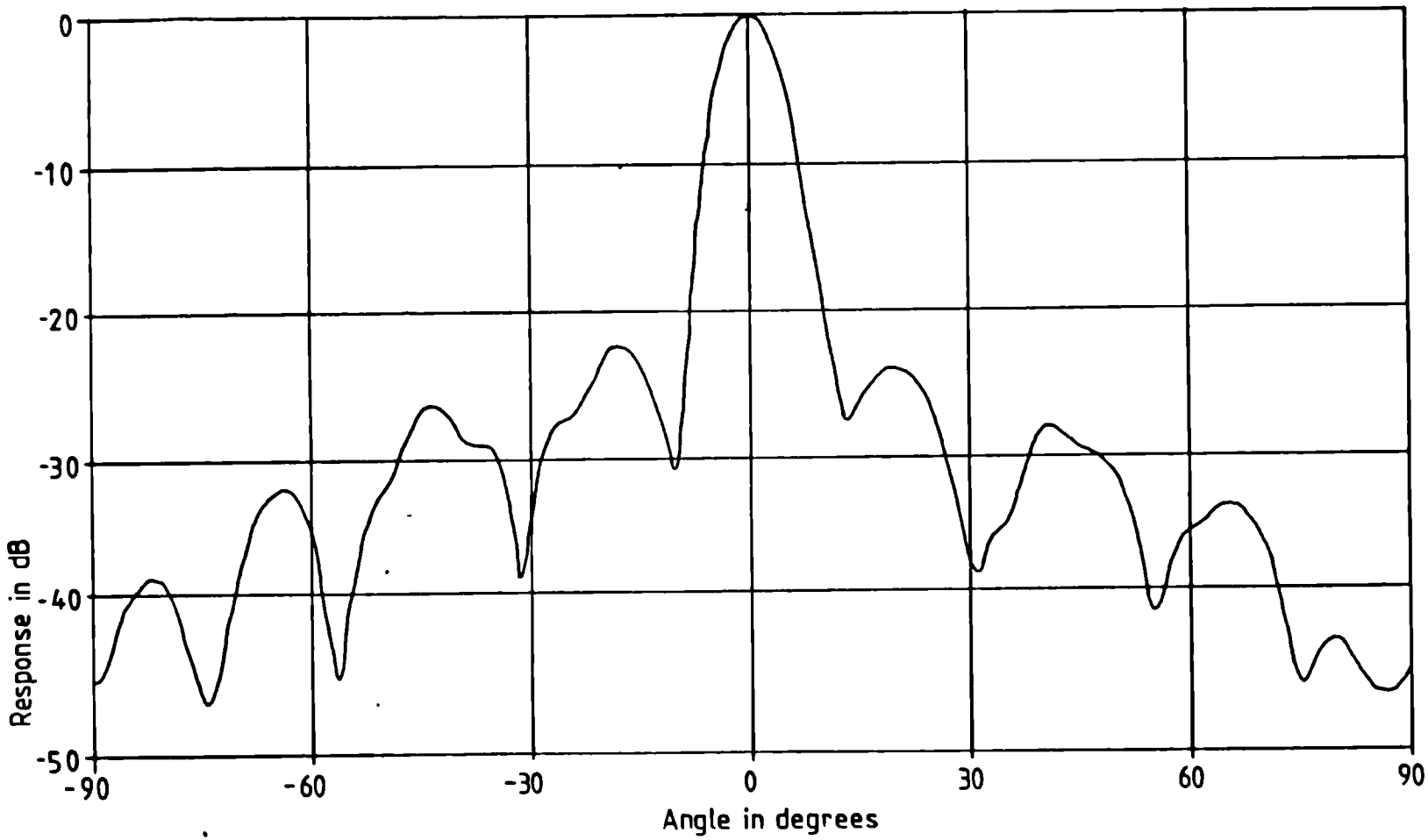

Fig 8.10. Radiation pattern of the 30cm parabolic dish in the E-plane.

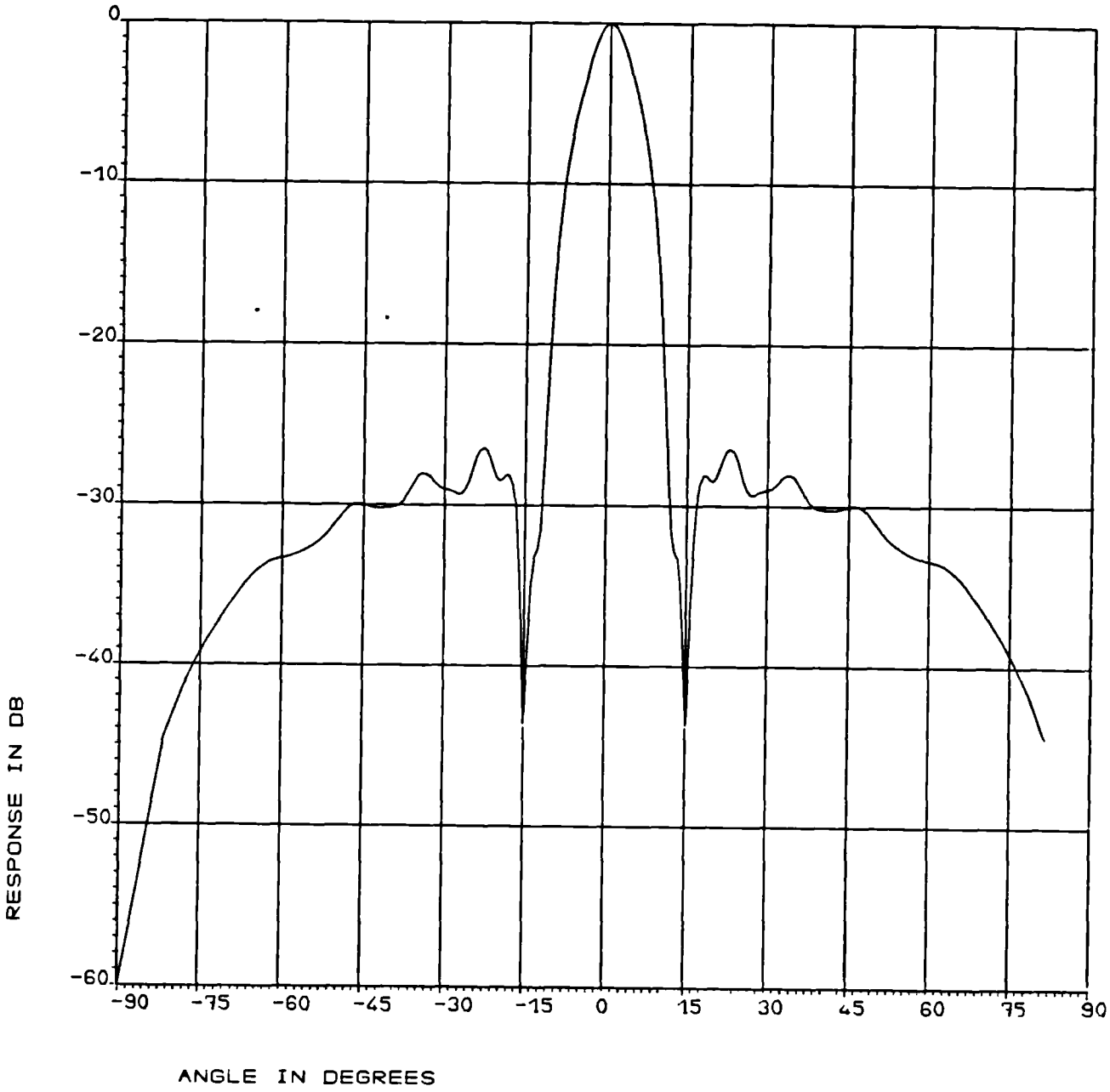

Fig 8.11. Computed radiation pattern for the 30cm dish in the E-plane.

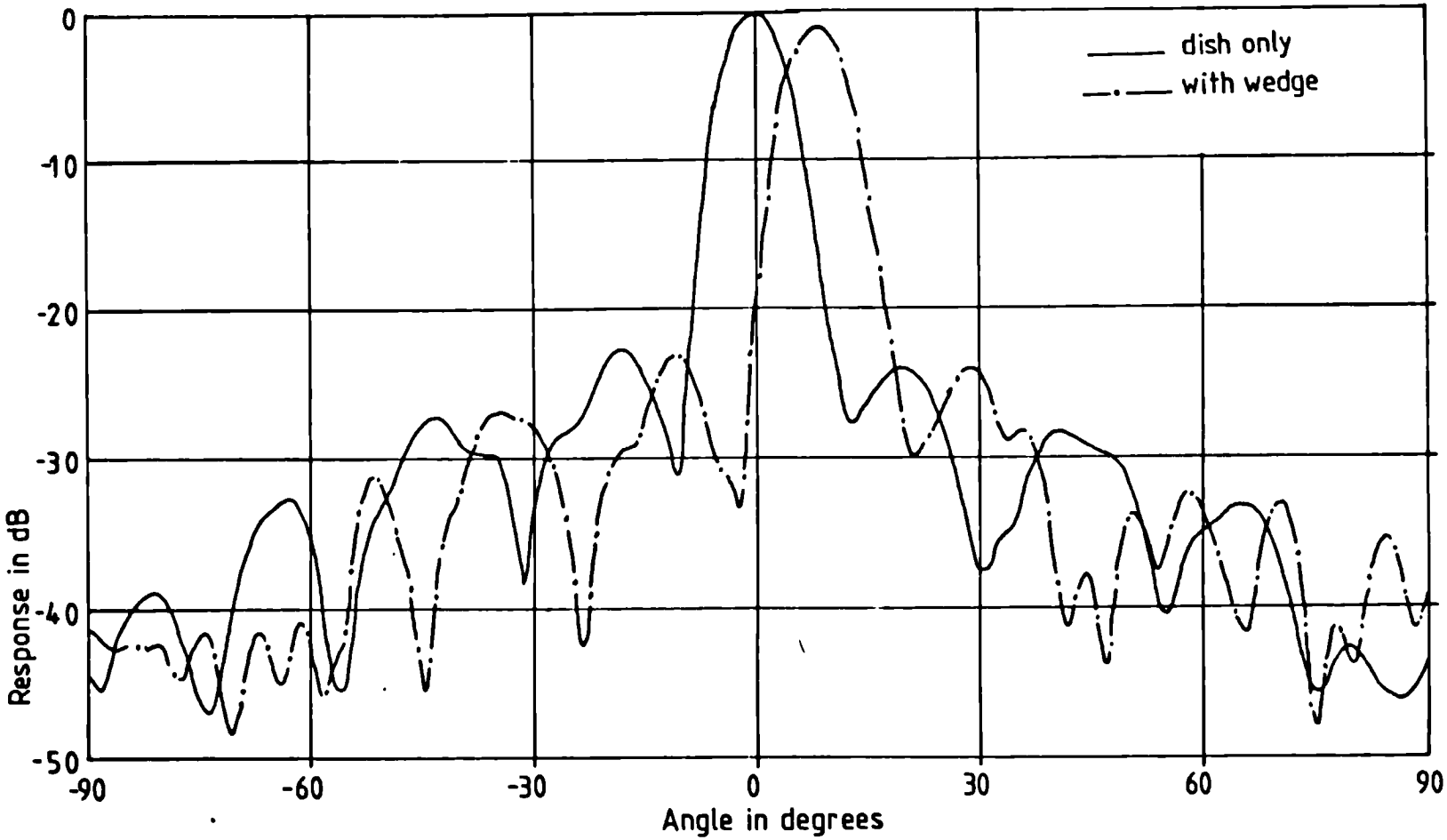

Fig 8.12. Steered pattern of the 30cm dish using a single wedge.

steered by 8^{o} and there is very little change in the sidelobe levels. Then both the wedges were placed in front of the dish and the radiation pattern was measured. As the turntable was capable of rotating in the horizontal plane only, the wedges were placed to provide the resultant deflection in the horizontal plane only. This condition was achieved by placing the second wedge at an angular position ψ and then placing the first wedge at $-\psi$ position. The angular position of the wedges was measured from the angle between the reference line of the wedges and the horizon. Fig(8.13) shows the radiation pattern for different values of ψ . Maximum deflection occurs at $\psi=0^{o}$, and produces a beam deflection of 16^{o}. Other than this, measurements for $\psi= 30^{o}$, 60^{o} and 90^{o} were also taken to obtain different deflection angles. Two more results for different frequencies are shown in figs (8.14) and (8.15). Steered patterns for different values of were computed at 12GHz using the relation developed in section(4.2), and are shown in fig(8.16). The sidelobe levels do not change by any significant amount in both the measured and the computed results. In all cases the sidelobes remain well below the -20dB. Steering angles for different wedge positions were also found from the charts presented in section(7.3). A comparison between the measured and the computed angles of beam steering are presented in table 8.1. They are in very good agreement and the error is less than 0.5^{o}. The error

Wedge position		Measured		Computed		Using chart	
1st wedge	2nd wedge	Azimuth	elevation	Azimuth	Elevation	Azimuth	Elevation
0°	0°	16°	0°	15.7°	0°	16°	0°
-30°	30°	13.5°	0°	13.5°	0°	13.7°	0°
-60°	60°	8.0°	0°	7.7°	0°	8.0°	0°
-90°	90°	0.3°	0	0	0	0	0

Table 8.1. Comparison between the measured and computed angles of beam steering for circular perspex wedges.

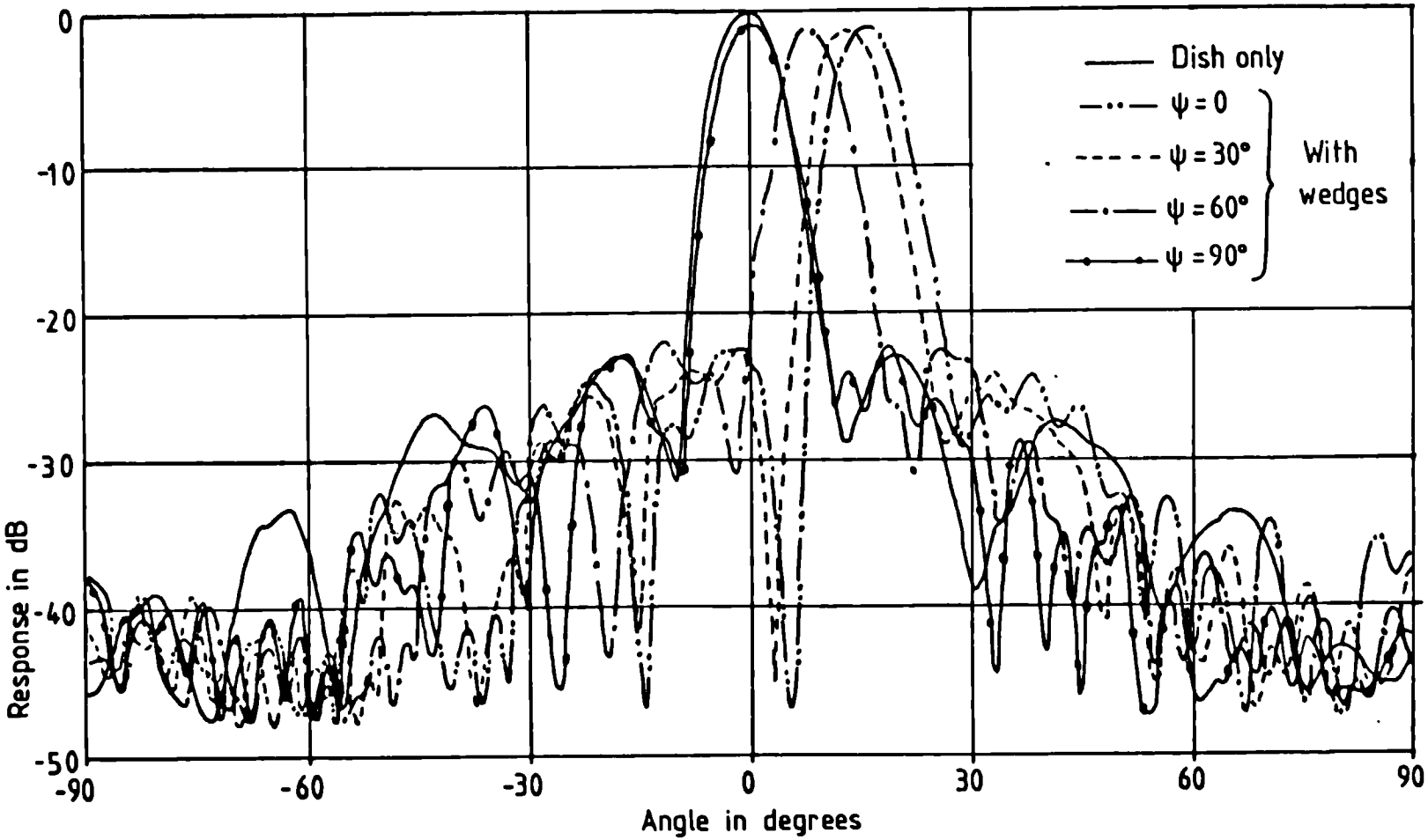

Fig 8.13. Steered radiation pattern of the 30cm dish for different values of ψ using two perspex wedges at 12GHz.

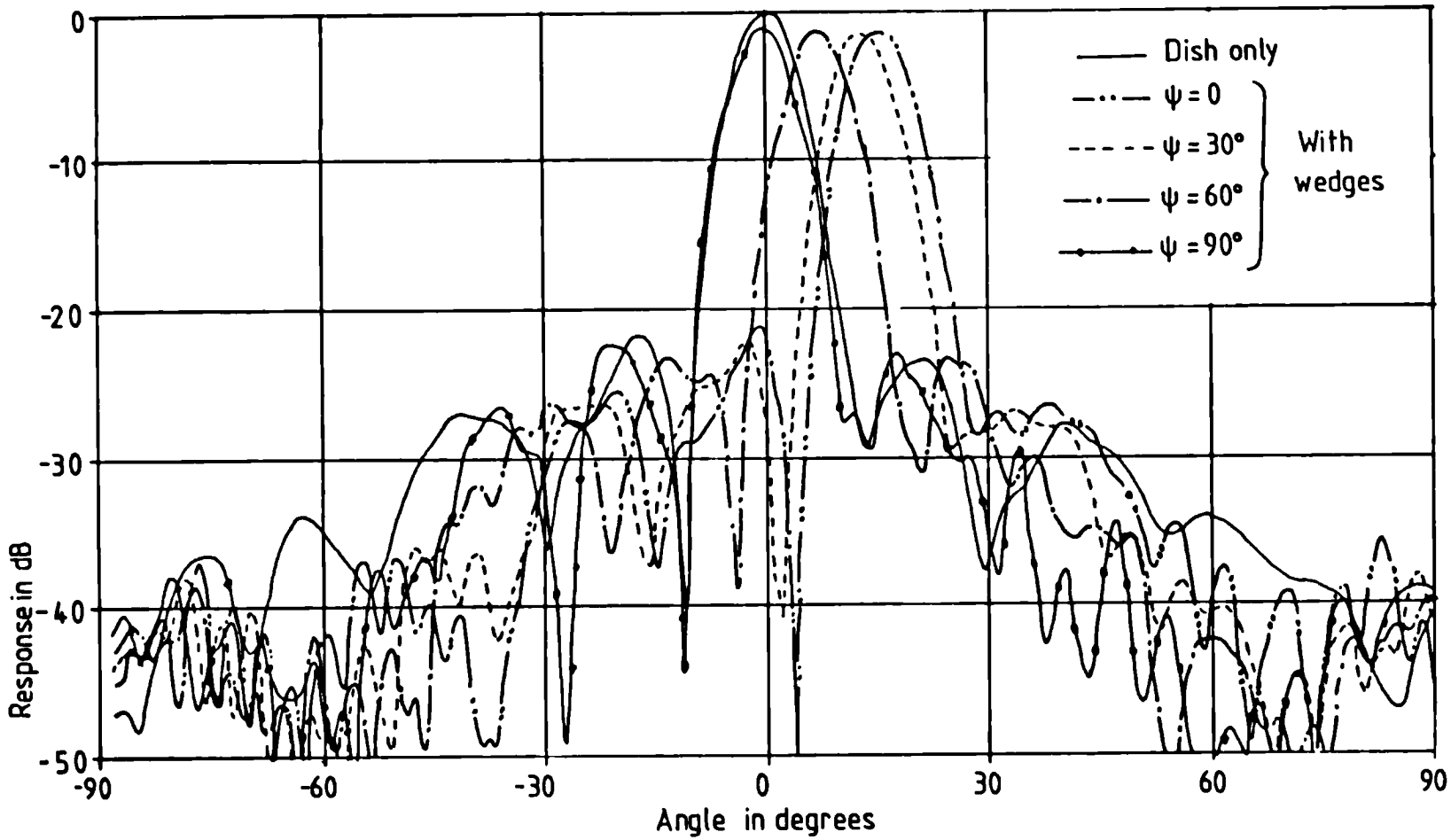

Fig 8.14. Steered radiation pattern of the 30cm dish using the perspex wedges at 12.3GHz.

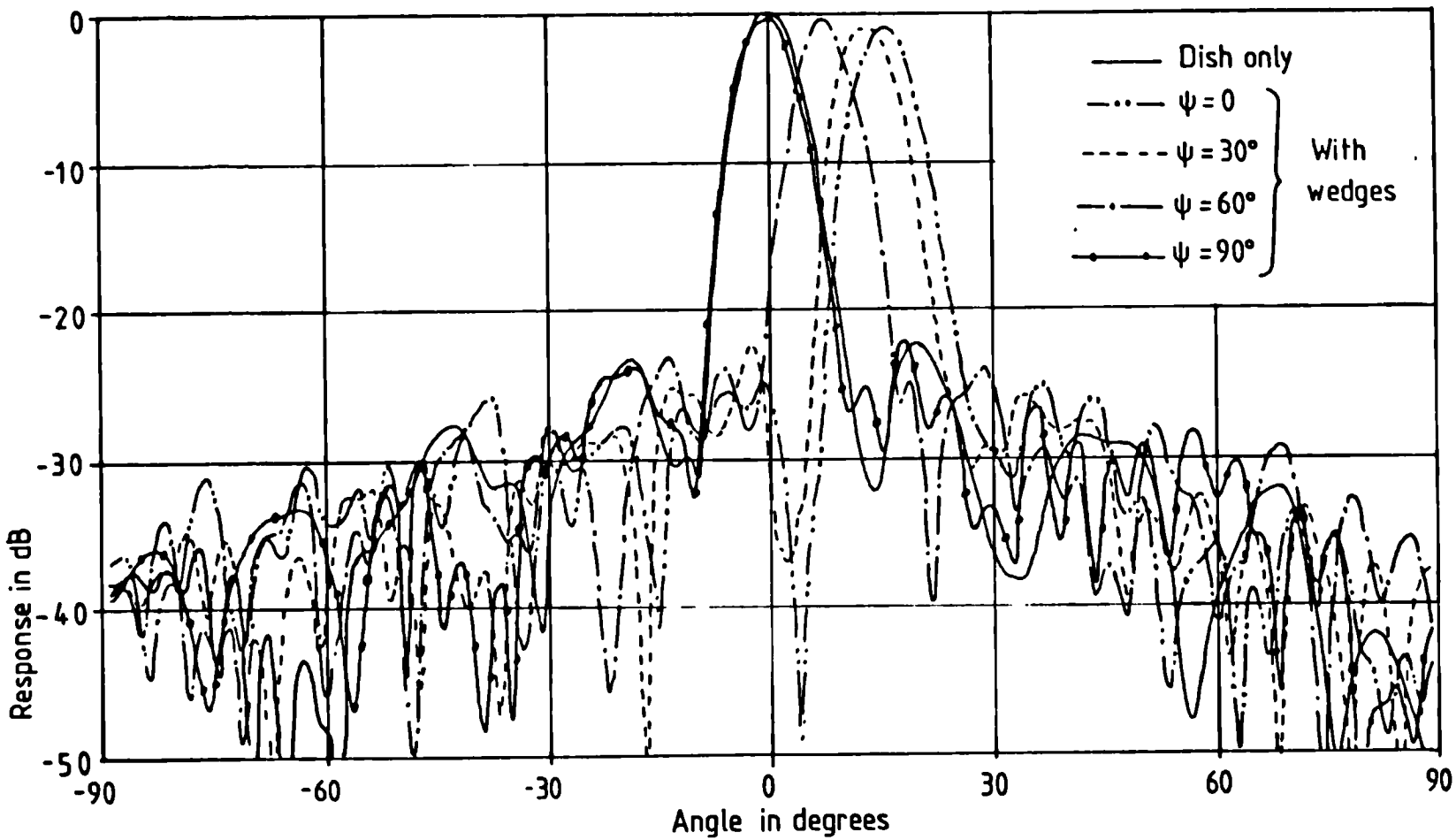

Fig 8.15. Steered radiation pattern of the 30cm dish using the perspex wedges at 11.7GHz.

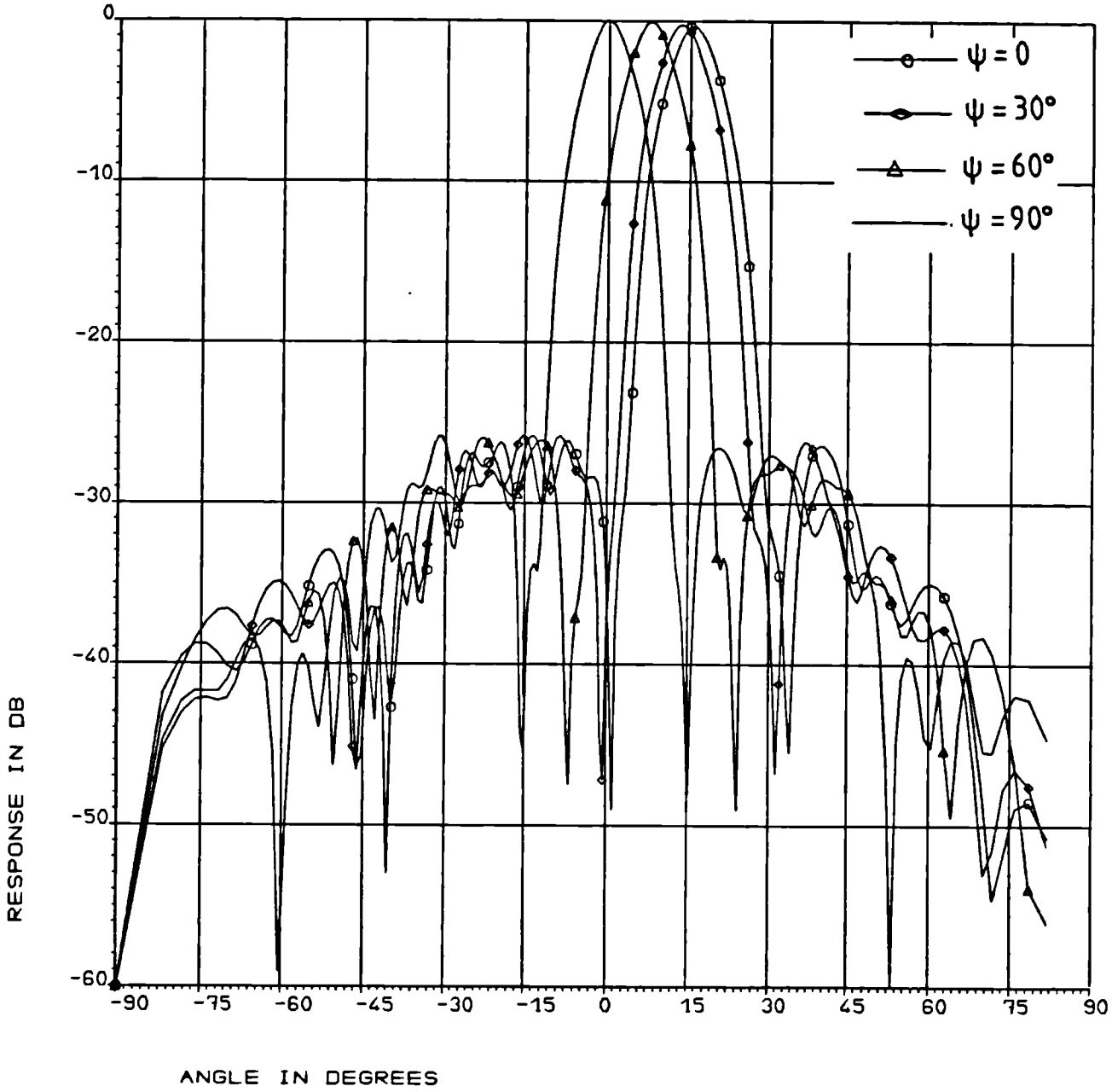

Fig 8.16. Computed radiation pattern of the 30cm dish steered by a pair of perspex wedges at 12GHz.

occurs due to the difficulty in reading the chart very accurately as the contours are plotted at intervals of 5%. It is also difficult to read the exact beam position, as the beam is quite broad (8^{o}).

Cross polarization due to the wedges is maximum for a polarization angle of 45^{o}, measured from the plane of incidence. So, we put the wedges corresponding to $\psi = 45^{o}$ to get the worst possible cross polarization for the pair of wedges. The measured cross polar patterns are shown in fig(8.17). We can see that the cross polar patterns have been steered by the wedges, but their levels remain approximately the same.

Due to the limitation of the measuring facilities, no measurements were taken for radiation patterns perpendicular to the plane of beam steering. However, computations were made to show that there should be no significant change in the pattern in the perpendicular plane due to the beam steering. Fig(8.18) shows the computed pattern of the antenna on its own, and fig(8.19) shows the pattern in the perpendicular plane when the beam is steered by 16^{o}.

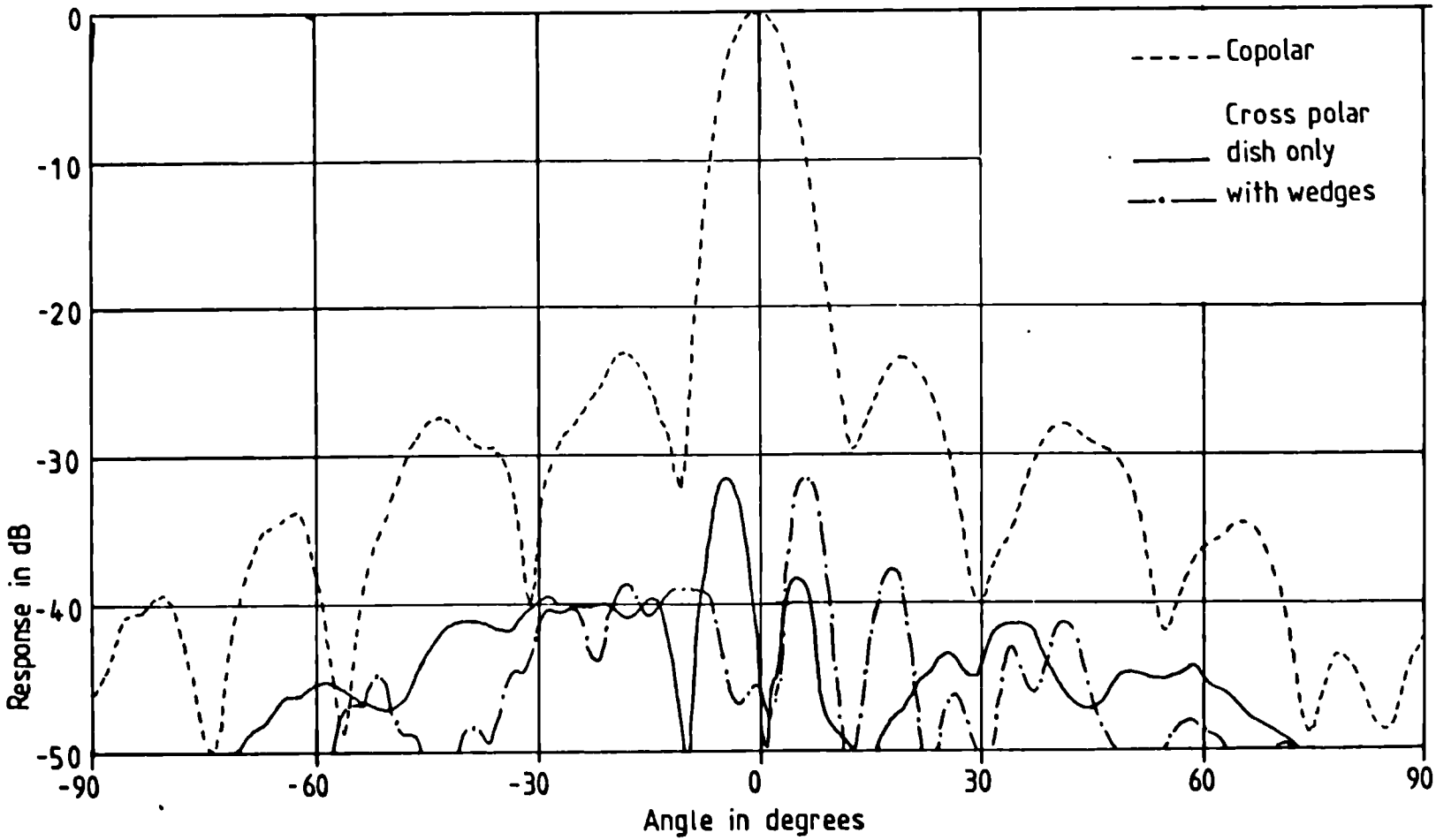

Fig 8.17. Cross polar pattern for the wedges with $\psi = 45^{o}$.

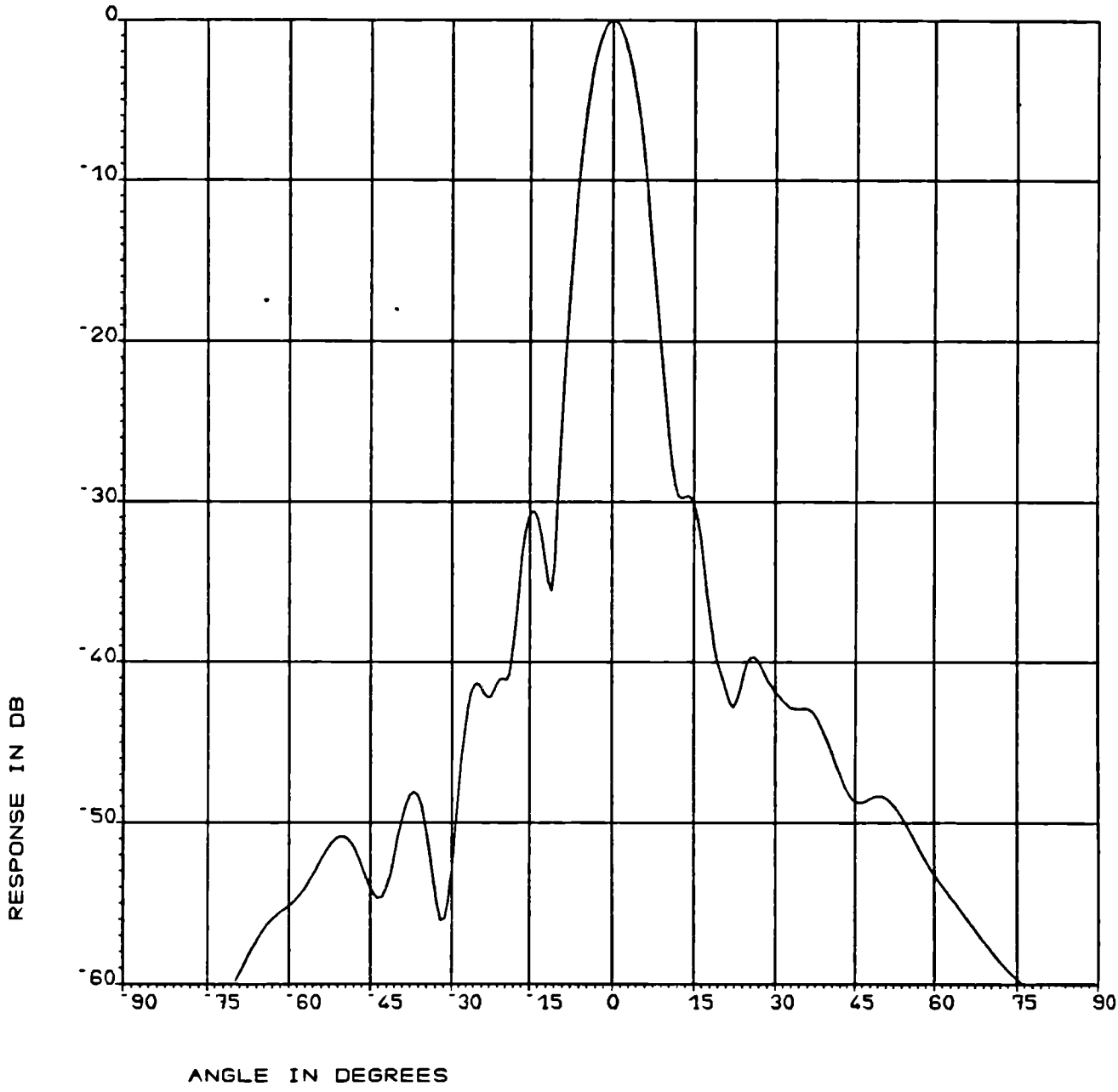

Fig 8.18. Computed pattern of the 30cm dish in the H-plane

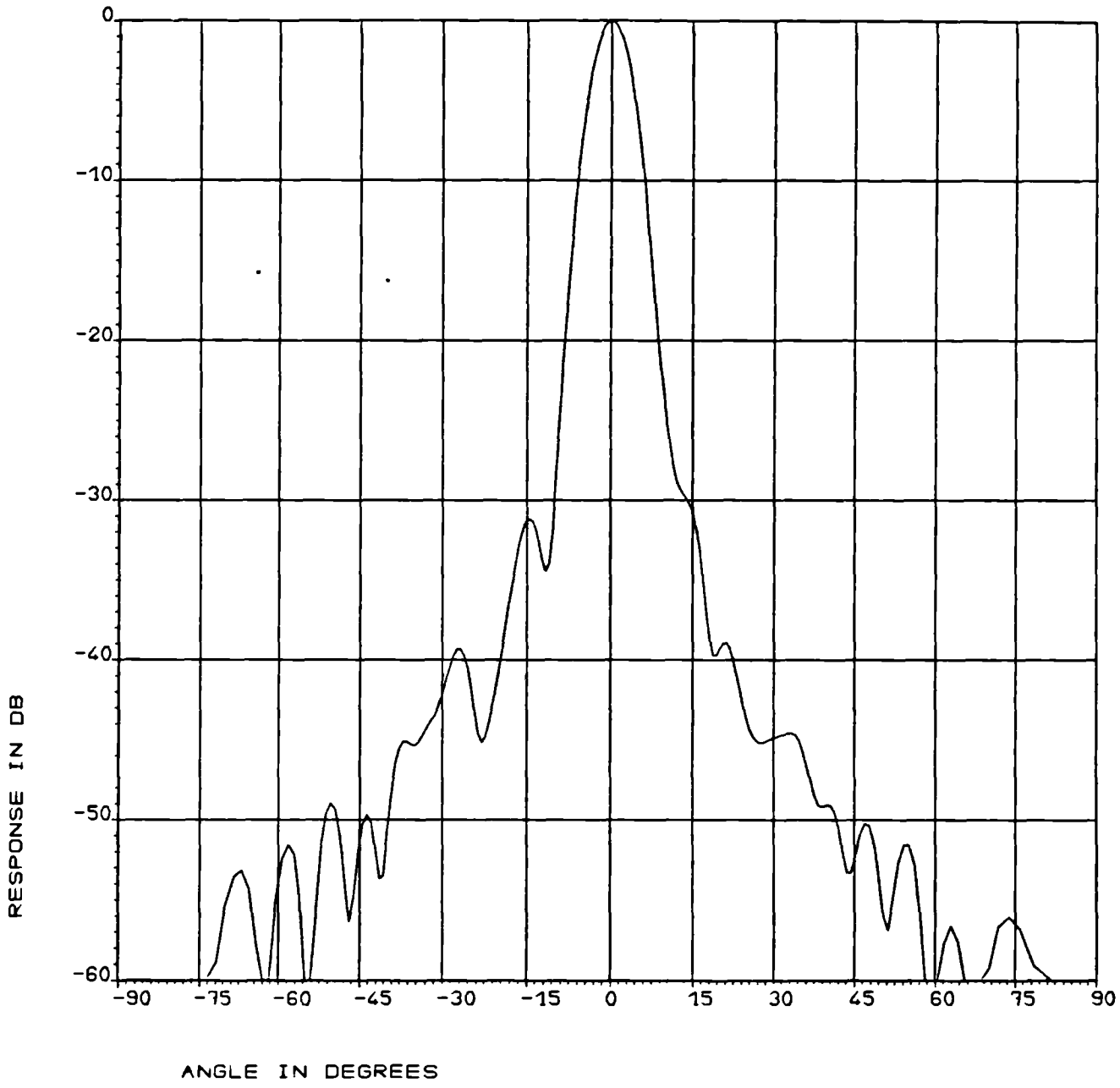

Fig 8.19. Computed pattern of the 30cm dish in the plane perpendicular to the plane of the beam steering.

8.4 Discussion

Section 8.2 has discussed the problems of using TiO_2 powder as a dielectric material for the wedges. However it is possible to use better quality TiO_2, mixed with polystyrene or PTFE to make the resultant dielectric material solid and the proportion of TiO_2 in them more uniform. But the weight is still a limiting factor for the large wedges.

Perspex wedges are much cheaper and can be easily machined to make wedges for small antennas. Although there is some discrepancy between measured and the computed patterns, the steered patterns in both cases are not substantially different from the pattern of the antenna alone. So, from the measured and the computed results we can safely conclude that the sidelobe levels do not change appreciably compared to the radiation pattern of the antenna. So, the reduction in the gain of the system comes mainly from the loss inside the wedge material, as the reflection and other losses are small. This is an attractive feature of the scheme, unlike the feed shifting technique in the parabolic dish. Even with phase shifters, such a performance can be achieved if the inter-element spacing does not exceed 0.5λ.

9. Conclusion

9.1. Summary

A novel scheme has been developed to steer the beam of an antenna using dielectric wedges. The technique uses a pair of dielectric wedges, having circular faces, placed in front of an antenna in the near field. Beam steering is achieved in any direction up to some maximum value determined by the dielectric constant and the wedge angle. Chapters 2 and 3 are devoted to the antenna fundamentals and the basics of the propagation of electromagnetic waves in a dielectric medium. These are vitally important for an insight into the mechanism of the beam steering technique.

The scheme has been theoretically and experimentally investigated in chapter 4 using the concept of angular spectrum. The effect of reflections on the radiation pattern is also examined in this chapter and a novel application of dielectric matching has been devised.

Some important aspects of the technique, like the possibility of stepping the wedges as a weight reduction scheme, cross polar performance of the wedges, size of the wedges in relation to the size of the antenna etc. are extensively analysed in chapter 6. It is concluded that the size of the wedges should be slightly larger than the size of the antenna to intercept a significant portion of the aperture. The cross polarisation can be neglected up

to a steering angle of about 30^{o}. Even beyond ihis angle the cross polar components due to the wedges are not very high. Experiments described in chapter 4 and chapter 8 confirm the low values of cross polarization for moderate steering angles (16^{o}). Some charts have been developed in chapter 7 to enable the user to determine the wedge positions for the corresponding beam position. The accuracy of the charts has been confirmed in the experimental measurements in chapter 8.

9.2 Applications and Limitations

The scheme was developed with particular reference to Direct Broadcast Satellite (DBS) antennas to obtain a useful amount of beam steering. The technique developed here is simple to apply to any type of antennas such as a parabolic dish or a flat plate array of radiating elements. Mechanical rotation of the wedges is simple, as they are independent of the antenna and the feed, and hence contain no rotating microwave joint. Pointing the beam in the right direction is also simple as the wedges have to be rotated by a much larger angle than the desired beam deflection.

The steered pattern is very nearly the same as the antenna pattern and steering changes the sidelobes by a very small amount. The angle of beam steering is independent of frequency. However, frequency limitations are set by the

matching layers on the wedges faces.

This technique can be applied to the antenna irrespective of its polarization. The performance is very nearly the same for linear or circular polarization. Hence using a polarizer at the front of the antenna can enable a linearly polarized antenna to be used to receive circularly polarized waves without disturbing the beam steering properties of the wedges.

This technique can be quite attractive for antennas on vehicles when used along with a servo mechanism. At X-band frequencies, the size of the antenna is large enough to make the wedges heavy, unless some artificial dielectric material can be fabricated. But at high frequencies like millimeter waves, the size of the antenna is smaller and the wedges can be made much lighter even with conventional dielectrics.

The maximum amount of beam steering using this technique is limited by the reduction in gain and the generation of cross polarization. The gain reduces rapidly at large angles due to the inclination of the main beam and due to significant internal reflection of the waves inside the wedges. Considering these factors, the upper limit of beam steering seems to be about 50^{o}.

9.3. Future Work

A search was made for high dielectric constant materials and it was found that they are quite heavy. Stepping the dielectric wedges can reduce the overall weight by a factor of 3 or 4. Although some theoretical analysis is given in chapter 6 to predict the deterioration of the radiation pattern, further work could be done to study the behaviour of the stepped wedges in more detail, both theoretically and experimentally.

It was pointed out in section 6 that the reduction in the gain of the antenna due to the inclination of the main beam can be compensated to a large extent by using fast wave structures like waveguides, to build up the wedges. Artificial dielectric materials with dielectric constant less than 1 can also be fabricated. However, further improvement is necessary in the design and construction of the artificial dielectric wedges to make them commercially attractive.

APPENDIX I

Gain claculation for DBS antennas

Let T_a be the antenna system noise temperature and T_s be the noise temperature of the amplifier. The noise temperature of sky, which is quite cool at these frequencies, is about $13^{o}K$ at 25^{o} of elevation [38]. Assuming an ambient temperature of $290^{o}K$,

$10Log(1 + T_s/290) = 8$ = Noise figure.

$T_s = 1537^{o}K$

Total noise = $1537 + 13 = 1550^{o}K$

$= 31.9$ dB

$G > 31.9 + 6 = 37.9$dB, as $G/T > 6$ dB/^{o}K.

For a frequency of 12GHz, $\lambda = 2.5$cm, which gives an effective area of the antenna

$A_e = G\lambda^2/4\pi = 3185.46\ cm^2$

Diameter = 63.7cm

For a parabolic dish, let us assume an aperture efficiency of 50%.

Diameter of a dish for the required gain = 90cm.

APPENDIX II

Scattering pattern of an 8-element array -

Consider an array consisting of omnidirectional elements fed with a corporate feed network, as illustrated in fig(A.1). Now consider a plane wave incident at such an angle that the elements are excited with uniform angle and phases of 0, $-\emptyset$, $-2\emptyset$, ... etc (taking the leftmost element is taken as zero phase). When the power from elements 1 and 2 arrives at the first junction in the feed network - point J_{11} - then some of the power will flow into the output arm and some will travel from one element directly to the other element and be reradiated. We can resolve the two signals into components in-phase and anti-phase with each other, where the in-phase components represent the power coupled to the next section of the feed line and the anti-phase components merely interchange between the elements. Fig(A.1c) shows the vector diagram corresponding to the situation at point J_{11}, and if we take account of the line lengths (as shown in the diagram) we can work out the excitation of each element. This corresponds to set 1 in the figure. We can then repeat the process for the other junctions between pairs of elements, then use the method again to take account of the other junctions J_{21} etc, and finally obtain three sets of excitations as shown in figure(A.1b). The resultant pattern is the sum of these three sets.

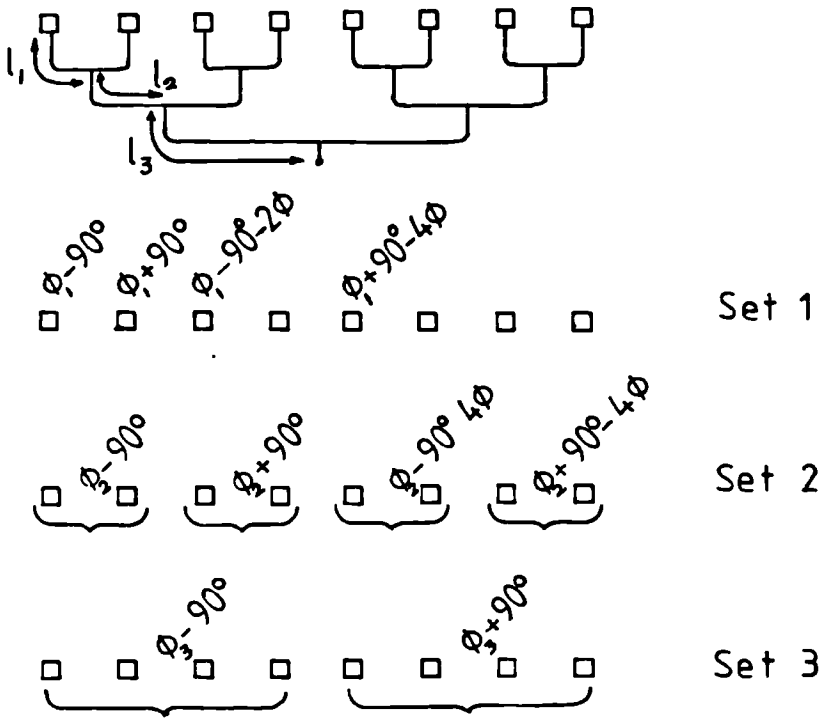

Set 1
Amplitude = $\sin\Phi/2$

$\Phi_1 = -\Phi/2 - 2\beta l_1$

Set 2
Amplitude = $\cos\Phi/2 . \sin\Phi$

$\Phi_2 = \Phi_1 - \Phi - 2\beta l_2$

Set 3
Amplitude = $\cos\Phi/2 . \sin\Phi . \cos 2\Phi$

$\Phi_3 = \Phi_2 - 2\Phi - 2\beta l_3$

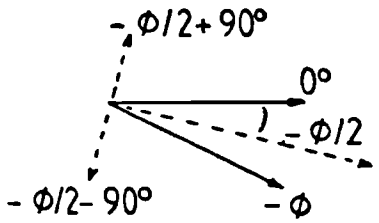

Fig A.1. Three sets of excitation for the scattering pattern of the 8-element array.

APPENDIX III

Measurements of ε and tanδ

This technique was first suggested by Roberts and Von Hippel [39]. The setup is shown in figure(A.2) below.

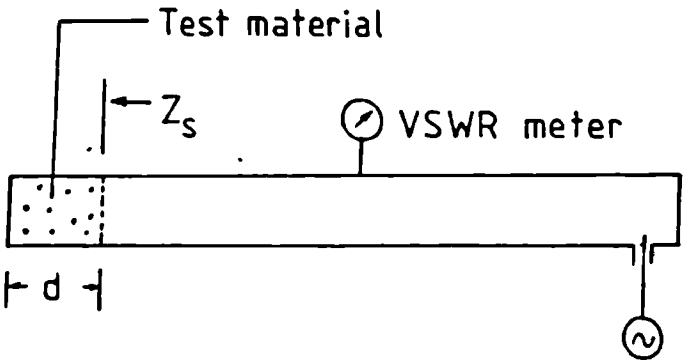

Fig A.2. Experimental setup for the measurement of and tanδ .

Let Z_o be the characteristic impadence of the waveguide when filled with air.

$$Z_o' = j\omega\mu_o / j\beta_o$$

Let Z_o be the characteristic impedance of the waveguide when filled with the dielectric material whose properties are to be measured.

$$Z_o = j\omega\mu_o/P \text{ , where } P = \alpha_d + j\beta_d$$

α_d= attenuation factor

β_d= propagation factor.

Hence from the figure,

$$Z_s' = Z_o \tanh(Pd)$$

$$Z_s/Z_o = Z'_o/Z_o \cdot \tanh(Pd)$$

$$= j\,\beta_o/P \cdot \tanh(Pd)$$

$$= j\,\beta_o d \quad \tanh(Pd)/(Pd)$$

This equation can be solved numerically. Roberts and Von Hippel [39] provided charts for the function tanh(Pd)/(Pd).

References

[1] Kingslake,R., "The Diffraction Structure of the Elementary Coma Image", Proc. Phys. Soc. (London), vol.6, pp 147-158, 1948.

[2] Born, M., Wolf,E., "Principles of Optics", chapt. 5 & 6, Pergamon, New York, 1959.

[3] Ruze,J., "Lateral Feed Displacement in Paraboloid", IEEE AP, vol.13 , page 660-665, Sept. 1965.

[4] Hansen,R.C., "Microwave Scanning Antennas", vol.3, chapt. 1, Academic Press, New York, London, 1966.

[5] Rotman,W.,Turner,R.F., "Wide angle microwave lens for line source application", IEEE AP - 11, pp 623-630, 1963.

[6] Fong,A.K.S., Smith,M.S., "Design and performance of a microstrip multiple beam forming lens", 3rd International Conference on Antennas and Propagation, pp 344-347,1983.

[7] Sole,G.C., Smith,M.S., "3-D Multiple beam forming lenses for planar arrays", 14th European Microwave Conference, pp 686-690, 1984.

[8] Silver, S., "Microwave antenna theory and design", Peter Peregrinus Ltd, 1984 pp 169-174.

[9] Booker, H.G., Clemmow, P.C., "The concept of Angular Spectrum of plane waves and its relation to that of polar diagram and aperture distribution" , IEEE vol. 97,1950, pp 11-17.

[10] Clark, R.H., Brown, J., "Diffraction theory and antenna", John Wiley and Sons Ltd., 1980 pp 70-71.

[11] Clark,R.H., Brown, J., ibid, pp 85-87.

[12] Clark,R.H., Brown,J., ibid, pp 41-43.

[13] Ramo, S., Whinnery, J.R., Van duzer, T., "Fields and waves in Communication Electronics", John Wiley and Sons Inc., 1965, pp 327-29.

[14] Collin,R.E., "Foundations for microwave engineering" McGraw Hill Book Co. Inc., 1966, pp 221-224.

[15] Collin,R.E., ibid ,pp 225-240.

[16] Ramo,S., Whinnery, J.R., Van duzer,T., ibid, pp 363-364.

[17] Dekker, A.J., "Electrical Engineering Materials", Prentice Hall Inc., New Jersey, U.S.A., 1959, pp 62-76.

[18] Mc Ewen, C.D., Khan,M.R.,"Beam Steering Method with Improved sidelobes using dielectric wedges for atellite TV reception", 14th European Microwave Conference, Sept. 1984,pp 681-85.

[19] Catalogue for RT/DUROID products, Mektron Circuit Systems Ltd.,Surrey, U.K.

[20] James,J.R., Hall P.S.,"Microstrip antenna theory and design",Peter Peregrinus Ltd, Stevenage, U.K., New York U.S.A., 1981.

[21] Clark,R.H., Brown, J., ibid, pp 181-183.

[22] Silver, S.,"Microwave Antenna Theory and Design",Peter Peregrinus Ltd,London, U.K.,1984, pp 351-55.

[23] Matthaei,G.L., Young L.,Jones ,E.M.T., "Microwave filters, impedance matching networks and coupling structures", McGraw Hill, New York, 1964, ch.4.

[24] Hamid ,M.A., Yunik,M.M.,"On the design of stepped

transmission line transformers", IEEE MTT-15, Sept.1967,pp 528-29.

[25] Arnold ,R.M., "Transmission line impedance matching using the smith chart", IEEE MTT-22, Nov.1974,pp 977-78.

[26] French ,G.N., Fooks ,E.H., "Double section matching transformers", IEEE MTT-17, Sept.1969, pp 719.

[27] Day, P.I., "Transmission line transformation between arbitrary impedances using the Smith chart", IEEE MTT-23, Sept. 1975, pp 772-73.

[28] Bramham, B.,"A convenient transformer for matching coaxial lines", Electronic Engineering vol.33, pp 42-44, Jan 1961.

[29] Von Hippel, A.R.,"Dielectric materials and applications", John Wiley and Sons Inc. NewYork, Chapman and Hall Ltd., London, 1954, pp 301-370.

[30] Barlow, H.M.,Cullen,A.L., "Microwave measurements", Constable and Co. Ltd.,London, U.K.,1950, pp 275-303

[31] Kock, W.E., "Metallic delay lenses", Bell System Technical Journal, vol.27, Jan 1948, pp 58-82.

[32] Jasik,H., "Antenna Engineering Hand Book", McGraw Hill Book Co. Inc.,1961, chapter 14,pp 21-41

[33] Collin, R.E., "Field Theory of Guided Waves", McGraw Hill Book Co. Inc.,1960, pp 509-547.

[34] Brown, J., "Microwave lenses", John Wiley and Sons Inc., New York, 1953, pp 52-68.

[35] Brown, J., "Microwave lenses", ibid, pp 7, 111 - 113.

[36] Jasik, H., ibid, chapter 14, pp 5-9.

[37] Silver, S., ibid, p 398.

[38] Skolnik, M.,"Radar Hand Book", McGraw Hill Book Co. Inc., 1970, chapter 2, page 31-32.

[39] Roberts, Von Hippel, "New method for measuring Dielectric constant and loss in the range of centimeter waves", J. of App. Phys.,vol. 17, no.7, 1946, p.610.